ABSTRACT OF THESIS

Name of Candidate MARGARET GRACE FERGUSON

Address 46 Dunnikier Road, Kirkcaldy

Degree Doctor of Philosophy *Date* August, 1967

Title of Thesis "STUDIES OF MOLECULAR EXCITATION PROCESSES IN GASES"

The thesis is divided into two parts.

Part one

A spectrophone technique is developed which allows measurement of the relaxation times, at room temperature, of molecules whose radiative lifetimes and collisional relaxation times are comparable. The relaxation times of CO, HCl, DCl, and HBr are determined. The relaxation times of the last three gases are much shorter than those predicted by standard vibration-translation energy transfer theory, and it is shown that the results are best explained in terms of vibration-rotation energy transfer.

Part two

Part two is concerned with the development of an electron impact spectrometer designed to study electronic excitation in molecules. The incident electron energy is chosen so that the optical selection rules are not expected to hold. Electron impact spectra of helium and argon are obtained. The usefulness of the method is discussed in the light of other work, and suggested improvements are considered.

Use other side if necessary.

STUDIES OF MOLECULAR EXCITATION PROCESSES IN GASES

BY

MARGARET G. FERGUSON

Thesis presented for the degree of

Doctor of Philosophy

University of Edinburgh August, 1967

PREFACE

This thesis is concerned with two types of excitation processes in molecules. Part One deals with the intermolecular transfer of vibrational energy, and Part Two with the excitation of electronic states of molecules by electron impact.

CONTENTS

PART ONE

MEASUREMENTS OF VIBRATIONAL RELAXATION TIMES BY THE OPTIC ACOUSTIC EFFECT

PART ONE

MEASUREMENTS OF VIBRATIONAL RELAXATION TIMES BY THE OPTIC ACOUSTIC EFFECT

Chapter One

Introduction

Vibrational Energy Transfer:

Molecular energy is distributed among vibrational, rotational and translational degrees of freedom. If the temperature of a particular degree of freedom is perturbed by an amount ΔT, then the return to equilibrium is governed by the equation

$$d(\Delta T)/t = -(\Delta T)/\tau$$

where τ is the 'relaxation time' of the process.

Collisional relaxation of the various molecular degrees of freedom shows enormous differences in rate. Equilibration of translational energy requires only a few collisions, and that of rotational energy rarely more than twenty. In contrast, vibrational relaxation usually requires between 10^3 and 10^{10} collisions.

This slow readjustment of vibrational energy has important consequences in both physics and chemistry. It affects gas dynamics by introducing a time dependence into the thermodynamic and transport properties of gases, and is important in such diverse fields as the design of rocket motors and infra-red gas lasers. Application in the field of gas lasers have recently been receiving increased attention, and an idea of the range of possibilities can be had from perusal of the supplement on Chemical lasers published by the Optical Society of America (1). In addition, since the activation and deactivation stages of many chemical reactions involve the conversion of kinetic energy of motion into vibrational energy, the relation between vibrational energy tranfer and chemical kinetics is a close one. The wide range of vibrational relaxation times offers a useful criterion against which to test our grasp of molecular interactions in systems which can be specified in detail.

The knowledge so acquired can then be applied to the more complex conditions prevailing when chemical reactions occur.

Vibrational energy may be transferred by collisional or radiative processes. The radiative lifetimes (τ rad) of most vibrationally excited states of molecules with electric dipole moments are of the order of milliseconds, so that, under normal experimental conditions many collisions occur during one radiative lifetime, and collisional relaxation predominates. However, in a few diatomic molecules with high fundamental vibration frequencies (greater than 2000 cm^{-1}) the two processes become competitive. Since radiative lifetimes are known from absorption intensity measurements this competition can be used to determine collisional relaxation times. The present work is concerned with the development of such a method.

The inefficiency of collisional transfer of vibrational energy is easily understood qualitatively. For changes in translational energy to affect the internal motion of a molecule it must experience, during collision with another, an oscillatory perturbation whose frequency corresponds to that of the internal motion. A rough analogy may be drawn to a vibrating spring; if the spring is compressed and released slowly there is no resulting change in its motion, but if sharply hit it starts vibrating. In molecular collisions the perturbation effecting energy transfer arises from the change in translational energy of the molecules as they approach one another in the repulsive region of the intermolecular potential. At moderate temperatures this change is slow compared with typical vibration frequencies. Vibrational energy transfer is therefore inefficient.

From this simple physical picture we deduce that relaxation times will decrease with increasing velocity of approach, increasing steepness of the intermolecular potential, and decreasing vibration frequency. The situation is complicated by the occurrence of 'complex collisions'.

As well as the simple case where vibrational energy is exchanged with translation, V-T transfer, there exists the possibility of vibrational energy exchange between the internal modes of the collison partners, V-V transfer. For near resonant collisions V-V transfer has been shown, experimentally and theoretically to be more efficient than the V-T process (2,3).

Refinements of the basic theory proposed by Zener (4) in 1931 have led to good agreement with experimental results for low energy vibrational modes of diatomic and simple polyatomic molecules. The original classical approach of Landau and Teller (5), and later semiclassical and quantum mechanical treatments lead to essentially the same results. Discussions of the theories of vibrational energy transfer are given by Herzfeld and Litovitz (6) and Cottrell and McCoubrey (7). The difficulty of a priori calculations for polyatomic molecules has resulted in a number of empirical correlations of experimental relaxation times. In a particularly useful one by Lambert and Salter (8), a plot of the logarithm of the number of collisions undergone by a molecule before energy transfer occurs (Z_{10}) against the lowest fundamental vibration frequency (ν min cm^{-1}) revealed that molecules containing two or more hydrogen atoms fall on a different straight line from those containing no hydrogen atoms. Compounds containing one hydrogen atom lie between the two lines.

A possible explanation of this phenomenon arose from work by Cottrell et al (9,10,11) on the relaxation times of a series of hydrides and their deuterated analogues. Theory predicts that the lower vibration frequency of the deuteride will be the controlling factor leading to a shorter relaxation time for the deuteride than for the hydride. Experimentally the opposite is true. The hydrides relaxed more rapidly than their corresponding deuterides. Cottrell suggested that, since the rotational velocity of the peripheral atoms is greater than the translational velocity of the molecule as a whole,

vibrational energy transfer into rotation might be more likely than into translation. Rotational-translational energy transfer is then rapid. A theoretical expression for V-R transfer was derived (11) and the calculated ratios of hydride to deuteride relaxation times agreed well with the measured values. Conclusive proof that rotation can play an important part in vibrational de-excitation come from work by Millikan and Osburg (12) on carbon monoxide relaxed by ortho and para hydrogen. And a recent correlation by Moore (13) supports the interpretation of relaxation in many polyatomic molecules in terms of vibration-rotation energy transfer.

In the present work a method is developed whereby the optic-acoustic effect is used to measure long relaxation times ($>10^{-3}$sec) and a value is obtained for the relaxation time of pure carbon monoxide. The same method is then used to determine the relaxation times of HCl, DCl and HBr. The values obtained indicate that vibration-rotation interactions play an important role in the vibrational relaxation of the last three gases.

Chapter Two

EXPERIMENTAL METHODS IN VIBRATIONAL ENERGY TRANSFER

Only a brief review of the more important methods in energy transfer will be given here. A detailed discussion can be found in reference (7) and in recent reviews.

2.1 Ultrasonic Methods:

Studies of the propagation of sound waves in gases have long provided the most important and accurate data on vibrational relaxation at or near room temperature. For a full account see reference (6).

(a) Measurement of Velocity:

In an ideal gas the velocity of sound is given by

$$V^2 = \frac{RT}{M}\left(1 + {}^{RT}/_{Cv}\right)$$

Where R is the gas constant, T the absolute temperature, M the molecular weight, and Cv the molar heat capacity at constant volume, being the sum of vibrational, rotational and translational contributions to the specific heat. At low sound frequencies the time between successive compressions and rarefactions of the gas is long enough to allow excess translational energy to relax into vibrational modes. As the frequency is raised the period of the sound wave becomes comparable with the vibrational relaxation time; the vibrational modes no longer contribute to the specific heat, and the velocity of sound rises - see Fig. 1(a). The midpoint of this dispersion curve corresponds to a sound wave whose frequency is proportional to the relaxation time.

(b) Measurement of Absorption:

The dispersion of sound is accompanied by a non-classical absorption of sound caused by the relaxation process (Fig. 1(b)). The frequency at the absorption maximum is again simply related to the relaxation time.

FIG 1 VELOCITY AND ABSORPTION OF SOUND AGAINST FREQUENCY FOR AN IDEAL GAS

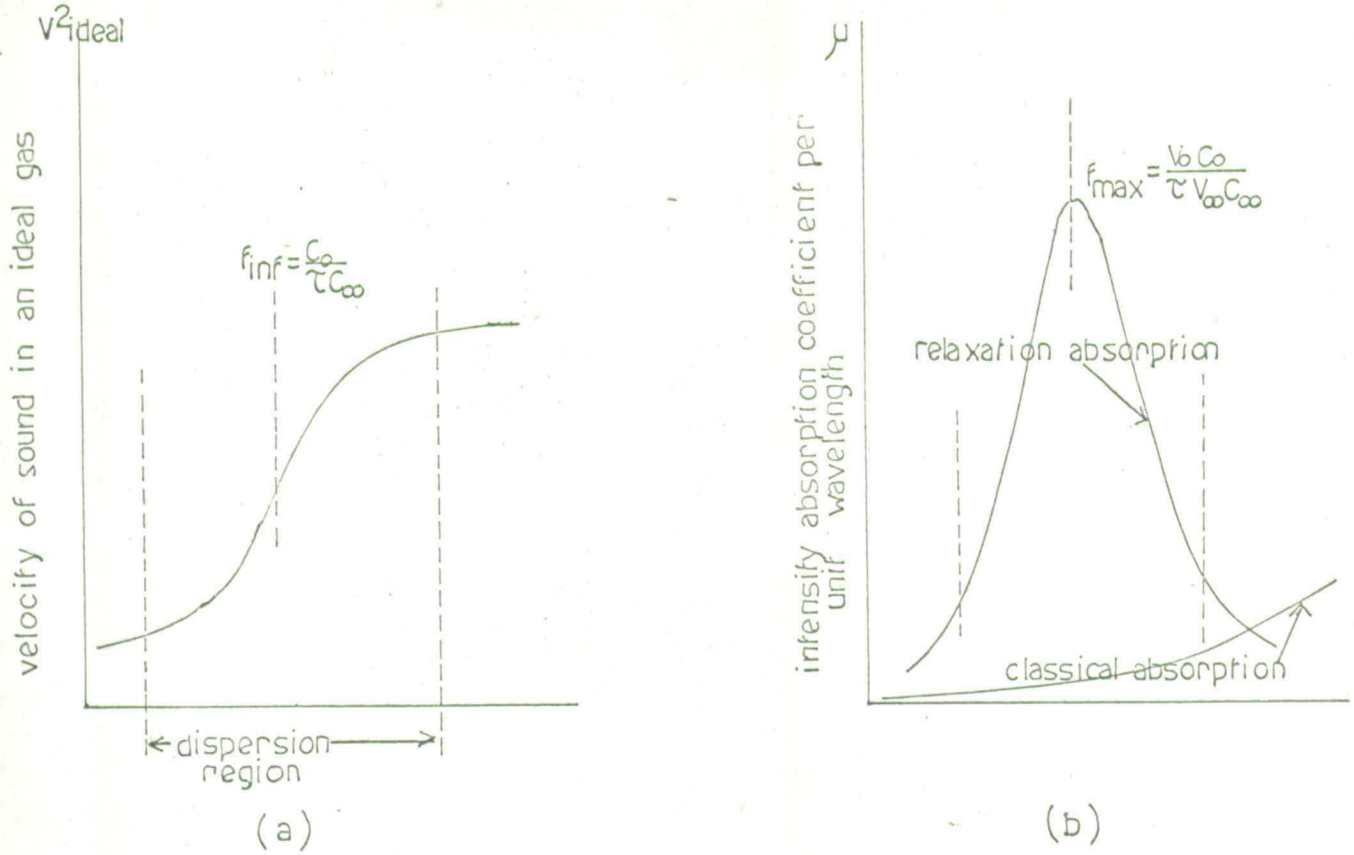

FIG. 2 PROPERTIES OF CARBON MONOXIDE BEHIND A MACH 8 SHOCK WAVE (INITIAL PRESSURE 10 TORR). — ref.

State 1 is the undisturbed gas.
State 2 represents the shocked gas conditions before vibrational relaxation.
State 3 is the region of energy equilibration.

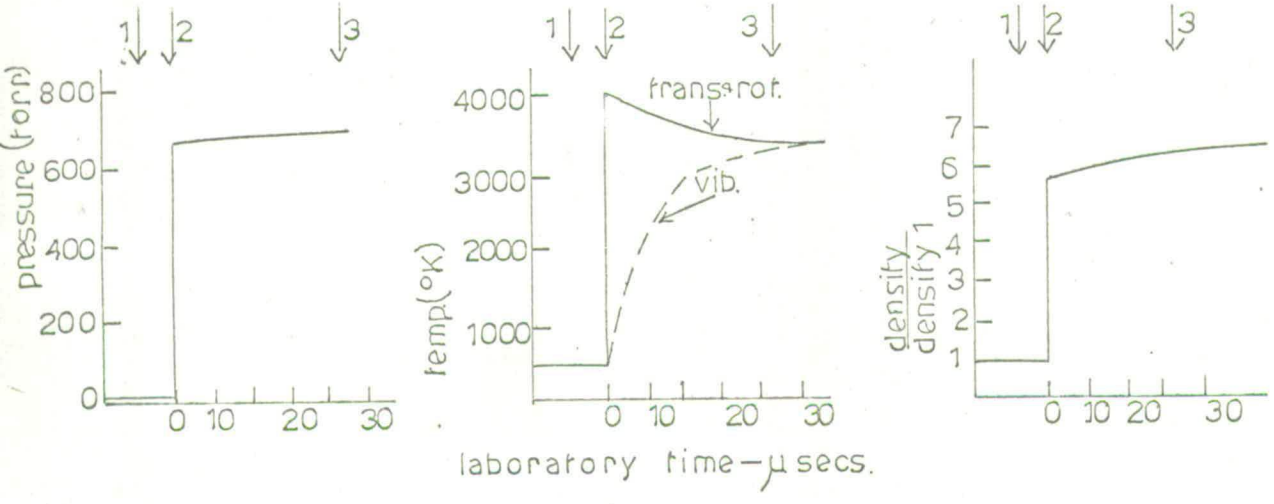

In both cases corrections must be made for the non-ideality of the gases.

A basic limitation of the above methods is that energy is supplied to translation. It can then relax into all accessible internal modes so that there is no way of examining preferentially the relaxation of one mode. Also, because the source of sound is a quartz crystal high temperature work is ruled out. This means that molecules with relatively high vibration frequencies (>1500 cm^{-1}) cannot be studied ultrasonically (14) since a sufficient proportion will not be excited to the first vibrational level.

2.2 Shock Waves:

As a shock wave travels through a gas the translational and rotational temperature immediately behind the shock rises to a value somewhat greater than the equilibrium temperature T_3 of the shocked gas, while the vibrational temperature remains at T_1, that of the unshocked gas. In the succeeding relaxation zone the vibrational temperature rises rapidly as energy is transferred into vibration; the translational temperature decreases towards T_3 and the density increases, until equilibrium conditions for the shocked gas are attained. (Fig. 2). Investigation of the shock front structure gives vibrational-translational relaxation times. The most generally applied method has been measurement of the density profile with an interferometer. Gaydon and co-workers (15) and Holbeche (16) have followed the vibrational temperature using a sodium line reversal technique. As with ultrasonic methods, shock waves give non-selective excitation of many vibrational levels. That this limitation can sometimes be overcome is shown in a few studies of infra-red emission from shock heated gases, leading to relaxation times for specific modes (17, 57).

Shock waves allow the measurement of vibrational relaxation times up to several thousand degrees and hence provide an important complement to ultrasonics. A recent review of the subject is given by Bauer (19).

FIG 3 TOP VIEW OF OPTICAL ARRANGEMENT FOR MILLIKAN'S FLUORESCENCE EXPERIMENT

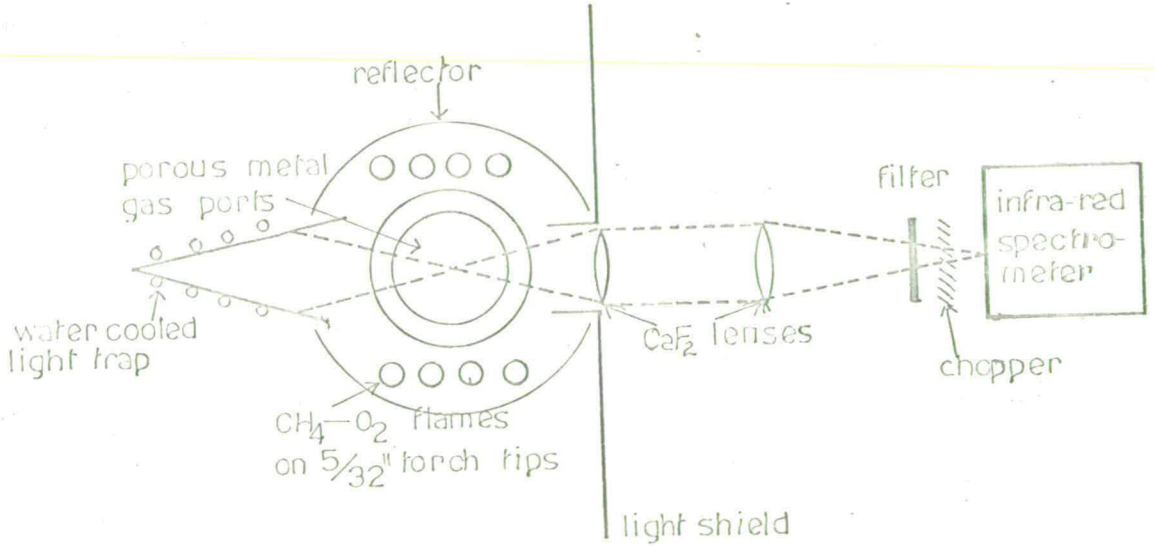

2.3 Quenching of Vibrational Fluorescence:

Millikan's work on infra-red emission from shock heated carbon monoxide gave a new method for determining the rates of vibrational relaxation of CO with many different collision partners near room temperature (20,21,22). He uses the fact that for pure CO, or CO mixed with Ar, the radiative process (1) is more important than the collision process (2). CO^* denotes vibrationally excited CO.

$$CO^* \longrightarrow CO + h\nu \qquad (1)$$

$$CO^* + M \longrightarrow CO + M + \text{kinetic energy} \qquad (2)$$

Thus at room temperature CO is expected to fluoresce. If this fluorescence is to be observed the CO used must be very pure and wall collisions must be eliminated. Millikan's experimental arrangement is shown in Fig.3. When a flow of extremely pure CO was contained in an annular flow of Ar of matched velocity an intense fluorescence signal was obtained. The addition of increasing amounts of a foreign gas M that is efficient at de-exciting CO^* caused quenching of the fluorescence. At half-quenching the rates of the radiative and collisional processes are equal. Since the rate of (1) is known, the collision efficiency of M is determined.

The fluorescence in pure carbon monoxide could be detected for 4 cms, or 0.2 secs, past the point of excitation implying that the collisional relaxation time at 286°K and 1 atmosphere pressure is of this order or longer. This value disagrees with the room temperature value of $\tau = 2 \times 10^{-3}$ secs. reported by Woodmansee and Decius (23) and the even shorter value of $\tau = 1.3 \times 10^{-5}$ secs. obtained by Delaney (24). Schaefer (25) measured $\tau = 3 \times 10^{-4}$ secs. All these workers were using spectrophone techniques which depend on detecting pressure signals arising from collisional energy loss. But Millikan showed that in pure carbon monoxide at room temperature radiative loss is predominant and CO should give no response in the spectrophone (20). The present work therefore began as an attempt to show that pure carbon monoxide

gave no optic acoustic signal.

2.4 The Optic Acoustic Effect:

A gas molecule absorbing radiation of the appropriate frequency will be raised to an upper vibrational level. If it then loses this vibrational energy by transfer to thermal energy during collisions with other molecules, the translational temperature of the gas increases, and in a constant volume system there is a concomitant increase in pressure. Periodic interruption of the incident radiation results in sound emission from the gas at the interruption frequency. This effect - the 'optic-acoustic' effect - was discovered independently by Tyndall (26), Rontgen (27), and Bell (28) in 1881. Bell named the instrument a spectrophone. Tyndall (26) used thermal radiation interrupted at an audible frequency to excite gas contained in a thin glass sphere, and detected the resultant pressure fluctuations with a small listening tube attached to the sphere. The lack of convenient sound detectors delayed further development until 1938 when, in a short time, three authors independently reported the use of the optic acoustic effect as a method of gas analysis (29, 30, 31). In 1945 Viengerov (32) successfully employed the optic acoustic effect to measure infra-red absorption spectra by using monochromatic exciting radiation.

Measurement of Vibrational Relaxation Times using a Spectrophone:

Gorelik (33) in 1946 first suggested the use of the spectrophone to determine rates of vibrational energy transfer. He pointed out that the time lag between the absorption of a vibrational quantum and its degradation to thermal energy would introduce a phase lag between the incident radiation and the emitted sound. He also showed that the amplitude of the optic acoustic signal has an added frequency dependence because of the relaxation effect. Cottrell (35) showed theoretically that if the mean number of vibrationally excited molecules depends on the frequency of modulation, the mean translational

temperature should vary with the frequency in a manner determined by the vibrational relaxation time. However, he overestimated the magnitude of the effect which is very small and outwith experimental measurement (24).

There are two theoretical approaches to the optic acoustic effect: Gorelik's original thermodynamic approach which was further developed by Cottrell (7), and the kinetic molecular approach adopted by Delany (24) and Kaiser (36). Both treatments lead to the same frequency dependence for the phase and amplitude of the sound wave. The relationships are shown in Fig, 4.

For the simple theory to hold, the rate of heat transfer from the gas to the environment must be negligible compared with the rate of the relaxation process. Thermal conductivity effects introduce a frequency dependent phase lead and decrease the amplitude of the signal, thus interferimg with both quantities used to determine relaxation times. Heat conduction effects can be overcome by making the modulation frequency sufficiently high. Delany (24) in an extensive study of the optic acoustic effect has confirmed experimentally the predictions of the simple theory.

In principle the optic acoustic effect offers an ideal method for obtaining vibrational relaxation times because energy is supplied to a selected vibrational mode. But the experimental difficulties are formidable. As well as phase and amplitude changes caused by relaxation and heat condution, further frequency dependent changes can be introduced by the apparatus. Such spurious phase shifts have proved to be one of the major problems in obtaining reliable relaxation times from the spectrophone - see, for example, reference (40).

Two experimental methods have been developed: measurement of the phase difference, and measurement of the frequency response of the signal amplitude. Slobodskaya's preliminary experiments in 1948 (34) formed the basis of work by Slobodskaya and Gasilevich on the relaxation of CO_2- N_2 mixtures (37).

FIG 4 FREQUENCY DEPENDENCE OF THE PHASE AND AMPLITUDE OF OPTIC ACOUSTIC SIGNALS

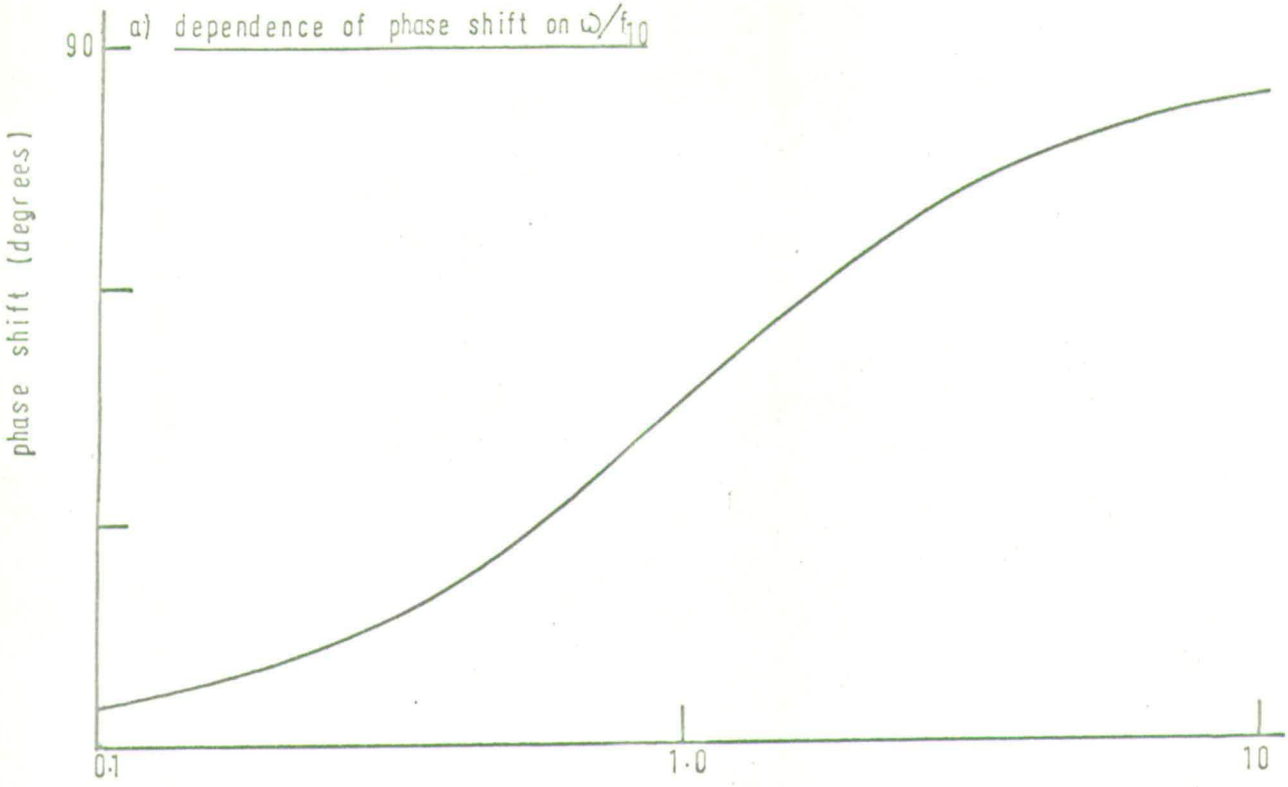

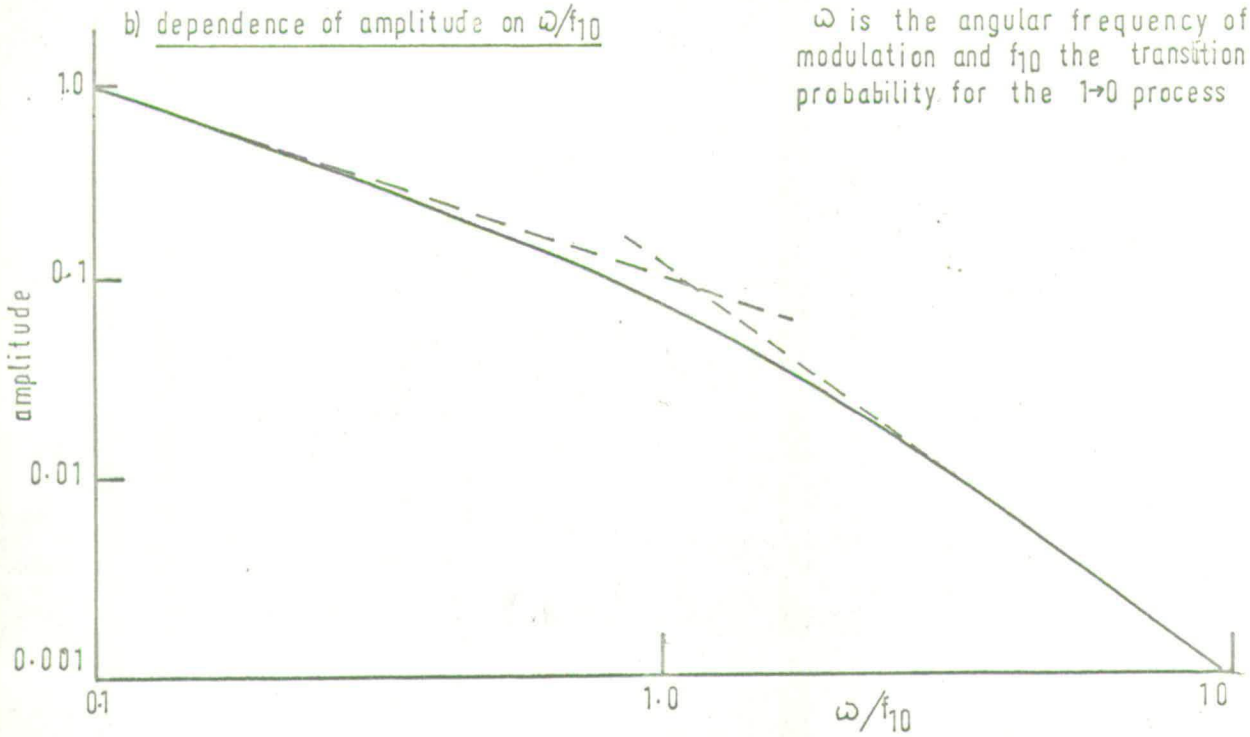

ω is the angular frequency of modulation and f_{10} the transition probability for the 1→0 process

In mixtures of high N_2 concentration the relaxation phase lags are large. They decrease with increasing CO_2 concentration until too small to be detected. The apparatus phase shift - the sum of phase shifts due to the electronics of the detecting system, the properties of the diaphragm, and variations in gas properties - was assumed to be independent of gas composition. The apparatus phase shift was then deduced from the fast relaxing end of the scale, where the relaxation phase shift was undetectable, and used to correct the slow relaxing end. The 2.7 and 4.5 μ bands of CO_2 were studied.

A much more satisfactory experiment becomes possible if the apparatus phase shift can be eliminated. Then the relaxation times of pure gases and gas mixtures can be obtained from the pressure dependence of their phase shifts; decreasing the pressure increases the relaxation time and hence the phase lag. This pressure dependence experiment was attempted by Jacox and Bauer (38). However, at a modulation frequency of 2.550 kc/s their results deviated markedly from the theoretical lines. It is possible that at the high frequency used their microphone would be near resonance, hence introducing pressure dependent phase changes which would destroy any relation between the measured phase shift and the desired relaxation time.

Delany (24) studied the relaxation times of CO and CO_2 using both Slobodskaya's method and the pressure dependence technique. He used a reciprocity technique to calibrate the microphone phase shift before each experiment and appears to have eliminated spurious phase changes. However, his gas purity was not high enough and he obtained rather short relaxation times - 2.3 μ s. for CO_2 and 13 μ s. for CO.

Cottrell's suggestion that apparatus phase shifts could be eliminated by using a double cell spectrophone was investigated by Read (39). The optic acoustic signals of equal amplitude in two volumes of gas separated by a microphone diaphragm will be in phase with one another when the diaphragm remains stationary and no signal can be detected. Hence phase shifts due to

diaphragm and electronic properties are eliminated. If gas properties are matched - and phase shifts due to gas thus eliminated - the phase lag which has to be introduced into the beam illuminating the fast relaxing gas is a direct measure of the relaxation lag characteristic of the gas being studied. Unfortunately, the system proved impracticable. Whilst the diaphragm had to be stiff to separate the two gases, the detection of small signals required it to be flexible. However, some of the advantages of the double cell spectrophone were retained in Read's two cell experiment (39). Here the reference signal for phase comparison came, not from a photocell, but from a second spectrophone filled with a fast relaxing gas. It was hoped that by matching gas properties and cell sensitivities most of the apparatus phase shift would be eliminated. CO_2, N_2O and CH_4 were studied at a modulation frequency of 189 c/s.

The two cell approach seemed promising; it was therefore further investigated by Macfarlane (40). However, he showed that phase lags were present which had no connection with relaxation processes. In fact the metal coated Melinex diaphragm used by Read was resonating in the region of 100 - 200 c/s. Also matching of either gas properties or cell sensitivities was found to be impossible. The two cell approach was therefore abandoned and Macfarlane proceeded to design a single cell experiment using Bruel and Kjaer Type 4132 condenser microphone. These highly developed microphones have a flat audio-frequency response and low inherent noise, permitting sensitive and faithful detection of optic-acoustic signals over a wide pressure range.

Phase measurements in methane, after correction for thermal diffusivity, gave a relaxation time of 1.6 μsecs., in excellent agreement with the ultrasonic value of 1.5 $\pm$ 0.2 μsecs. The apparatus was then used to measure the relaxation times of a variety of gases and gas mixtures (41, 42).

Macfarlane's value of $\tau = 7.0 \pm 0.5\,\mu$secs. for the ν_3 band of CO_2 differs from that obtained by Lavercombe (43, 44) who also used a phase difference technique. However there appear to be errors in Lavercombe's plots of phase difference against pressure, and some of the phase differences measured were greater than 90°, which is not possible if a purely relaxation process was being studied (see Fig. 4). Also he used ethane to calibrate his apparatus and may thus have introduced a constant error because of neglect of the difference in the velocity of sound between ethane and carbon dioxide.

Since this chapter was written Slobodskaya has published results of relaxation measurements in undiluted CO_2 (67). The apparatus, with some modifications, was the same as that used in reference (37). Here, apparatus phase shifts were eliminated by studying the relaxation of two bands in the same gas - the 4.3 and 14.8μ bands of CO_2. The total phase shift for the first band, relaxation time τ_1, is $\psi_1 + \phi_o$ and the total phase shift for the second band, relaxation time τ_2, is $\psi_2 + \phi_o$, where ϕ_o is the apparatus phase shift. The difference between the phase shifts is then

$$\Delta\psi = \psi_2 - \psi_1 = \arctan\omega\tau_2 - \arctan\omega\tau_1$$

(see equation (1) of chapter four). She obtained the relaxation times by two methods:

(1) From the dependence of phase shift on chopping frequency

and (2) From the dependence of phase shift on pressure.

Her results are: by method (1) $\tau_{4.3} = 4.4 \pm 0.7\,\mu$ secs.

$\tau_{14.8} = 0.5\,\mu$ secs.

by method (2) $\tau_{4.3} = 4.1 \pm 0.9\,\mu$ secs.

$\tau_{2.7} = 0.6 \times \tau_{4.3}$

Macfarlane's value for the 2349 cm^{-1} (4.3μ) band is $\tau = 7.0 \pm 0.5\,\mu$ secs., longer than those of Slobodskaya. Assuming that both experimental techniques are adequate, the discrepancy may be caused by differences in gas purity. No details of gas purification are given in Slobodskaya's paper and water is known to be extremely efficient at deactivating CO_2.

The alternative approach adopted by Decius is to study the variation of signal amplitude with frequency. Woodmansee and Decius (23) reported the use of this method to measure the relaxation time of carbon monoxide. But their measurements were also complicated by the presence of a resonance in the cell. Redesign of the cell removed the resonance and relaxation in the CH_4, CH_3D, CH_2D_2 and CHD_3 series has been studied(45).

All spectrophone techniques have given collisional relaxation times for CO which are much too short. Theoretical calculations, high temperature measurements, and Millikan's low temperature work all indicate that at room temperature the collisional relaxation time is so long that CO should fluoresce and one would therefore expect little or no spectrophone signal. The very fact that previous workers were able to measure the collisional relaxation time in a spectrophone probably means that their CO contained impurities which greatly shortened the relaxation time. A simple spectrophone was therefore designed to show that, if very pure, CO did give no optic acoustic signal.

Chapter Three

THE VIBRATIONAL RELAXATION OF CARBON MONOXIDE

3.1 Introduction:

Early measurements of the vibrational relaxation time of carbon monoxide are inaccurate because the investigators did not realise the extreme importance of impurity effects in this gas. This applies particularly to the early low temperature work of van Itterbeck and Marieus (46) and Bender (47). Sherrat and Griffiths (48), using an ultrasonic interferometer under conditions far from ideal for this technique, obtained $\tau = 10\mu s$ independent of temperature between 1073 and 1273°K. In the light of later work this must be wrong.

More recently, the relaxation time of carbon monoxide has been studied by Windsor, Davidson and Taylor (49) who observed the rate of increase of infra-red emission behind reflected shock waves. At high temperatures, where the collisional relaxation time is short, the effect of impurities is not nearly so great as at room temperature. Hence the results of shock tube work are quite reliable if the technique used is adequate. The discrepancy between the results of Windsor, Davidson and Taylor and those of later workers probably arises from their use of reflected shocks. This makes the calculation of shocked gas conditions difficult and the method they adopt - based on an incident, unrelaxed reflected shock - gives an upper limit to the attainable shocked gas temperature. Matthews (50) has determined the relaxation time by following density changes behind incident shock waves, and Gaydon and Hurle (15) used a sodium line reversal technique. The latest high temperature results of Hooker and Millikan (17) agree well with those of Matthews and Gaydon and Hurle (see Fig. 5). A plot of the logarithm of the relaxation time against $T^{-1/3}$ is a straight line as predicted by the basic Landau-Teller theory.

FIG. 5 VIBRATIONAL RELAXATION TIME FOR PURE CARBON MONOXIDE AT ONE ATMOSPHERE PRESSURE AND HIGH TEMPERATURE

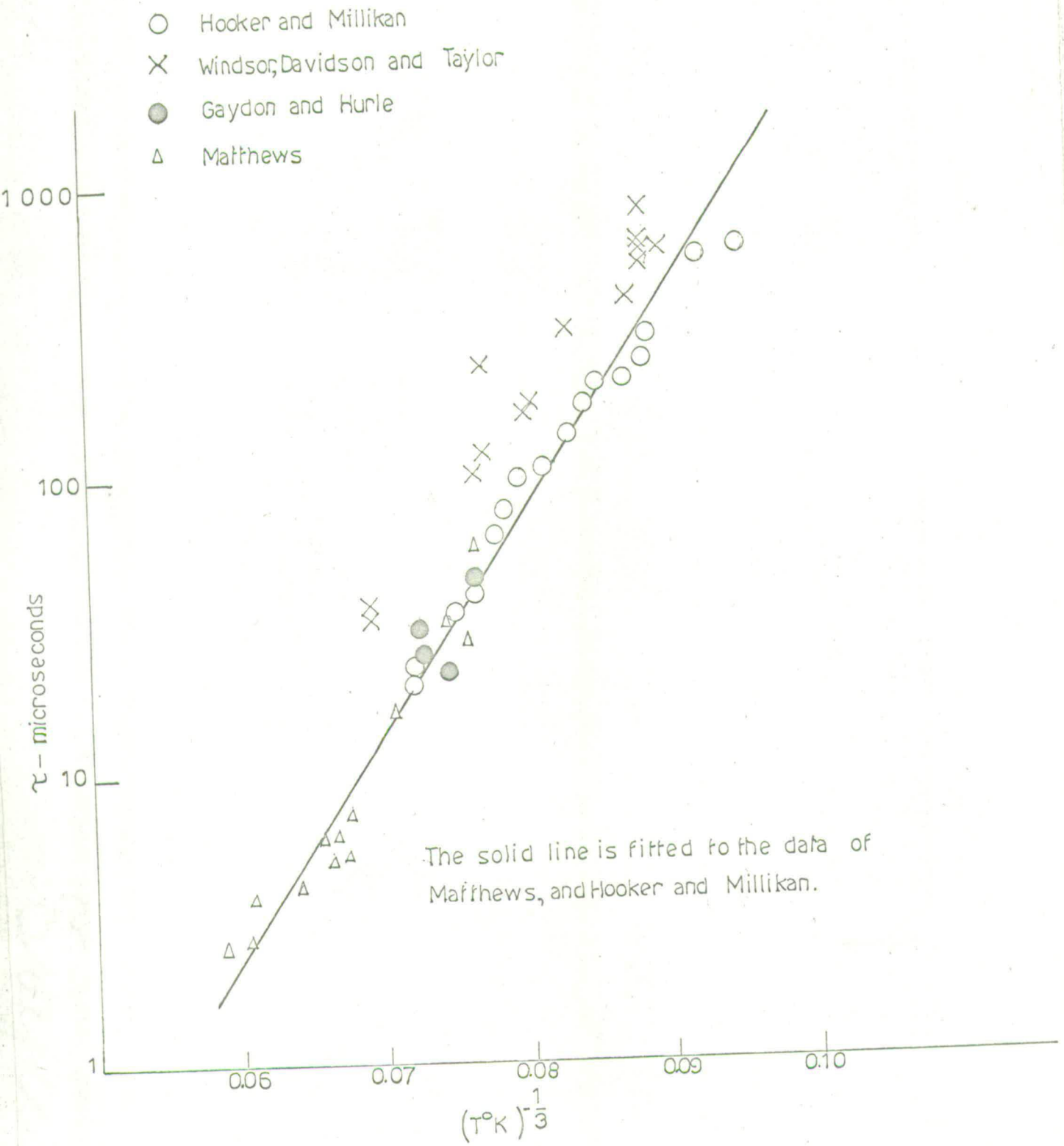

FIG 6 THEORETICAL RELAXATION TIME FOR CARBON MONOXIDE

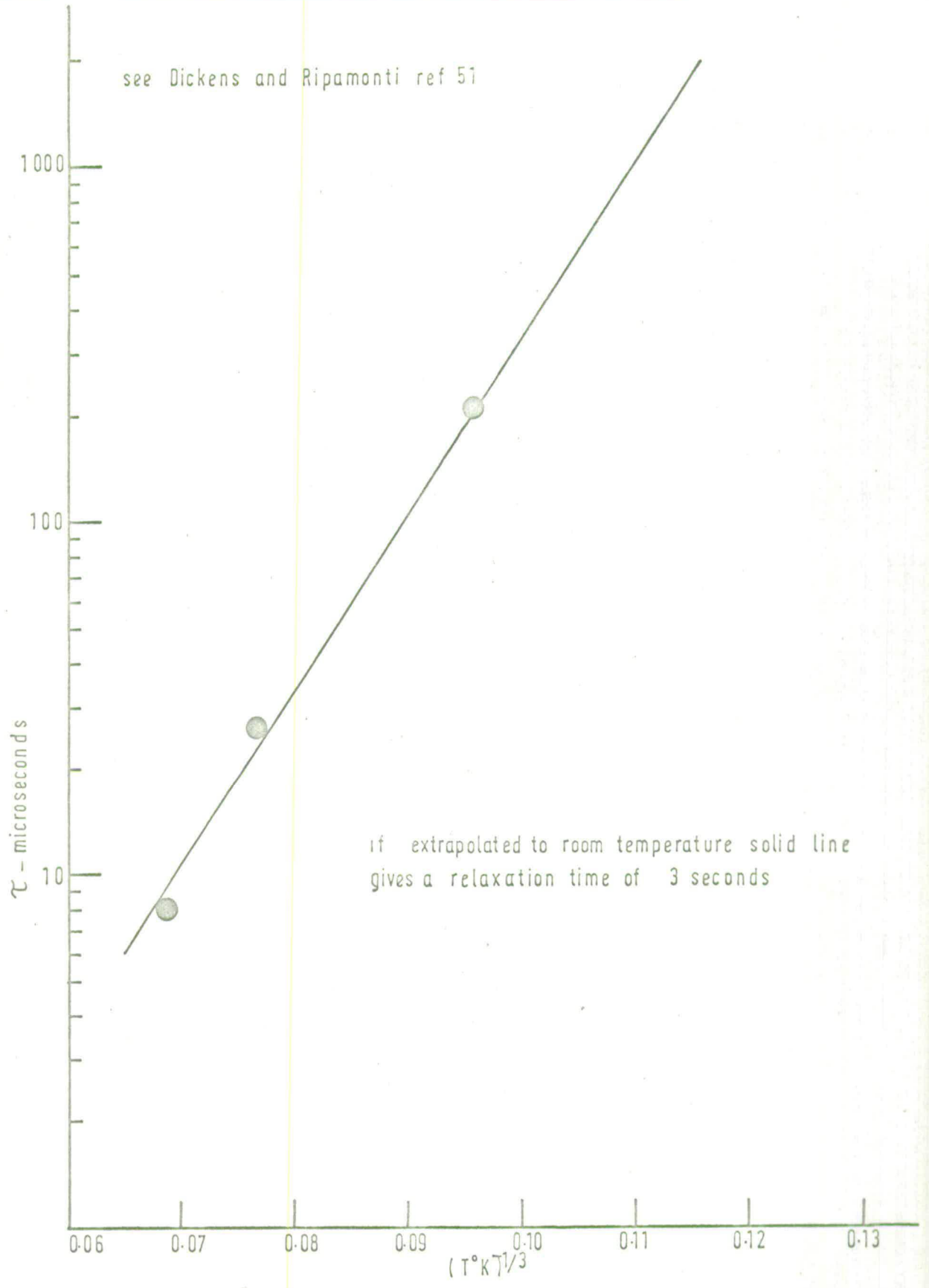

The solid line in Fig. 5 is fitted to the data of Matthews, and Hooker and Millikan and if extrapolated to room temperature indicates a relaxation time of 5 secs.

The relaxation time of carbon monoxide has been calculated by Dickens and Ripamonti between 1400 and 3000°K and is in excellent agreement with experimental results (51). The calculated results are plotted in Fig.6 and also indicate a relaxation time of the order of seconds at room temperature.

These predictions are confirmed by Millikan's fluorescence work which was discussed in Chapter two. McCaa and Williams have also studied the vibrational fluorescence of carbon monoxide using a radiation chopping technique (52). They found results in agreement with Millikan and evidence supporting a stepwise degradation of the $v = 2$ level. However, their carbon monoxide was not pure enough to allow them to determine the relaxation time accurately.

3.2 Experimental:

The Spectrophone: The spectrophone (Fig.7) is made of brass in two parts vacuum sealed by means of a Viton 'O' ring. A 'Melinex' diaphragm (30 gauge) metallised on one side is clamped between two brass rings screwed to the cell over an adjustable tensioning ring. The position of the backplate is also adjustable for maximum sensitivity. The pressure in the cell equilibrates through leaks of a long time constant across the diaphragm, tensioning ring, and backplate. The absorption cell is a cylinder 2.5 cm. in diameter and 2 cm. long with calcium aluminate glass windows. (Barr and Stroud Type BS39) sealed to both ends with Viton 'O' rings. A metal needle valve connects the cell to a conventional high vacuum system (Fig. 8) and is closed during runs to give acoustic isolation of the cell. In order to reduce degassing from the cell walls the spectrophone can be baked to 120°C.

FIG 7 SPECTROPHONE CELL

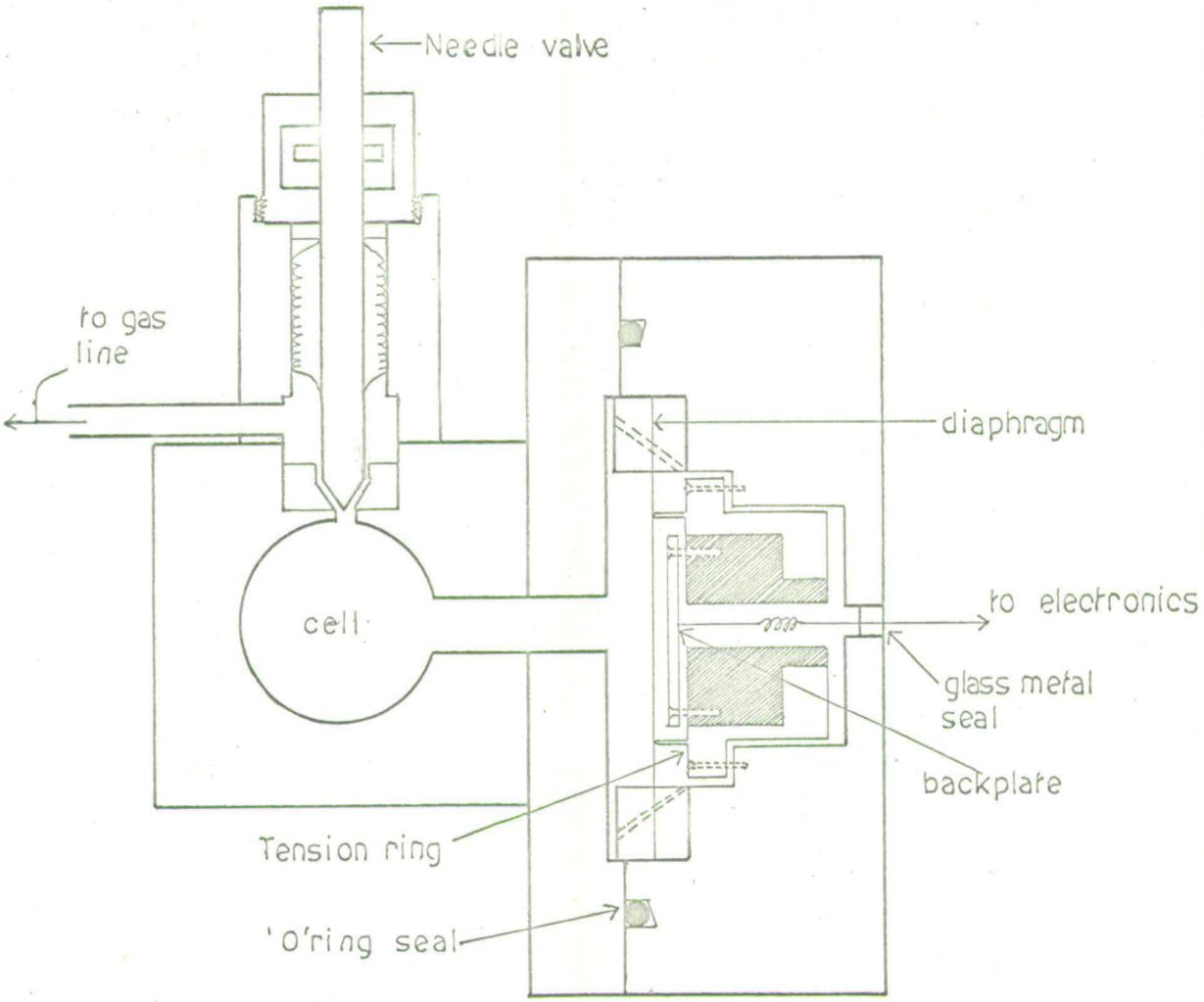

FULL SCALE

FIG. 8 GAS HANDLING SYSTEM

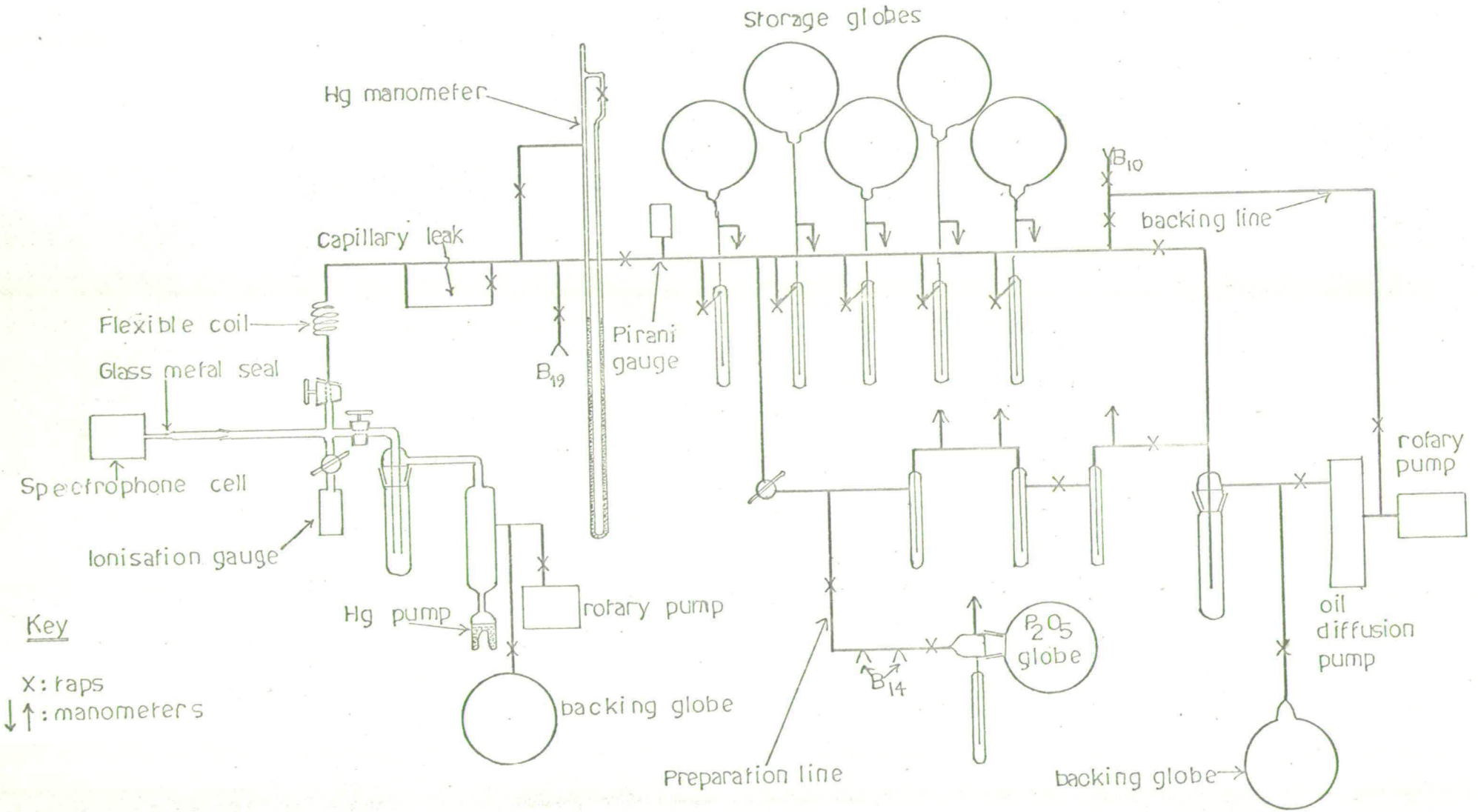

Optical System and Electronics: Fig. 9. Infra-red radiation from a Nernst filament is focussed by a front silvered mirror, through a modulating disc into the cell.

Variations in capacity of the microphone caused by the acoustic pressure frequency modulate a 10.7 Mc/s oscillator at the chopping frequency. The output, monitored by a conventional frequency-modulated ratio detector, is preamplified and fed to a selective amplifier of 2.5 mv. full scale sensitivity. In later runs this was increased by 50 μv. full scale sensitivity. The d.c. output from the detector is used to give an indication of diaphragm position while filling and emptying the cell.

The sensitivity of the entire system could be checked at any time by noting the signal from a standard pressure of N_2O.

Materials: Carbon monoxide was obtained from a cylinder (I.C.I. Limited). Mass spectrometer analysis indicated small amounts of CO_2 and H_2O. The gas was further purified by passage through several cold traps at -196°C., one containing pellets of alumina (20), and dried over P_2O_5.

3.3 Results:

The first object was to show that pure CO gave little or no optic acoustic signal. The cell was filled with CO to a pressure of 40 cms Hg and at a chopping frequency of 140 c/s with the selective amplified at 2.5 mV. sensitivity no signal could be observed for 5 hours after filling the cell. The signal then rose to a steady value over a period of 40 hours. It seemed probable that this rise was caused by impurity molecules desorbing from the cell walls, and shortening the collisional relaxation time. To test this the cell was baked at 120°C. for 40 hours. The pressure fell from 3×10^{-5} to 3×10^{-6} torr, and the pressure rise from 2×10^{-3} torr per hour to 4×10^{-4} per hour. When the cell was filled with CO as before the signal had not reached a steady value after 140 hours, confirming the above hypothesis. Hereafter the cell was baked before each experiment.

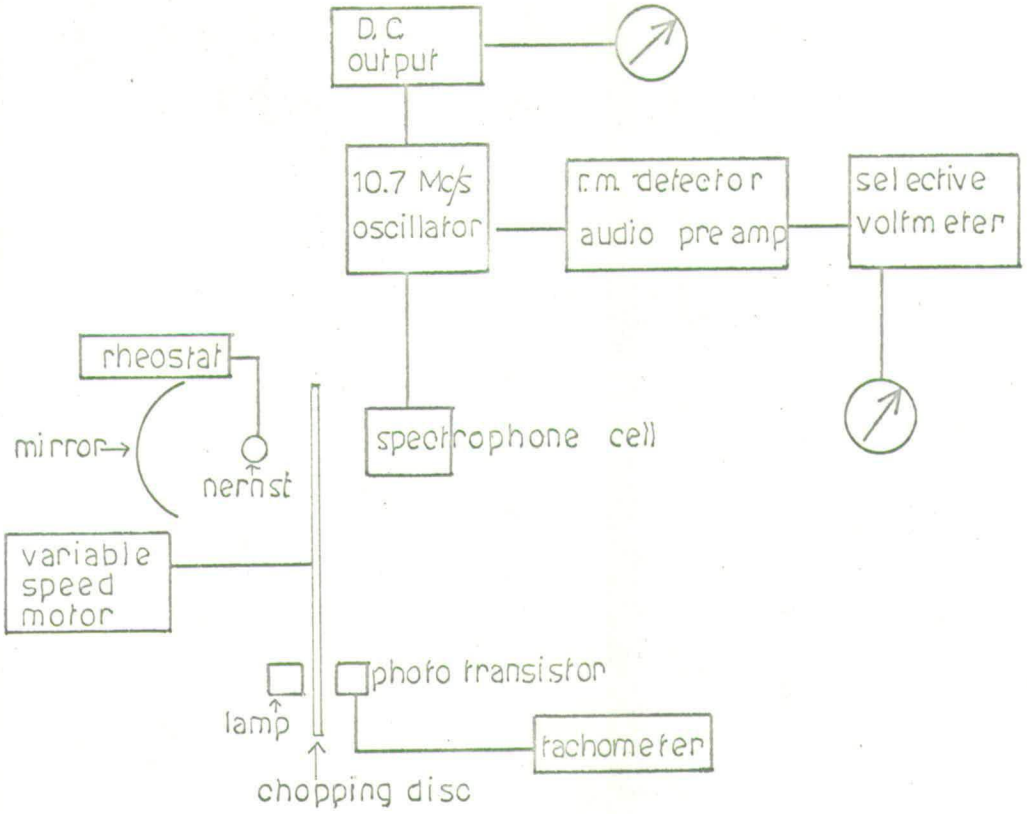

FIG. 9 EXPERIMENTAL ARRANGEMENT

Now, even in pure CO a little vibrational energy will still be lost by collision, the exact amount depending on the relative rates of the collisional and radiative processes. Increasing the sensitivity of the system enabled the small signal corresponding to this energy loss to be detected. Hydrogen, which is known to be efficient at de-exciting CO was allowed to diffuse into the cell. ($\tau_{CO.H} = 10^{-4}$ secs. at room temp. - see ref. 20). The rate of the collision process increased until all the absorbed energy was transferred by collision, and the spectrophone signal rose to a steady maximum.

The initial signal is proportional to the energy lost by collision in pure CO: i.e. it is proportional to $f_{10} n_1 \; h\nu \; \text{sec}^{-1} \; \text{cm}^{-3}$, where f_{10} is the transition probability per molecule per second for the 1-0 process, n_1 is the number of vibrationally excited molecules per unit volume, ν is the vibration frequency, and h is Planck's constant (36). Assuming that the radiation density remains constant and that the added H_2 ($\sim$ 10%) does not affect the absorption process, i.e. that n_1 remains unchanged, then the final signal is proportional to the total energy loss in pure CO by collision and radiation. This is given by $(f_{10} + A_{10}) n_1 h\nu$, where $A_{10} = 1/\tau_{rad}$ is the Einstein coefficient for spontaneous emission and τ_{rad} is the radiative lifetime. Since $f_{10} = 1/\tau_{CO.CO}$ (7), then

$$\frac{\text{initial signal}}{\text{final signal}} = \frac{1/\tau_{CO.CO}}{1/\tau_{CO.CO} + 1/\tau_{rad}} \qquad 3.1$$

$\tau_{CO.CO}$ being the collisional relaxation time in pure CO. The radiative lifetime can be calculated from available measurements of the total absorption intensity of the vibration rotation band, and hence $\tau_{CO.CO}$ can be obtained.

Calculations of Radiative Lifetimes from Absorption Intensities:

A convenient formula for the calculation of radiative lifetimes from absorption intensities is derived by Penner (53). He shows that the integrated absorption S_{lu} for the transition from a lower quantum state l to an upper state u is given by

$$S_{lu} = \frac{c}{8\pi\nu^2_{lu}} \frac{N_l}{p} A_{ul} \frac{g_u}{g_l} \left[1 - \exp\left(-\frac{h\nu}{kT}lu\right)\right] \qquad 3.2$$

c is the velocity of light, ν_{lu} the frequency for the transition, N_l the number of molecules in the lower quantum state, p the partial pressure of the absorber, A_{ul} the Einstein coefficient for spontaneous emission, g_u and g_l the degeneracies of the two states and k is the Boltzmann constant.

If $h\nu \gg kT$ then the contribution from the induced emission term can be neglected and 3.2 written

$$S_{lu} = \frac{c}{8\pi\nu^2_{lu}} \frac{N_l}{p} A_{ul} \frac{g_u}{g_l}$$

For an ideal gas at S.T.P. values of S_{lu} in cm^{-2} atm^{-1} may be converted to A_{ul} in the case where nearly all the molecules are in the ground state, and $g_u = g_l$, by noting that

$$\frac{N_l}{p} = \frac{6.0247 \times 10^{23}}{82.056 \times 273.16}$$

giving $$S_{lu} = 3.210 \times 10^{28} A_{ul}/\nu^2_{lu} \qquad 3.3$$

S_{10} for carbon monoxide has been found by Benedict, Herman, Moore and Silverman (54) to be 235.6 cm^{-2} atm^{-1}, agreeing well with the results of earlier workers. Using equation 3.3 $\tau_{rad} = 1/A_{10}$ is found to be 0.033 secs. (since $h\nu/kT \gg 1$ contributions to τ_{rad} from the radiation field can be ignored).

At a pressure of 39 cm Hg the initial signal from pure CO was 15 μv rising to a final signal of 780 μv. This gives a relaxation time for pure CO at room temperature and one atmosphere pressure of 0.8 secs.

FIG 10 CARBON MONOXIDE — SIGNAL AMPLITUDE AGAINST TIME

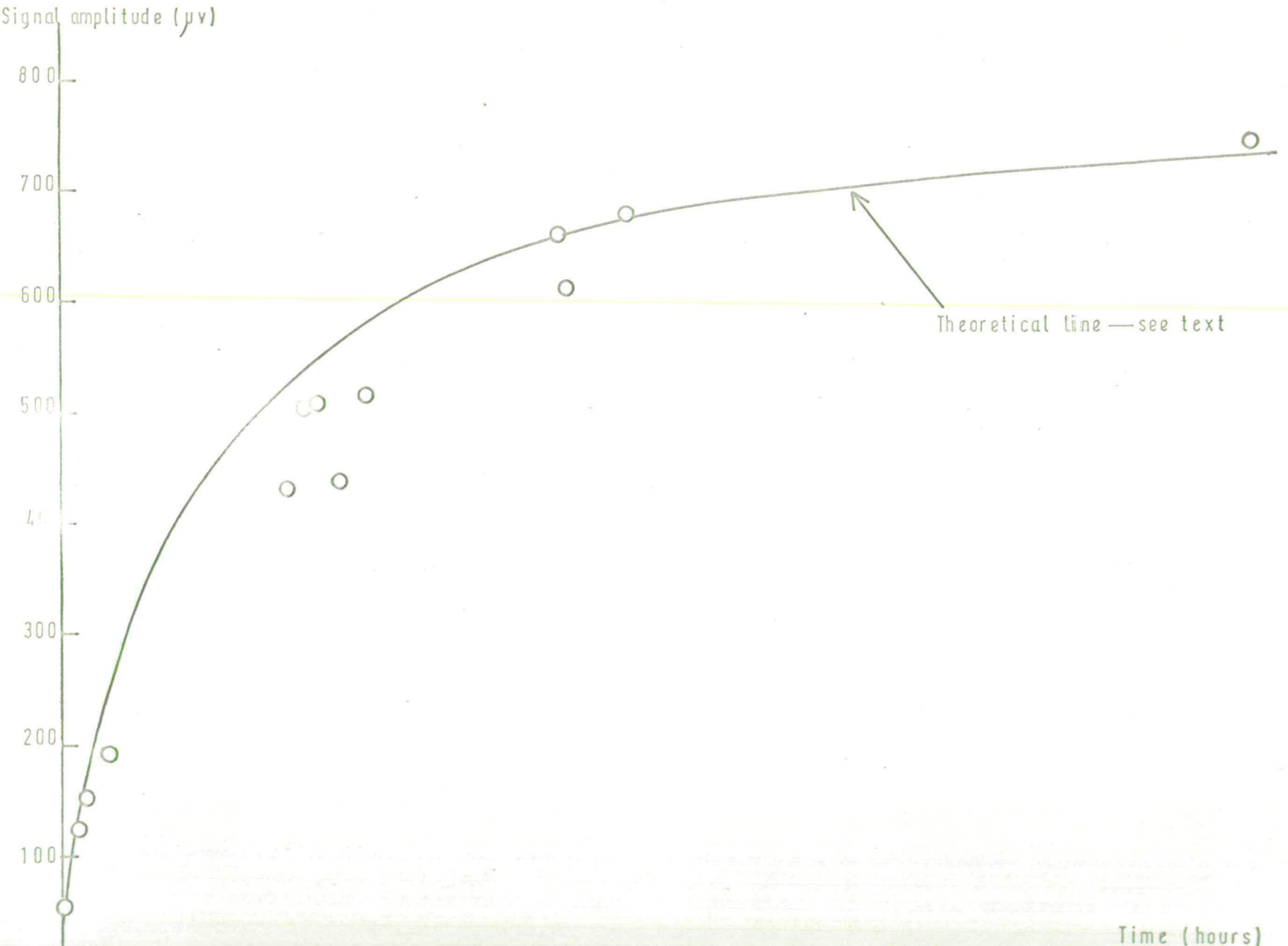

Collisional relaxation times are inversely proportional to pressure. To test the experimental method the measurement was repeated at two pressures, the same gas sample being used for each measurement in order to minimise slight differences in purity. The initial signal at 40 cms was found and the pressure reduced as rapidly as possible to find the initial signal at 20 cms. The final signals at both pressures were then measured. The results are shown in Table I.

From the figures at 40 cms and the final signal at 20 cms, the initial signal expected at 20 cms is 10 μv , instead of the experimental value of 20 μv . However, this discrepancy is easily accounted for by impurity desorbing from the cell walls during the time taken to lower the pressure from 40 cms. to 20 cms.

Table I.

Spectrophone signals from Carbon Monoxide

Chopping frequency 140 c/sec.

P cm Hg	Initial signal μv .	Final signal μv .
20	20	460
40	30	760

To investigate the effects of impurity in more detail measurements were made on a sample of CO left in the cell for 90 hours. The results are shown in Fig. 10. The theoretical curve was calculated using the equation for the relaxation time of the mixture:

$$1/\tau_{mixture} = 1 - X_B/\tau_{CO.CO} + X_B/\tau_{CO.B}$$

B is the impurity molecule, probably water, and X_B its molefraction. It was assumed that B was desorbing from the walls at a steady rate - taken as the degassing rate in the empty cell - and a relaxation time of $\tau_{CO.B} = 1 \times 10^{-6}$ secs. gave the best fit of the calculated line to experimental points.

This compares well with Millikan's finding that a few p.p.m. of water quenched the fluorescence of CO.(20).

3.4 Discussion:

The value obtained here is a lower limit to the true relaxation time in pure CO; difficulties with gas purity in a static system mean that the initial signal represents an upper limit to the signal due to CO.CO collisions since impurity reduces the relaxation time and more energy is therefore lost by collision than in pure CO. All measurements were carried out at chopping frequencies greater than 70 c/sec. so that it is unlikely that energy loss to the walls will be significant (7). This is confirmed by McCaa and Williams (52) who observed fluorescence from CO at approximately the same pressure, using a modulation frequency of only 13 c/sec.

The main source of error in this experiment, apart from impurity, is reabsorption of the resonance fluorescence. This has been studied in some detail for CO by Henry and Doyenette (55, 56). They investigated the variation of the radiative relaxation time, τ rad, with gas pressure and cell diameter and their results are shown in Figs. 11 and 12. Above 300 torr they found that τ rad became independent of pressure and varied with the square root of the cell dimensions. Using the dimensions of the present cell a τ rad = 0.15 secs. is deduced instead of the calculated τ rad = 0.033 secs., giving $\tau_{CO.CO}$ = 4 secs. This is in good agreement with the extrapolation of high temperature shock tube data (Fig. 5) and theoretical prediction Fig. 6. The agreement between experimental and theoretical curves in Fig. 10 is reasonable considering the assumptions involved and it emphasises the extreme efficiency of polyatomic molecules as collision partners for CO.

This apparatus can be used to study the relaxation of other molecules with relaxation time so long that they cannot be measured ultrasonically, or with the phase difference spectrophone. The hydrogen halides are just such molecules.

FIG 11 VARIATION OF THE RADIATIVE RELAXATION TIME WITH PRESSURE IN CELLS OF DIFFERENT DIAMETER

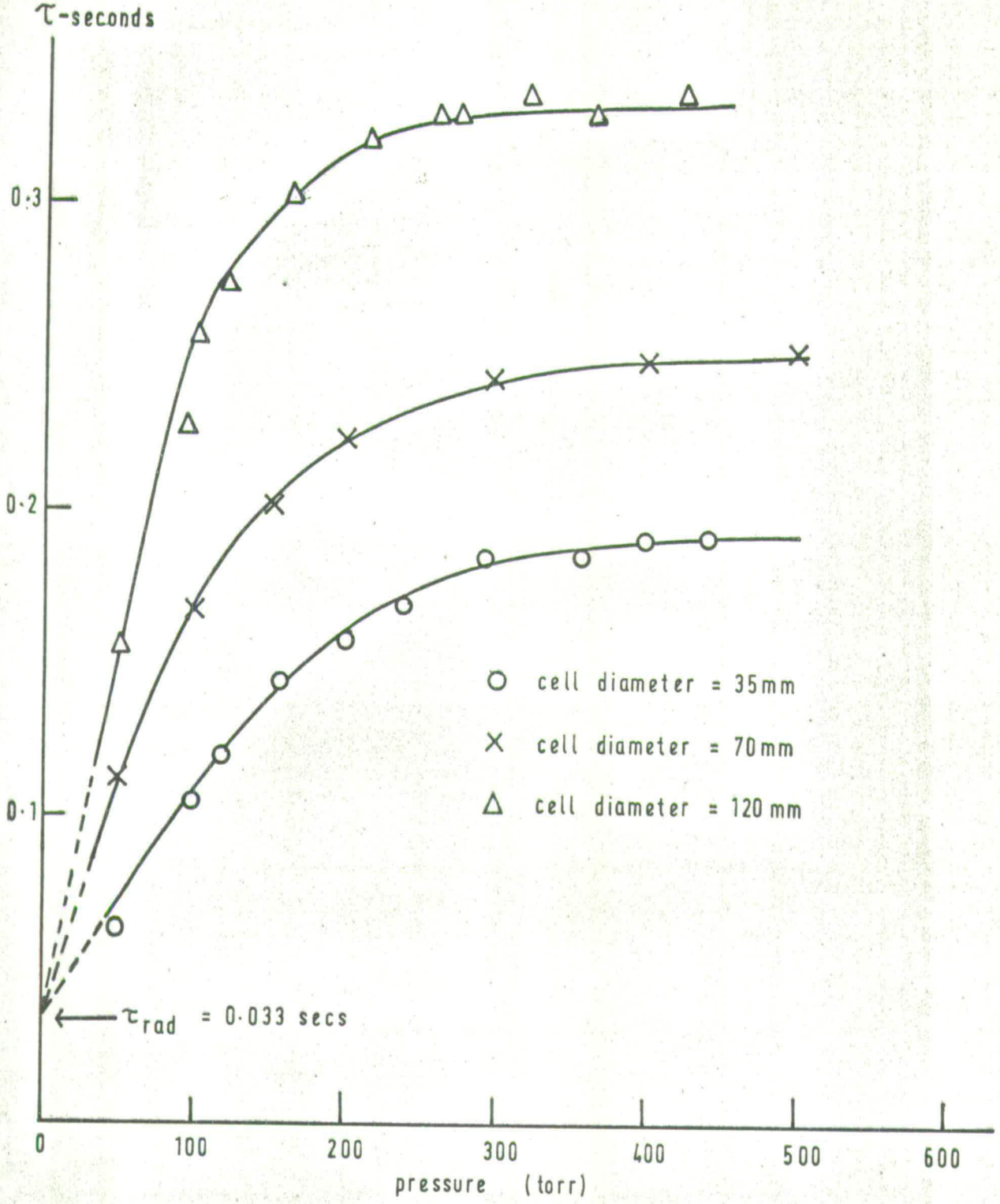

FIG 12 VARIATION OF THE RADIATIVE RELAXATION TIME AS A FUNCTION OF THE SQUARE ROOT OF THE CELL DIAMETER FOR PRESSURES GREATER THAN 300 TORR

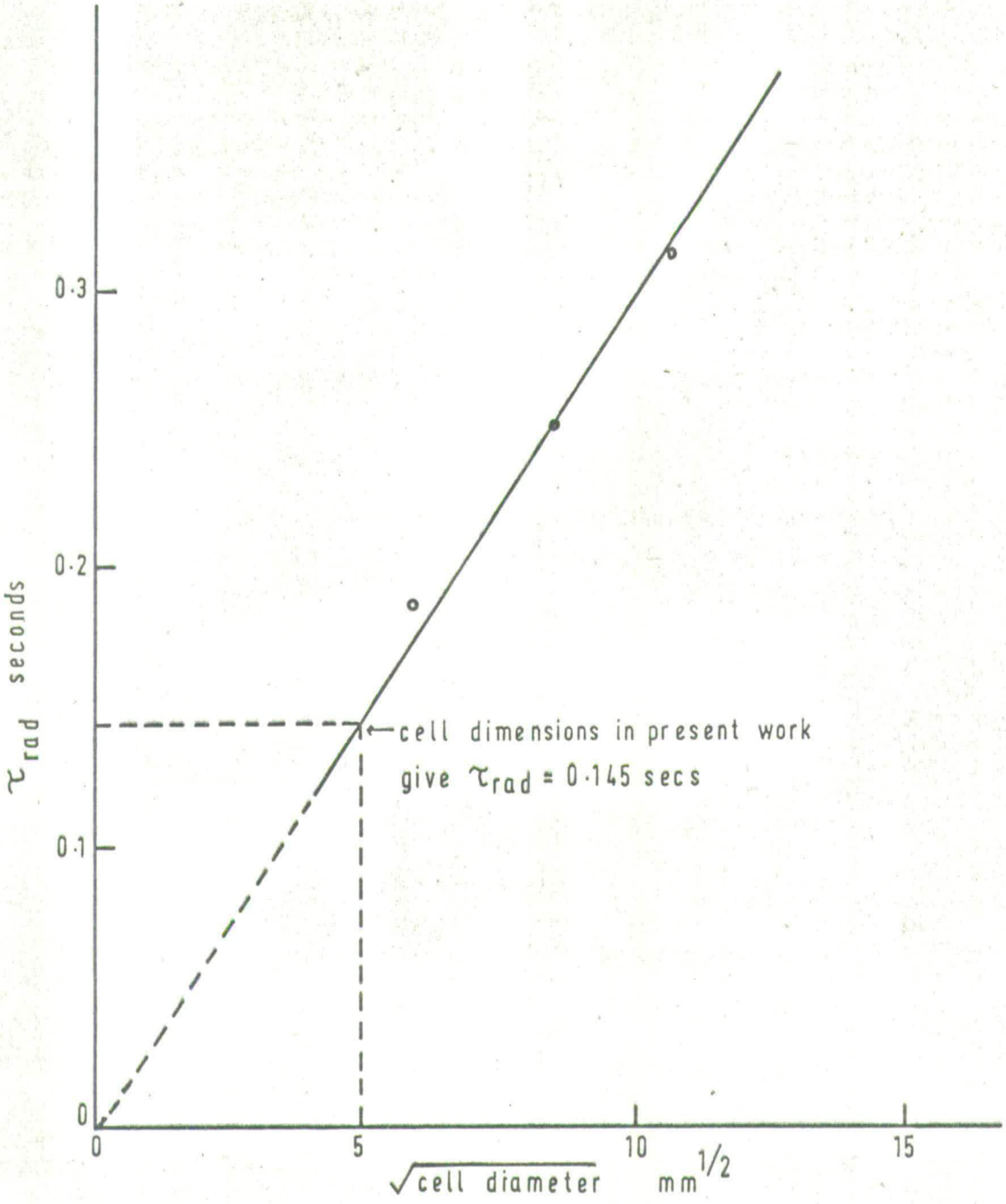

Chapter Four

VIBRATIONAL RELAXATION OF THE HYDROGEN AND DEUTERIUM HALIDES

4.1 Introduction:

Very little is known about the vibrational relaxation of the hydrogen and deuterium halides. Borrell (57) has studied infra-red emission from shock-heated HCl and HBr and found that their relaxation times are several orders of magnitude shorter than theory predicts. Chow and Greene (58) obtained similar results for HI. This large discrepancy between theory and experiment is greater than any previously found for diatomic molecules. It is therefore important to know the relaxation times of these molecules and their deuterides at lower temperatures. But their vibration frequencies are high ($> 2000\ cm^{-1}$) and prevent the use of the ultrasonic interferometer; nor can the phase difference spectrophone be used. The simple theory for the phase difference spectrophone predicts the relation

$$\tan \phi = \omega\tau/p \qquad 4.1$$

between the phase lag ϕ, and the relaxation time τ . p is the pressure in atmospheres and ω the modulation frequency in radians per second. In a study of CO_2-N_2 mixtures Macfarlane found that at high N_2 concentrations the simple tangential relationship no longer held (40, 42). The theory involves the assumption that the rate of energy transfer from vibration to translation (α) is much faster than the rate of energy loss to the cell walls (β). In CO_2-N_2 mixtures at high N_2 concentration α becomes very small and the theoretical relationship breaks down. This is illustrated in Fig.13, where we can see that at low pressures (α becoming very small) the experimental points deviate markedly from the theoretical lines. Thus this spectrophone could not be used to measure relaxation times greater than 100 μs at atmospheric pressure. The range could possibly be extended by increasing the modulation

FIG 13 BREAKDOWN OF SIMPLE SPECTROPHONE THEORY

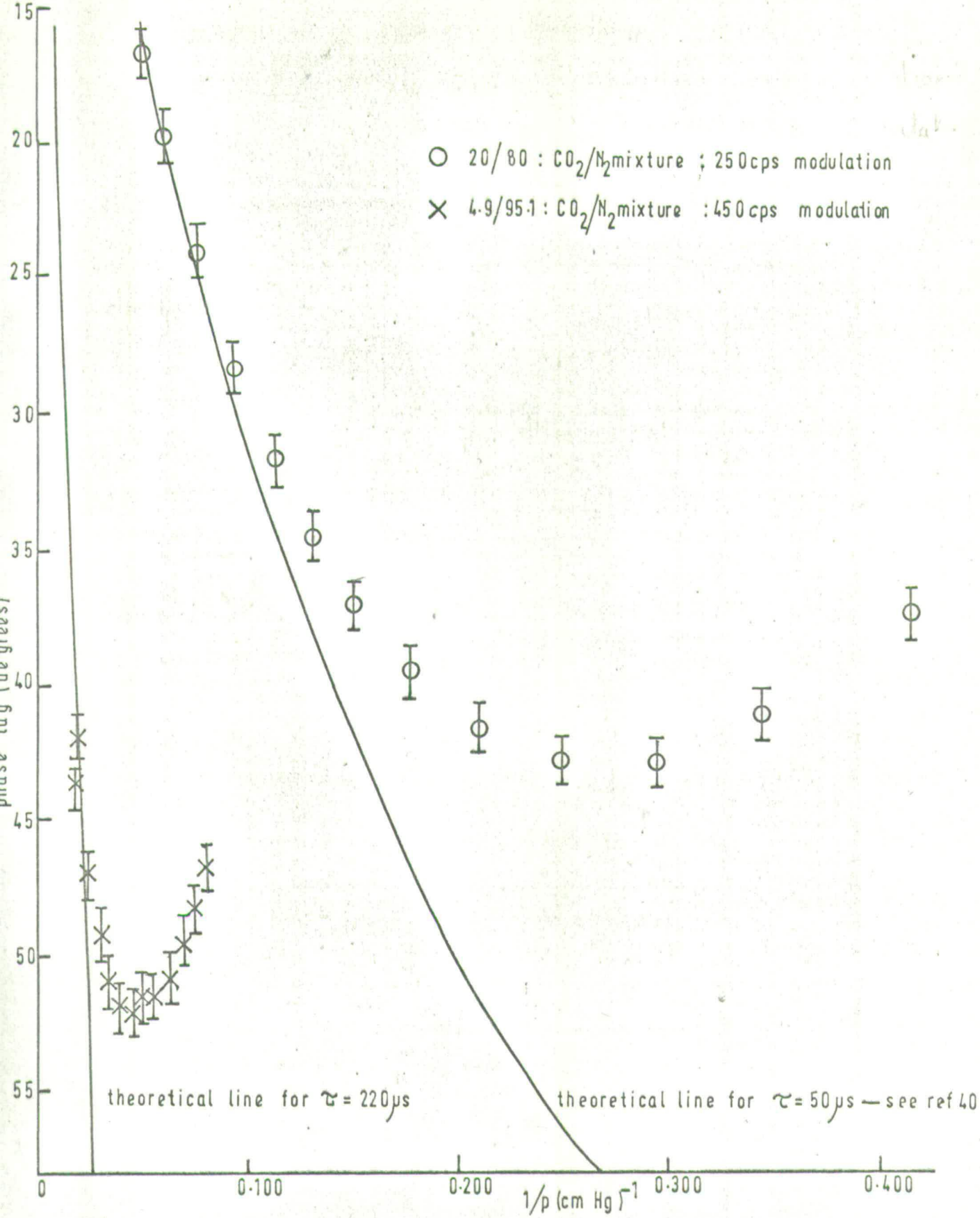

frequency (decreasing β) but only at the expense of microphone sensitivity. Since the relaxation times of the halides are expected to be very much greater than 100 μs measurements were attempted using the amplitude spectrophone.

4.2 Theoretical Vibration-Translation relaxation times for HCl, HBr, DCl and DBr at 290°K.

Collisional relaxation times were calculated using the semiclassical treatment of Cottrell and McCoubrey (7). The expected number of transitions f per molecule per unit time is given by

$$f = \frac{4\pi}{\sqrt{3}} N Br_o^2 v^* \exp\left(- 3y^* + \frac{h\nu}{2kT} + \frac{\phi_o}{kT} \right) \qquad 4.2$$

where $B = 32\pi^4 m^2 \nu / h \alpha^2 M$,

$v^* = (4\pi^2 kT\nu / \alpha m)^{\frac{1}{3}}$

and $y^* = (2\pi^4 m \nu^2 / \alpha^2 kT)^{\frac{1}{3}}$

N is the molecule density, r_o the classical distance of closest approach, ν the vibration frequency; m the reduced mass for the encounter, M the reduced mass of the oscillator, and v^* that velocity of approach for which energy transfer is most probable. α - a reciprocal length - is a measure of the steepness of the intermolecular potential. The second and third terms in the exponent take account of the symmetrisation of approach and recession velocities, and the part played by the attractive part of the potential respectively. ϕ_o is the minimum value of the intermolecular potential.

Values of α were obtained by fitting a Morse potential

$$V = V_o \exp(-\alpha r) - \phi_o \qquad 4.3$$

to the Krieger potential

$$V = 4\epsilon \left[\left(\frac{\sigma}{r}\right)^{12} - \left(\frac{\sigma}{r}\right)^{6} - \delta^* \left(\frac{\sigma}{r}\right)^{2} \right] \qquad 4.4$$

$$\delta^* = \tfrac{1}{2} u/\epsilon\sigma^3$$

at the points $r = r_A$, $r = r_o$. r_A is the value of r, the intermolecular

distance, for which the Krieger potential is zero, and μ is the dipole moment of the molecule. We then have (51)

$$v^* = (4\pi^2 kT\nu/\alpha m)^{1/3} \qquad 4.5$$

and

$$\alpha = (\ln F)/r_A - r_o \qquad 4.6$$

where

$$F = (\tfrac{1}{2}mv^{*2} - \phi_o)/ - \phi_o$$

α is obtained by iterative solution of 4.4 and 4.5.

Potential constants of the Krieger potential for HCl and HBr are given by Monchick and Mason (59). The calculated α values are shown in Table 2.

Table 2.

Potential Constants and derived values for HCl and HBr.

Molecule	μ(debye)	δ^*	σ(Å)	ϵ/k (°K)	α(Å)$^{-1}$
HCl	1.08	0.34	0.36	328	5.84
HBr	0.80	0.14	3.41	471	5.90

It was assumed that α for the deuterides was the same as for the hydrides - i.e. that substituting a deuterium atom did not significantly change the shape of the intermolecular potential. This has recently received experimental confirmation from a molecular beam experiment in which the scattering of HBr and DBr by potassium was studied (66). When the above α values were substituted in equations 4.2 the following relaxation times were obtained.

Table 3

Collisional Relaxation Times of HCl, DCl, HBr and DBr at 290°K and atmospheric pressure

Molecule	$\nu(sec^{-1})$	m(g)	$\alpha(cm)^{-1}$	τ (secs)
HCl	8.651×10^{13}	$3,052 \times 10^{-23}$	5.84×10^{8}	6.5
DCl	6.271×10^{13}	3.136×10^{-23}	5.84×10^{8}	1.6×10^{-2}
HBr	7.672×10^{13}	6.755×10^{-23}	5.90×10^{8}	5×10^{4}
DBr	5.518×10^{13}	6.858×10^{-23}	5.90×10^{8}	1.4×10^{1}

The predicted relaxation times are very long due to the combination of large mass and high vibration frequency in these molecules. This is particularly noticeable in the case of HBr. A similar effect has been found in the calculation of the relaxation time of AsH_3 (11).

4.3 Radiative Lifetimes of HCl, HBr, DCl and DBr.

The absorption intensities of HCl and DCl were measured by Benedict, Herman, Moore and Silverman (60). That of HBr has been measured by Penner and Weber (61), and by Babrov (62). The more recent value of Babrov is used here. The absorption intensity of DBr has not been measured but is calculated roughly from the known intensities of the other gases. Radiative lifetimes were derived from absorption intensities as before. (Table 4).

Table 4.

Radiative Lifetimes of HCl, HBr and DCl.

Molecule	$\nu(cm)^{-1}$	$S_{01}(cm^{-2}atm^{-1}$ at 300°K)	τ_{rad} (sec)
HCl	2886	130	0.03
DCl	2091	66.6	0.12
HBr	2560	35.8	0.15

Radiative Lifetime of DBr:

Although the absorption intensity of DBr has not been measured, it is possible to obtain an approximate value if one assumes that the shape of the dipole moment function is the same as that of HBr. To check the accuracy of the calculation radiative lifetimes of HCl, DCl and HBr were calculated in the same way.

For a 1-0 transition a linear approximation to the dipole moment function is adequate (60) i.e.

$$M = M_o + M_1 (r - r_e) \qquad 4.7$$

Where M_o is the permanent dipole moment, and r_e the equilibrium internuclear distance. Using this approximation the matrix element for the transition is shown to be (53)

$$\left|R_{n+1,n}\right| = M_1^2(n+1)/2\alpha$$

$$= M_1^2(n+1)B_e r_e^2/\omega_e \qquad 4.8$$

with $2\alpha = \omega_e/B_e r_e^2$ 4.9

$$B_e = h/8\pi^2 c\, m_r\, r_e^2 \qquad 4.10$$

M_1 being the reduced mass and ω_e and B_e have their normal spectroscopic meaning.

Thus with $\theta = M_o/M_1 r_e$

$$\left|R_{10}\right|^2 = M_o^2\ B_e/\theta^2\omega_e \qquad 4.11$$

$\left|R_{10}\right|^2$ was calculated from this expression and compared with experimental results.

Table 5.

Comparison of Theoretical and Experimental Matrix Elements for the 1-0 transitions in HCl, DCl, HBr and DBr.

Molecule	M_o(debye)	B_e(cm^{-1})	(cm^{-1})	θ	$\lvert R_{10}\rvert^2$ calc.	$\lvert R_{10}\rvert^2$ expt.	$\lvert R_{10}\rvert^2$ expt. / $\lvert R_{10}\rvert^2$ calc.
HCl	1.050	10.59	2990	0.988	4.00×10^{-3}	449×10^{-3} (a)	1.12
DCl	1.085	5.445	2091	0.988	$3.15 \times$ "	3.17 " (a)	1.01
HBr	0.80	8.473	2650	0.120	1.42 "	1.3 " (b)	0.97
DBr	0.83	4.291	1885	0.120*	1.09	------	------

* assumed.

(a) ref. (60)

(b) ref. (62)

Now $$A_{10} = \frac{64\pi^4}{3\,h\,c^3}\,\nu^3\left|R_{10}\right|^2 = 1/\tau_{rad}$$

Substituting the above values for $\left|R_{10}\right|^2$ we obtain the following predictions for A_{10}.

Table 6.

Einstein Coefficients for spontaneous emission of HCl, DCl, HBr and DBr

Molecule	A_{10} (calc) sec^{-1}	A_{10} (expt) sec^{-1}	A_{10} (calc)/A_{10} (expt)
HCl	30.6	33.86	0.89
DCl	9.10	9.10	1.0
HBr	7.4	7.2	1.03
DBr	2.2	----	

The radiative lifetime of DBr is therefore approximately 0.5 secs. The determination of collisional relaxation times by the present method depends on the completion between the two processes.

$$DBr^* \longrightarrow DBr + h\nu \qquad (1)$$

and $$DBr^* + DBr \longrightarrow DBr + DBr + \text{kinetic energy} \qquad (2)$$

The range which can be studied is determined by the absorption intensity of the gas and the relative rates of (1) and (2). If the rate of (1) is slow compared with (2) then most of the energy is transferred by collision anyway and no rise in signal can be detected in the spectrophone with the addition of a more efficient collision partner. By lowering the pressure the relative rates of the two processes can be altered. But the extent to which the pressure may be lowered is limited by the difficulty of detecting any signal at all at low pressures.

Since DBr has a long radiative lifetime compared with the collisional lifetime, its collisional relaxation cannot be studied by this method.

4.4 Experimental:

The spectrophone and experimental arrangement were the same as those for CO except that a General Radio Company Tuned Amplifier and Null Detector Type 1232A was used for final amplification of the signal. Frequent replacement of the Melinex diaphragm was necessary in these experiments because the halides slowly attacked the aluminium coating.

Materials: Hydrogen chloride was prepared in two ways: from NH_4Cl and H_2SO_4, and by reaching conc. HCl with conc. H_2SO_4. In both cases the gas was dried with H_2SO_4 and P_2O_5, condensed at -196°C, degassed and distilled into the spectrophone. Hydrogen bromide was obtained from a cylinder (Matheson Co. Ltd., minimum purity 99.8%), dried over P_2O_5 and further purified as was HCl.

Some trouble was experienced in obtaining pure deuterium chloride. At first it was prepared by dropping D_2O on hot benzoyl chloride. The evolving gas was passed through a trap at 0°C, collected at -196°C, degassed and dried over P_2O_5. Infra-red analysis revealed that the resulting sample of DCl contained approximately 20% HCl. This was despite baking the gas line before reaction. A more satisfactory preparation appeared to be the

FIG 14 HCl —— SIGNAL AMPLITUDE AGAINST TIME

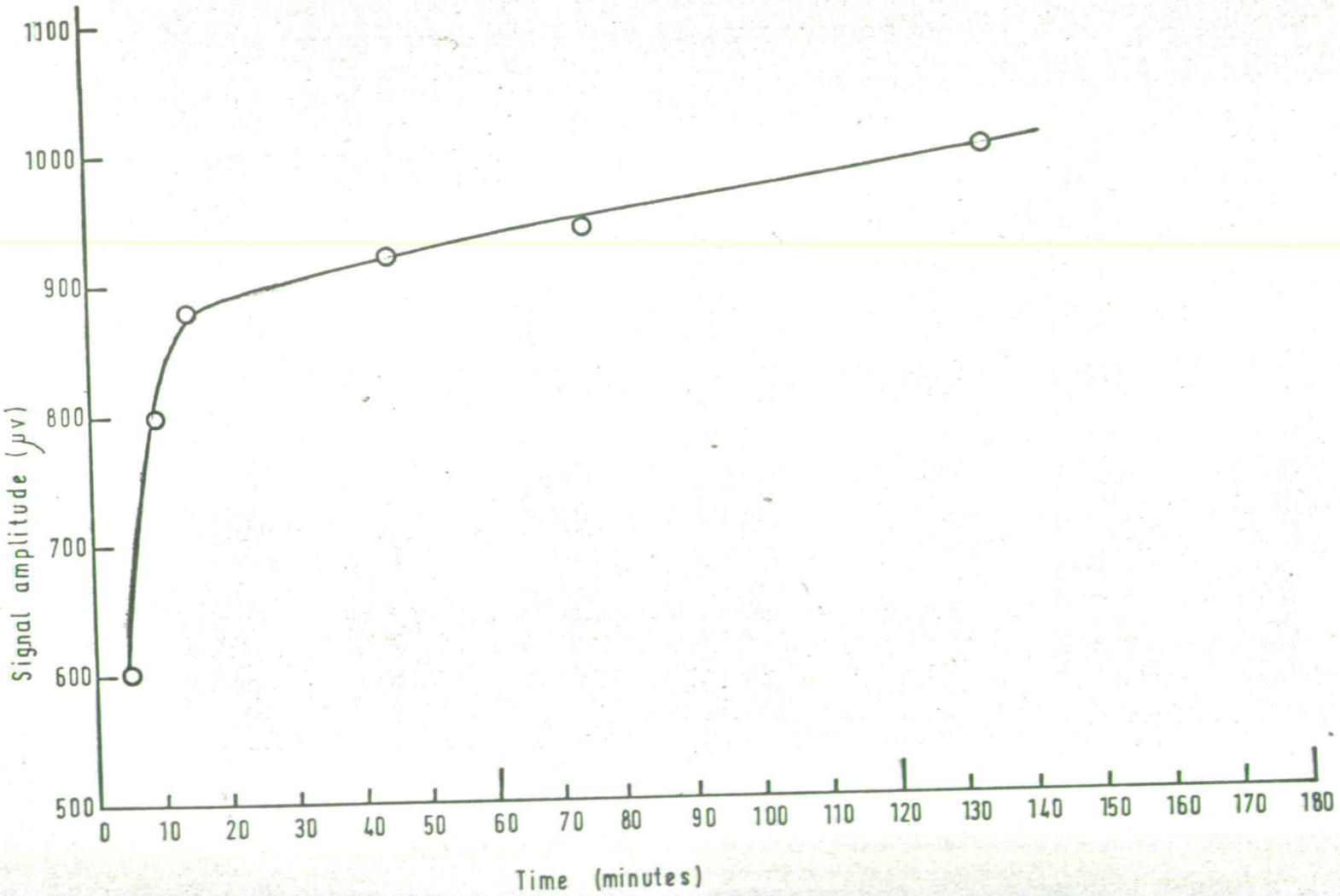

reaction of D_2O with $SiCl_4$ at -80°C. (63). The gas was collected at -196°C, degassed and distilled at -120°C. However, it again contained 10-20% HCl, which may have originated from an exchange mechanism with water absorbed on the walls of the generating system, despite the precautions taken to eliminate such contamination. This idea was confirmed when the percentage of HCl fell with continued preparation in the same vessel. Other workers have found similar effects (65). In later runs DCl was obtained from a cylinder (Merck, Sharpe and Dohme). Even then it was necessary to "deuterate" the gas line before pure DCl could be obtained. This was simply done by filling the line with DCl, leaving it for some time, pumping the gas away and repeating the process until the percentage of HCl decreased. A fresh sample of DCl was used for each experiment.

4.5 Results:

A carefully purified gas sample was allowed to diffuse, as rapidly as possible, into the baked, degassed spectrophone and the initial signal found. After several hours in the cell the signal had risen to a steady value. As with CO this rise is caused by impurity desorbing from the cell walls and shortening the relaxation time until all the absorbed energy is lost by collision. The curve of signal amplitude against time (Fig.14) is of the same shape as that for CO. Measurements on mixtures of HCl and H_2 (10%) that would be expected to have short relaxation times showed no such rise, indicating that it is not caused by effects unrelated to relaxation, such as attack on the microphone diaphragm.

From the initial and final signals the relaxation times (τ) were calculated as before:

$$\frac{\text{initial signal}}{\text{final signal}} = \frac{1/\tau}{1/\tau + 1/\tau_{rad}} \qquad 4.12$$

FIG 15 VIBRATIONAL RELAXATION TIMES OF HCl AND DCl AS A FUNCTION OF PRESSURE

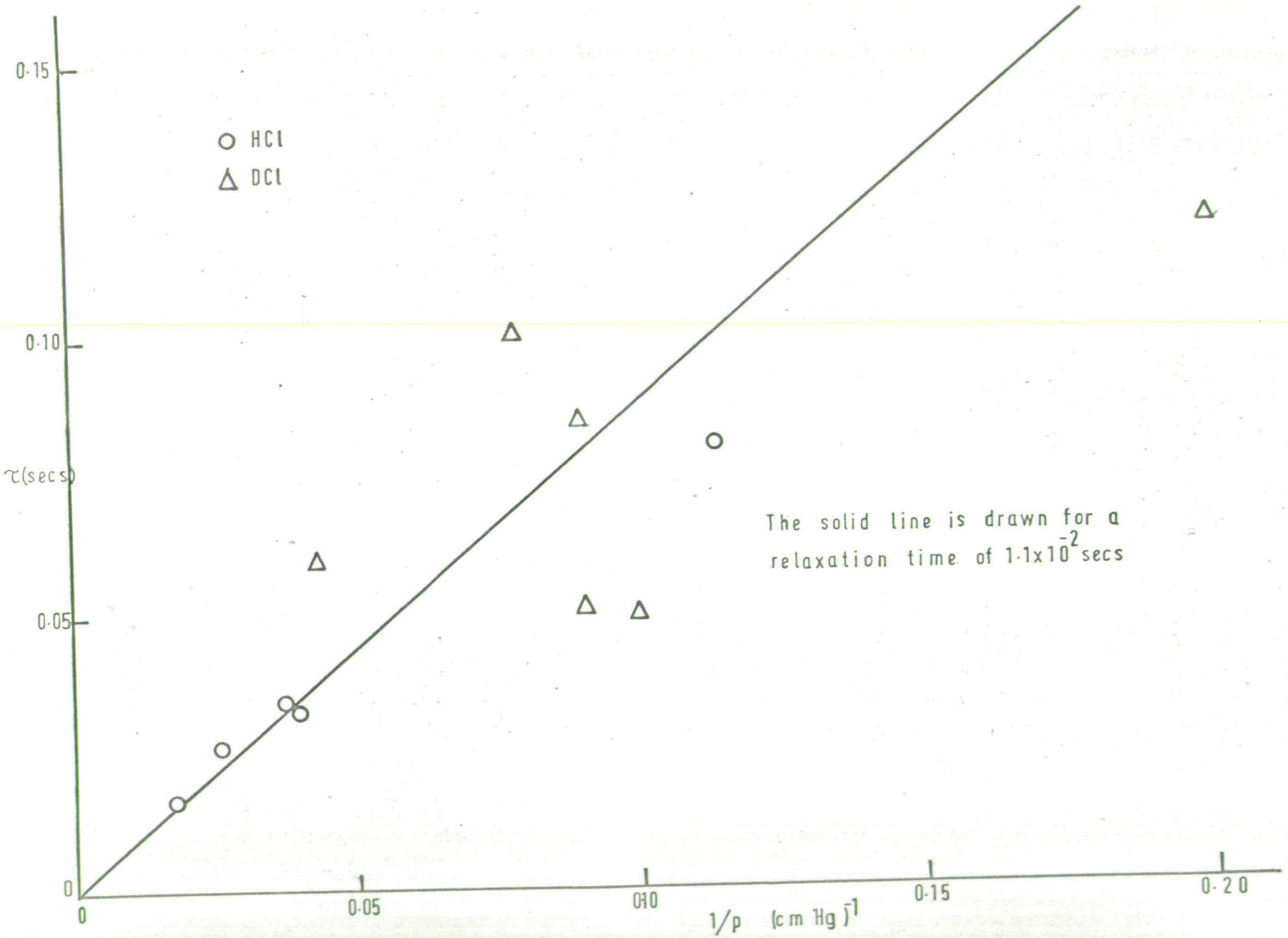

For each gas measurements were carried out over a range of pressures.

The results for HCl are shown in Table 7 and a plot of relaxation time against 1/pressure in Fig. 15. At atmospheric pressure the relaxation time is 1.1×10^{-2} secs.

Table 7.

Experimental Relaxation Times for HCl.

P (cm Hg)	ω (c.p.s.)	initial signal (μv)	final signal (μv)	τ (secs)
57	240	600	900	1.6×10^{-2}
39	79	1180	2160	2.6×10^{-2}
26.5	240	600	1260	3.4×10^{-2}
25	240	600	1200	3.2×10^{-2}
8.8	240	120	420	8.0×10^{-2}

The results for HBr are given in Table 8 and Fig. 16. The relaxation time at one atmosphere is 1.5×10^{-3} secs.

Table 8.

Experimental Relaxation Times for HBr.

P(cm Hg)	ω (c.p.s.)	initial signal (μv)	final signal (μv)	τ (secs)
11.6	240	350	380	2.0×10^{-2}
7.2	"	480	550	2.2×10^{-2}
5.6	"	140	220	2.4×10^{-2}
2.2	"	170	240	6.2×10^{-3}
1.6	"	70	100	6.3×10^{-3}

The results for DCl are shown in Table 9. There is a large scatter of values, almost certainly due to small but varying amounts of HCl in the samples of DCl. The points are plotted in Fig. (15), along with those for HCl. The relaxation time at one atmosphere is approximately 1×10^{-2} secs.

FIG 16 VIBRATIONAL RELAXATION TIME OF HBr AS A FUNCTION OF PRESSURE

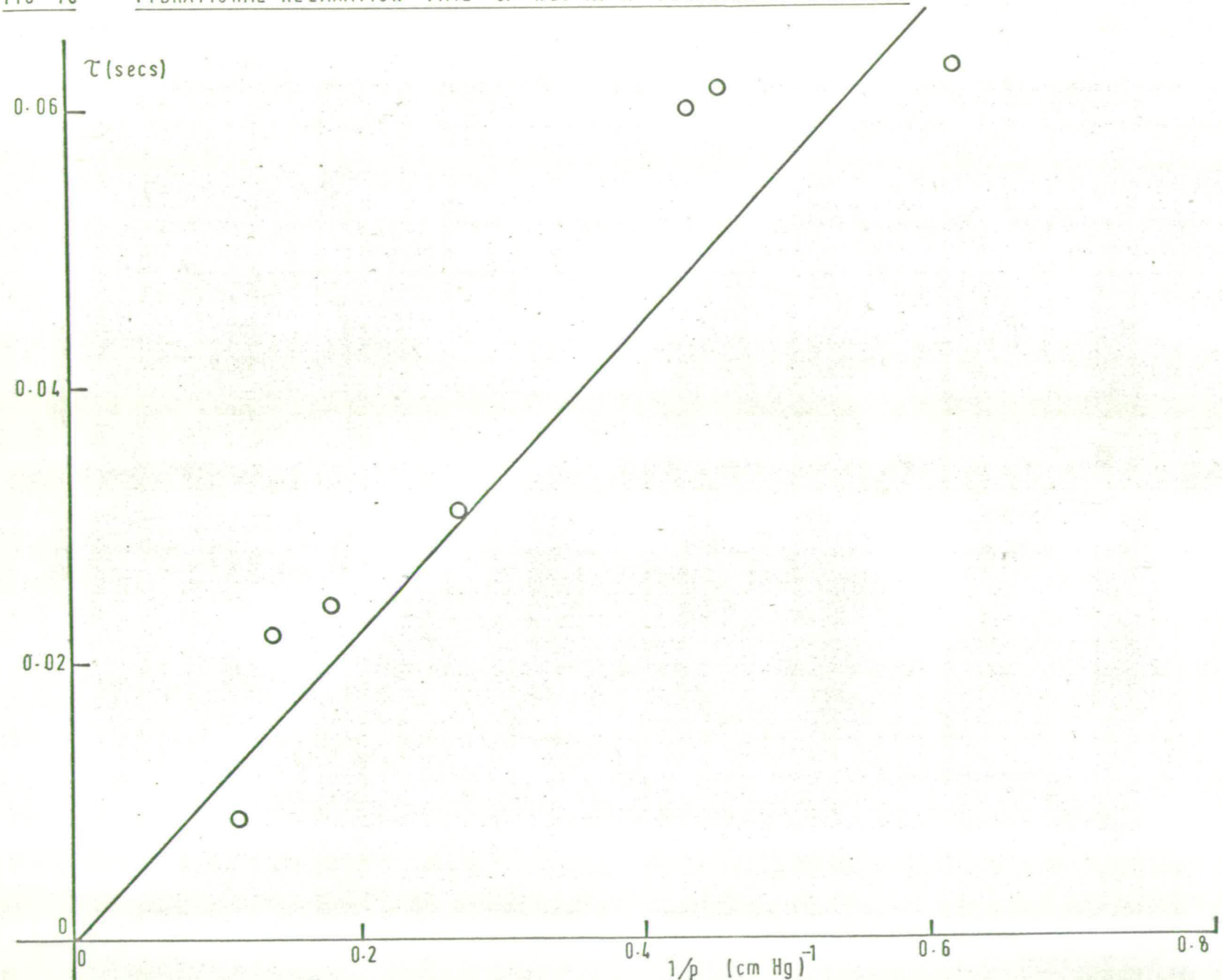

Table 9.

Experimental Relaxation Time of DCl.

P (cm Hg)	ω (c.p.s)	initial signal (μv)	final signal (μv)	τ (secs)
23	240	600	900	6×10^{-2}
14.5	140	800	1500	10.5×10^{-2}
11.0	140	700	1200	8.5×10^{-2}
11.05	240	400	570	5.1×10^{-2}
9.95	240	250	350	5.0×10^{-2}
5.0	80	550	975	12×10^{-2}

4.6 Discussion:

The above relaxation times must be regarded as shorter limits to the true relaxation times. Small traces of impurity - with such long relaxation times even a few p.p.m. of water can have a considerable effect - and reabsorption of the resonance fluorescence both shorten the measured relaxation time. The first of these effects is most important at low pressures and the second at high pressures. However, apart from DCl - where the purity problem is most acute - the plots of relaxation time against ^{1}/pressure are fairly good straight lines, indicating that impurity effects have probably been largely overcome. Also reabsorption of the resonance fluorescence will be less important in HCl and HBr than in CO because the pressures used are lower and the collisional relaxation times are shorter. Experimental and theoretical relaxation times (from Table 3) are compared in Table 10. It can be seen that the discrepancy between theory and experiment is far greater than experimental error.

Table 10.

Comparison of experimental and theoretical relaxation times for HCl, DCl and HBr.

Molecule	τ theor. (secs.)	τ expt. (sec.)	τtheor./τexptl.
HCl	6.5	1.1×10^{-2}	596
DCl	1.6×10^{-2}	1×10^{-2}	1.6
HBr	5.1×10^{4}	1.5×10^{-3}	3.4×10^{7}

While the relaxation time for DCl is very nearly correct, those for HCl and HBr are much too long. The same theory, however, gives very good results for other diatomic molecules with long relaxation times such as O_2, N_2 and CO. It therefore seems probable that vibrational energy in the hydrogen halides is transferred by some mechanism other than direct vibration-translation energy transfer. This mechanism might be vibration-rotation energy transfer, as suggested by Cottrell and Matheson (9) and the possibility of vibration-rotation energy transfer is discussed in detail in the next chapter.

Results for the 3-0 transition in HCl have recently been obtained by Borrell and Gutteride (18). The v = 3 band of HCl would be expected to relax rapidly to the v =1 level by resonance collisions of the type.

$$HCl\ (v = 3) + HCl\ (v = 0) \longrightarrow HCl\ (v = 2) + HCl(v = 1)$$

$$HCl\ (v = 2) + HCl\ (v = 0) \longrightarrow HCl\ (v = 1) + HCl(v = 1)$$

so that the 3-0 relaxation time should be effectively that of the 1-0 process which will be much slower than the resonance processes. The two sets of results can therefore be directly compared. Fig (15) shows the present result, those of Borrell and Gutteridge, and the approximate results for the 1-0 process obtained by Borrell. The temperature dependence is very different from that predicted by vibration-translation theory. This will be discussed in the next chapter.

IG 17 TEMPERATURE DEPENDENCE OF THE RELAXATION TIME OF HCl :

VIBRATION TRANSLATION THEORY

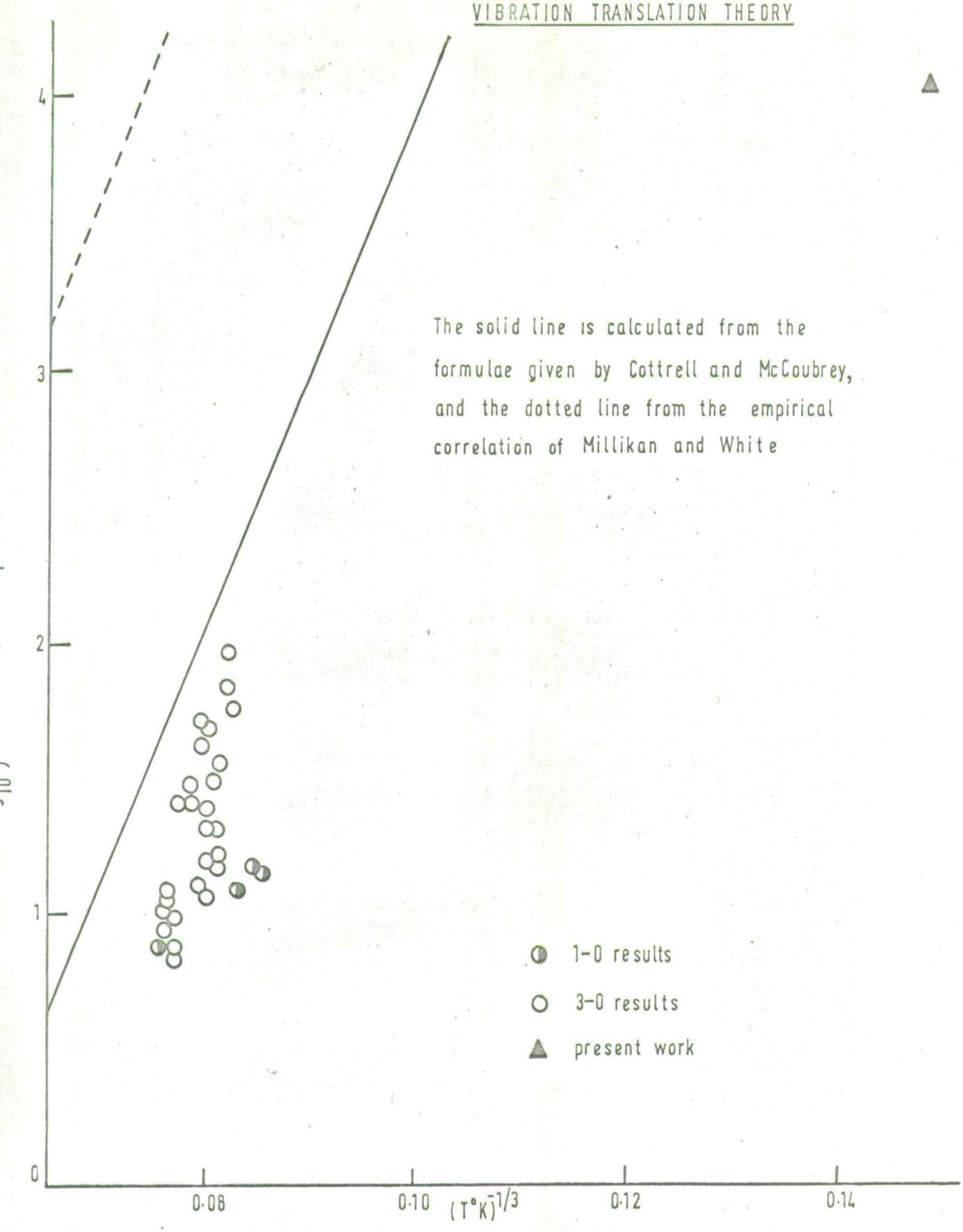

Chapter Five

VIBRATION-ROTATION ENERGY TRANSFER

5.1 Introduction:

The relaxation times of most diatomic and heavy atom polyatomic molecules can be satisfactorily explained in terms of vibration-translation energy transfer (6,7). Lambert and Salter (8) showed that there is a correlation between the number of collisions required for vibrational deactivation Z_{10} and the fundamental vibration frequency of the molecule, ν min. However, the picture is not a simple one. They were able to distinguish two classes of compound: heavy atom polyatomics lay on a straight line represented by

$$\log_{10} Z_{10} = 7.3 \times 10^{-3} \nu \text{ min}(cm^{-1}),$$

and those containing two or more hydrogen atoms lay on the line whose equation is

$$\log_{10} Z_{10} = 3.7 \times 10^{-3} \nu \text{ min}(cm^{-1}) \qquad (64)$$

Molecules containing one hydrogen atom lay between the two lines. This effect could not be explained at the time and the situation was further complicated when more recent data, especially on deuterated molecules, led to a large spread of points rather than to straight lines.

A possible explanation appeared when Cottrell and co-workers measured the relaxation times of a series of deuterides and hydrides and found that, contrary to the predictions of vibration-translation theory, the hydrides relaxed more rapidly than their deuterated analogues (9, 10, 11). On the basis of simple theory the slightly greater mass of the deuteride leads to a slower relative translational velocity and hence a slightly longer relaxation time for the deuteride than for the hydride. But this is outweighed by the lower fundamental vibration frequency of the deuteride which results in an increased probability of energy transfer and hence a shorter relaxation time.

Refinements can be made to the vibration-translation theory but in no case has it been successful in explaining the relative relaxation times of hydride molecules and their corresponding deuterides.

Cottrell suggested that in molecules with low moments of inertia, and therefore high rotational velocity, vibrational energy may be transferred into rotation rather than into translation. Rotation - translation energy transfer is then rapid. Qualitatively since the hydrides have a lower moment of inertia and higher rotational velocity than the deuterides it is possible, in this theory, that they could have shorter relaxation times than the deuterides. A simple calculation showed that vibration-rotation theory can account for the observed relative vibrational relaxation times of the hydrides and deuterides of elements in groups 4 and 5. The model adopted is shown below:

Model for vibration rotation energy transfer

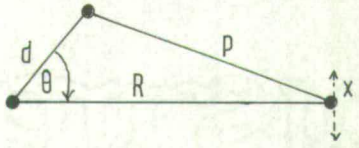

The force causing the interaction was assumed to arise between the peripheral atom of the rotator and the atom moving in the vibration. It is therefore a function of the distance p. d is the radius of the rotator and R the distance between the centre of the rotator and the equilibrium position of the vibrator. The rotator makes an angle θ with the line of centres and the displacement X of the vibrator is at right angles to this line. The probability of de-excitation of the vibrator was calculated using time dependent perturbation theory.

The calculated ratios are shown in Table 11.

Table 11.

Ratios of Reduced Relaxation Times for Lowest Mode for deuterides and hydrides (10)

Molecule	Theoretical $\beta D / \beta H$		Experimental $\beta D / \beta H$
	Vib-Rot.	Vib-Trans.	
CD_4, CH_4	1.7	0.58	1.7 (8)
SiD_4, SiH_4	1.5*	0.25	1.5 (8)
PD_3 , PH_3	1.5	0.13	1.5 (9)
AsD_3, ASH_3	1.2	0.04	0.6 (10)

* interpolated.

The vibration-rotation ratios agree remarkably well with experimental values. However, these results must be treated with some caution. Absolute values calculated using this theory are very many orders of magnitude too short, and the excellent agreement obtained in the ratios may be fortuitous.

Another consequence of vibration-rotation theory becomes apparent in the dependence of the relaxation time on molecular weight. According to the standard theory of vibrational energy transfer the probability of transfer depends on the extent to which the vibrational period and the duration of the encounter are matched. Because typical vibration periods are so short (3×10^{-14} secs. for a 1060 cm^{-1} vibration frequency) the rare high velocity collisions are mainly responsible for energy transfer. Therefore in two molecules with similar modes of vibration and vibration frequencies, but different molecular weights, the probability of energy transfer in the heavier gas will be very much less than in the lighter gas which has higher average translational velocity. However, in vibration rotation transfer the relative probabilities should depend on the rotational velocity, and hence the moment of inertia, rather than on the translational velocity and molecular weight.

Cottrell et al compared the relaxation times of PH_3 and AsH_3, (Table 12) whose moments of inertia are similar.

Table 12.

Molecular Parameters and Relaxation Times of PH_3 and AsH_3.

	AsH_3	PH_3
lowest vibration frequency (cm^{-1})	906	992
form of vibration	bending	bending
X - H distance ($\mathring{A}$)	1.42	1.50
Molecular weight	34	78
boiling point	-87	-55

The vibration frequencies are close and the intermolecular forces are probably similar as shown by the boiling points.

Relaxation Times:

	Vib-trans.	Vib-Rot.	Expt.
$\beta AsH_3 / \beta PH_3$	150	1	1.5

Again vibration-rotation theory seems to give better agreement with experiment.

Recently Moore correlated all the available data on vibrational relaxation in molecules with small moments of inertia (13) and his treatment will be followed here. He derived an explicit expression for the dependence of the probability of vibration-rotation energy transfer on molecular constants using a simple model of a peripheral atom, distance d from the centre of mass of the rotator, colliding with an atom of the stationary vibrating molecule.

Model for vibration-rotation energy transfer

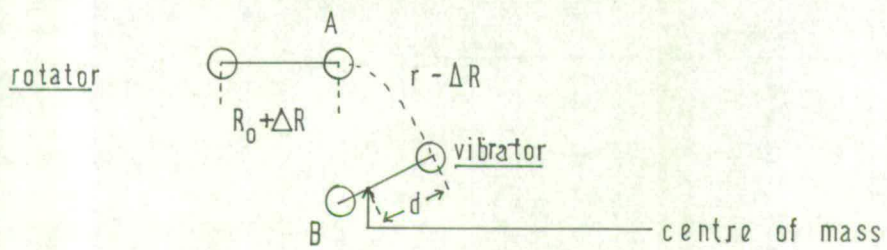

Several assumptions are made: that the translational velocity is slow compared with the rotational velocity, that only one rotational degree is considered, and that only head-on collisions with the rotational velocity parallel to the vibrational normal coordinate need be considered. It is assumed that the potential interaction between A and B effecting transfer is represented by

$$V = Vo \exp(-\alpha R)(1 + \alpha \Delta R) \qquad 5.1$$

where ΔR is the vibrational displacement, and r the distance between the colliding atoms with $\Delta R = 0$. The rate of change of distance between atoms A and B is ωd, ω being the angular frequency of the rotator.

Using semi-classical time-dependent perturbation theory Cottrell and McCoubrey (7) derive the following expression for the transition probability for vibration-translation energy transfer:

$$P_{10} = \frac{32\pi^4 m^2 \nu}{h\alpha^2 M} \exp\left(-\frac{4\pi^2 \nu}{\alpha v}\right)$$

The probability of vibration-rotation energy transfer is obtained by substituting (ωd) for the relative translational velocity v, and (I/d^2) for the reduced mass, m, in the above equation. I is the moment of inertia of the rotator and M the reduced mass of the vibrational normal coordinate. Hence for vibration rotation energy transfer

$$P_{10} = \frac{32\pi^4 I^2 \nu}{h\alpha^2 M d^4} \exp\left(-\frac{4\pi^2 \nu}{\alpha \omega d}\right) \qquad 5.2$$

and averaging over the thermal distribution of rotational velocity

$$\frac{dN(\omega)}{N} = \left(\frac{I\omega}{kT}\right) \exp\left(-\frac{I\omega^2}{2kT}\right) d\omega \qquad 5.3$$

gives

$$P_{10} = \frac{1}{Z_{10}} = \int P_{10}\omega \frac{dN(\omega)}{N} = \frac{32\pi^4 (2\pi)^{1/16}}{\sqrt{3}} \left\{ \frac{I^{13/6} \nu^{4/3}}{d^{13/3} (kT)^{1/6} M (\alpha)^{7/3}} \right\} \exp\left[-3 \left\{ \frac{2\pi^4 I \nu^2}{d^2 \alpha^2 kT} \right\}^{\frac{1}{3}} \right] \qquad 5.4$$

The change in velocity due to an increase of rotational energy $h\nu$ during collision has been neglected. When this is accounted for, and when a steric factor Zo, greater than one is included to take account of non-linear collisions, equation 5.4 becomes

$$\frac{1}{Z_o} \left\{ \frac{17.1\ I^{13/6}\ \nu^{4/3}}{d^{13/3}\ T^{1/6}\ M(\alpha)^{7/3}} \right\} \exp.\left[-1.78 \left\{ \frac{I\nu^2}{d^2\alpha^2 T} \right\}^{\frac{1}{3}} \right] \exp.\left[\frac{0.7194\nu}{T} \right] \qquad 5.5$$

From equation 5.5, the radial velocity for which energy transfer is most probable is given by

$$(wd^*) = \left(\frac{4\pi k \nu T d^2}{\alpha I} \right)^{\frac{1}{3}} = 0.995 \times 10^4 \left(\frac{I \nu d^2}{\alpha T} \right)^{\frac{1}{3}} \text{ molecular units} \qquad 5.6$$

and the optimum initial angular momentum quantum number

$$J^* = \frac{2\pi I w^*}{h} = 0.157 \left(\frac{I \nu T}{d\alpha} \right)^{\frac{1}{3}} \text{ molecular units} \qquad 5.7$$

In Table 13 the most probable rotational velocities for energy transfer (ωd^*) are compared with the average translational velocities for the hydrogen and deuterium halides. For comparison the figures for a few other molecules in which vibration-rotation energy transfer is important are included.

Table 13.

Rotational velocities and energies for vibration-rotation energy transfer

Molecule	$(\omega d)^*$ x 10^{-5} cm	$\bar{c}_{rel.}$ sec^{-1}	Ji*	Jf*	2BJi* cm^{-1}	2B Jf* cm^{-1}
HCl	6.5	0.42	13	21	270	445
HBr	6.1	0.28	14	22	237	373
DCl	4.6	0.41	18-19	27	196-206	294
DBr	4.43	0.28	20	29	170	246
HI	6.15	0.16	15	24	196	314
CH_4	3.4	0.63	17	23	178	242
CD_4	2.0	0.56	24	31	127	164
SiH_4	3.0	0.48	20	27	115	155

$\bar{c}_{rel} = \left(\frac{4RT}{\pi M}\right)^{\frac{1}{2}}$ is the average translational velocity.

$J_i^* = \left(\frac{2\pi I \omega}{h}\right)^*$ is the rotational quantum number for which $P_{i}d\omega\, dN(\omega)$ is a maximum.

$J_f^* = (J_i^* + \nu/B)^{\frac{1}{2}}$ is the rotational quantum number after vibrational energy transfer.

B is the rotational constant in cm^{-1}.

The ratio of $(\omega d)^*$ to the average translational velocity in the halides ranges from 38 for H I to 11 for DCl. It is as low as 3 for CD_4 and for the bulk of molecules considered by Moore is near 5. Thus the error caused by neglect of translational motion in the halides will be relatively small. A more serious error is likely to be caused here by the large rotational energy spacing of the halides; as much as half of the energy

separating successive rotational levels must be transferred to translation and the larger this energy is the smaller the transition probability. To account for this a translational factor should be included in equation 5.2. However using the simple theory only, the expected collision numbers at room temperature for HCl, DCl and HBr were calculated.

5.2 Vibration-Rotation Energy Transfer in the hydrogen and deuterium halides.

The collision numbers of Z_{10} for HCl, DCl and HBr were calculated from the expressions (from ref. 13)

$$\frac{1}{Z_{10}} = \frac{1}{c} \exp -1.78 \left(\frac{I\nu^2}{d^2 \alpha^2 T}\right)^{\frac{1}{3}} \qquad 5.8$$

$$\frac{1}{Z_{10}} = \frac{1}{Z_o} \exp \left[\frac{17.1\ I^{13/6}\ \nu^{4/3}}{d^{13/3}\ T^{1/6}\ M(\alpha)^{7/3}}\right] \exp \left[-1.78 \left\{\frac{I\nu^2}{d^2 \alpha^2 T}\right\}^{\frac{1}{3}}\right] \qquad 5.9$$

and from equation 5.5

Moore found that a plot of

$$\log_{10} Z_{10}\ (\text{expt}) \quad \text{against} \quad \left(\frac{I\nu^2}{d^2 \alpha^2 T}\right)^{\frac{1}{3}}$$

gave an order of magnitude fit with a straight line whose slope corresponded to $\alpha = 8.04\ \text{Å}^{-1}$, and $c = 13$.

A plot of

$$\log_{10} Z_{10}(\text{expt.}) \frac{17.1\ I^{13/6}\ \nu^{4/3}}{d^{13/3}\ T^{1/6}\ M(\alpha)^{7/3}} \quad \text{against} \quad \left(\frac{I\nu^2}{d^2 \alpha^2 T}\right)^{\frac{1}{3}}$$

gave a straight line for which the best parameters were

$$\alpha = 3.80\ \text{Å}^{-1} \quad \text{and} \quad Z_o = 6.75$$

Table 14.

Comparison of Calculated Vibration-Rotation Energy Transfer Collision Numbers with Experimental Values.

Molecule	T °K	I amu Å^2	d Å	ν cm^{-1}	M amu	Z_{10} calc. Eqn 8	Z_{10} calc. Eqn 9	Z_{10} calc. Eqn 5	Z_{10} exptl.	$\log_{10}\frac{Z_{10}(\text{eqn 5})}{Z_{10}\text{ exptl.}}$
H I	2465	2.57	1.591	2230	1.0	37	12	14	6.4×10^3 (b)	-2.7
H I	1370	2.57	1.591	2230	1.0	125	81	83	1.25×10^4 (b)	-2.2
HCl	2000	1.592	1.239	2886	1.0	181	105	139	1.33×10^4 (c)	-2.0
HCl	290	1.592	1.239	2886	1.0	1.29×10^5	2.29×10^6	7.29×10^4	5.4×10^7 (a)	-2.8
HBr	1000	1.99	1.396	2560	1.0	563	752	634	1.08×10^5 (a)	-2.3
HBr	290	1.99	1.396	2560	1.0	3.4×10^4	5.44×10^5	2.21×10^4	5.11×10^6 (a)	-2.3
DCl	290	3.075	1.206	2091	2.0	6.31×10^4	4.35×10^6	6.01×10^5	4.87×10^7 (a)	-2.7

(a) present work

(b) C.C. Chow, E.F. Greene, J. Chem. Physics, 1965, 43, 324

(c) P. Borrell, Chemical Society Special publications No.20. 'Molecular Relaxation Processes' Academic Press, 1966

And a plot of

$$\log_{10} Z_{10}(\text{expt}) \propto \left[\frac{17.1\ I^{13/6}\ 4/3}{d^{13/3}\ T^{1/6}\ M(\alpha)^{7/3}}\right] \exp.\left[\frac{0.7194\nu}{T}\right] \text{ against } \left[\frac{I\nu^2}{d^2\alpha^2 T}\right]^{\frac{1}{3}}$$

corresponded to a straight line whose slope gave $\alpha = 2.94\ \text{Å}^{-1}$ and intercept $Z_o = 4.97$.

Using these parameters Z_{10} is calculated for all three expressions and compared with experimental Z_{10}s. Hard sphere collision numbers are calculated from

$$Z = \frac{4.75 \times 10^{10} \sigma^2}{T^{\frac{1}{2}}\ M^{\frac{1}{2}}}$$

and $Z_{10} = Z\tau(\text{expt})$. σ is in Å, T in °K, M in a.m.u., and τ in secs. The results are shown in Table 14 along with those of other workers.

The agreement between theory and experiment has been greatly improved by the use of vibration-rotation energy transfer theory, particularly in the case of H Br. This is most clear when the ratios of the relaxation times predicted by the two theories are compared (Table 15).

Table 15.

Ratios of Relaxation times of HCl, HBr and DCl at 290°K.

Ratio	vib-trans.theory	vib-rot.theory	expt
τ HCl/τDCl	4.1×10^2	1.1×10^{-1}	1
τ HCl/τHBr	1.3×10^4	2.5	7.3

The effect noted by Cottrell in the $\beta AsH_3/\beta PH_3$ ratio is clearly important in the ratio of τ HCl/τ HBr. HBr has a vibration frequency about 12% lower than that of HCl, but in vibration-translation theory the much greater weight of HBr, and hence its lower relative translational velocity,

FIG 18 VIBRATION–ROTATION RELAXATION FOR MOLECULES CONTAINING LIGHT ATOMS

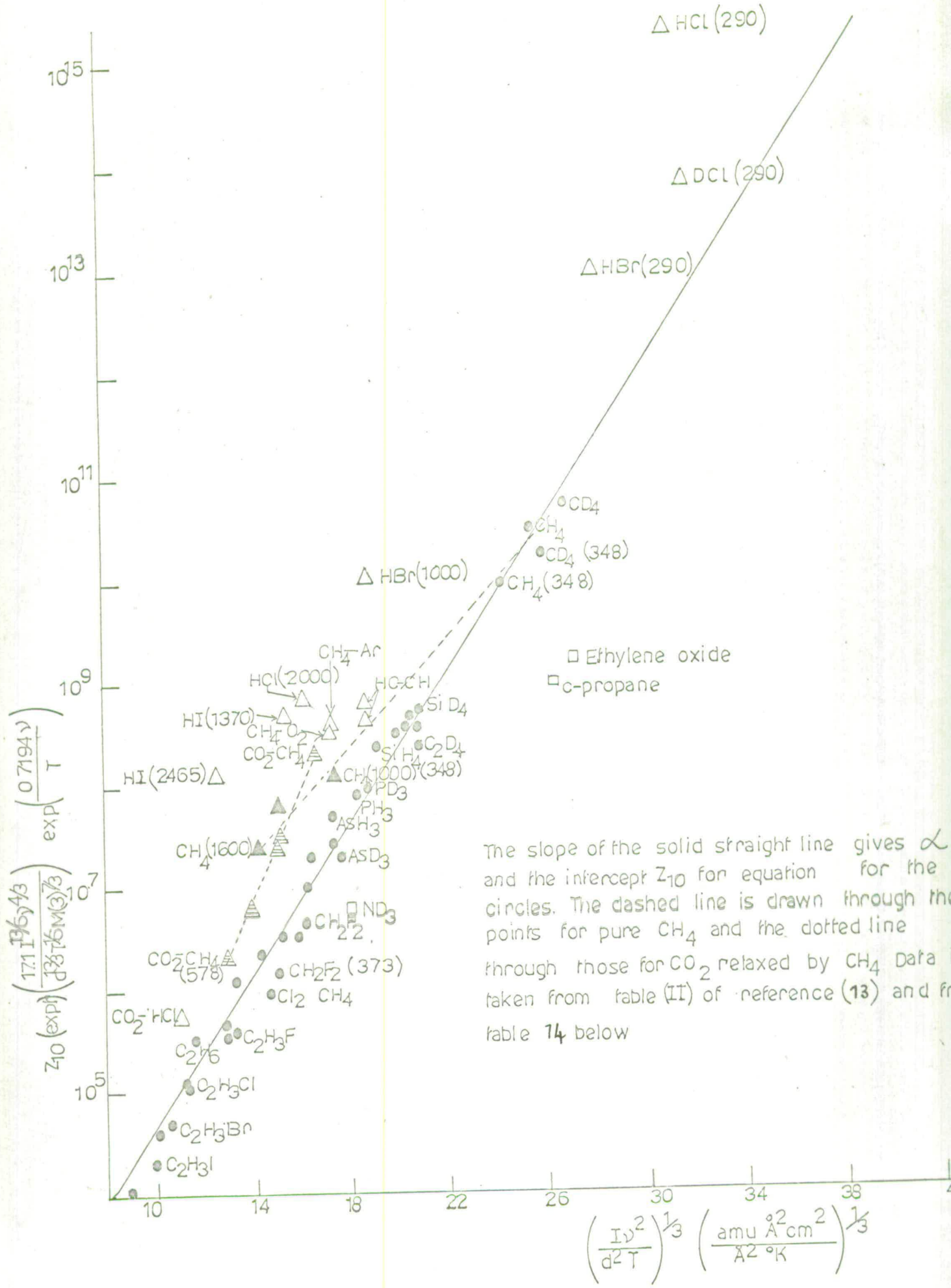

The slope of the solid straight line gives α and the intercept Z_{10} for equation for the circles. The dashed line is drawn through the points for pure CH_4 and the dotted line through those for CO_2 relaxed by CH_4 Data taken from table (II) of reference (13) and fr table 14 below

becomes the dominant factor leading to a much longer relaxation time for HBr than for HCl. However the moments of inertia of the two molecules are similar and vibration-rotation theory predicts that they will have similar relaxation times. It can be seen that this prediction is in agreement with the experimental finding.

Although the experimental result for DCl is not reliable because of traces of HCl in the sample it is obvious that the relaxation time of DCl is not 400 times smaller than that of HCl as predicted by vibration translation theory since the effects of impurity and reabsorption of the resonance fluorescence are such as to make the present result a lower limit to the true relaxation time.

A plot of

$$\log_{10} Z_{10}(\text{expt}) \times \left[\frac{17{\cdot}1\ I^{13/6}\ \nu^{4/3}}{d^{13/3}\ T^{1/6}\ M(\alpha)^{7/3}}\right] \exp\left[\frac{0\ 719 4\nu}{T}\right]$$

against $\left(\frac{I\nu^2}{d^2 T}\right)^{\frac{1}{3}}$ is shown in Fig. (18). It can be seen that the halides require approximately 100 times the number of collisions predicted by vibration-rotation theory. However the temperature dependence is very much closer to experiment - Fig. (19). This is a great improvement on the temperature dependence expected from vibration-translational theory (Fig. 17).

As was pointed out before an error could arise from neglect of the translational motion. In the halides the rotational spacing 2 BJ* is large (Table 13) and a significant amount of vibrational energy must be transferred to translation; these molecules have low translational velocity because of their mass and hence the overall probability of energy transfer is decreased. A complete understanding of vibration rotation energy transfer in the halides would require a quantum treatment of rotation, and separate calculations for all possible values of the initial and final rotational quantum number.

FIG 19 TEMPERATURE DEPENDENCE OF THE RELAXTION TIMES OF HCl AND HBr — VIBRATION ROTATION THEORY

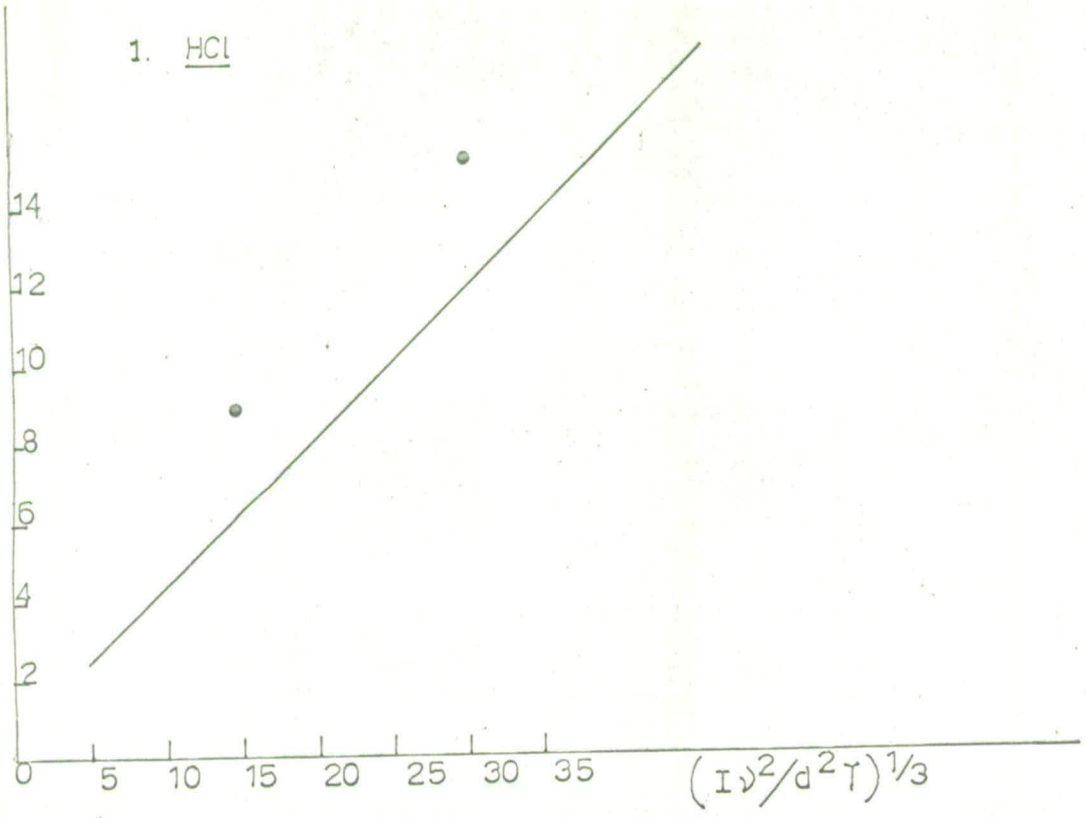

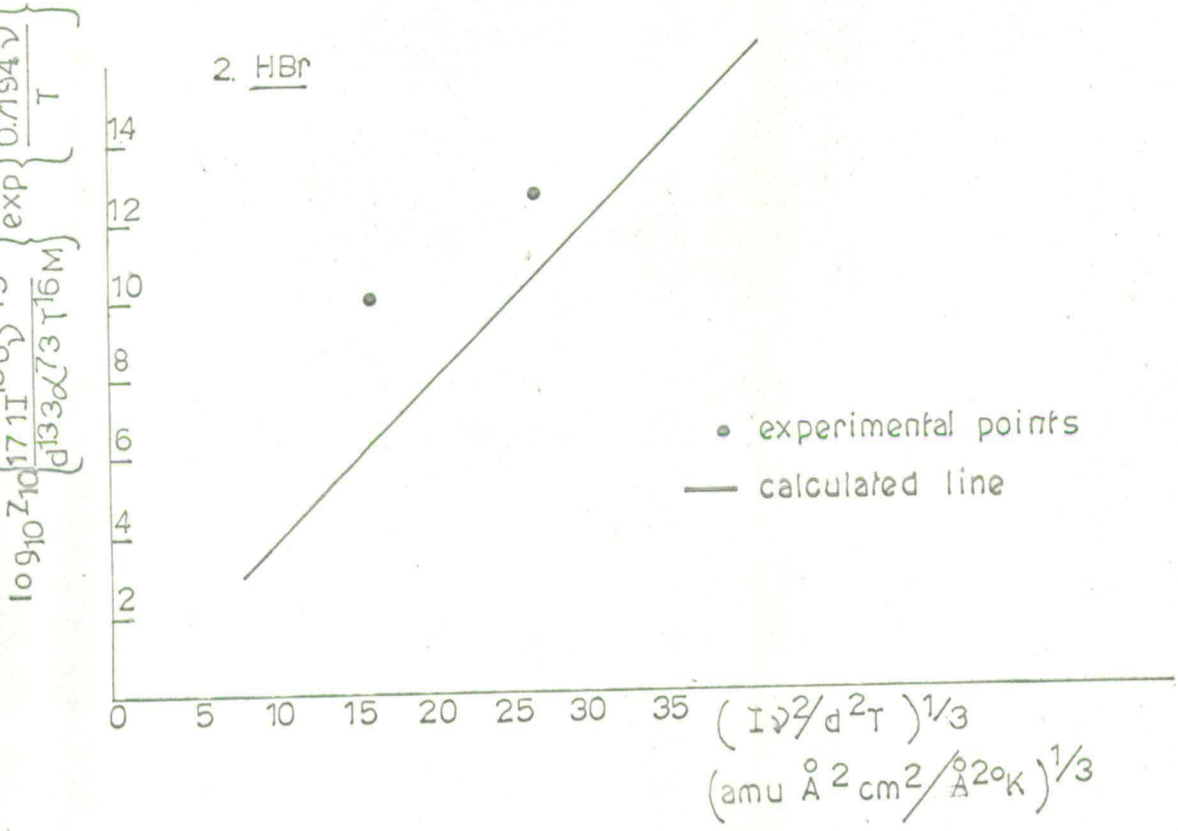

Conclusion:

The experimental results obtained in this work indicate that vibration-rotation energy transfer plays an important role in the collisional deactivation of vibrationally excited HCl, DCl and HBr. While it is true that no really satisfactory mechanism has so far been put forward by which such energy transfer can occur, nevertheless no other theory can account for the observed relaxation times, especially the ratio of τ hydride to τ deuteride. A comparison of, for example, a Lambert-Salter plot, with Moore's semi-empirical correlation shows the vast improvement achieved by interpreting the relaxation times of molecules with low moments of inertia in terms of vibration-rotation energy transfer.

REFERENCES

1. J. Applied Optics, Supplement 2 "Chemical Lasers", 1965.
2. R.C. Millikan, D.R. White, J. Chem. Physics, 1963, 39, 98.
3. R.N. Schwartz, Z.I. Slawsky, K.F. Herzfeld, J. Chem. Physics, 1952, 20, 1591.
4. C. Zener, Phys. Rev, 1931, 37, 556; 38, 227.
5. L. Landau, E. Teller, Phys. Zeit. Sowjetunion, 1936, 10, 34.
6. K.F. Herzfeld, T.A. Lifovitz 'Absorption and Dispersion of Ultrasonic Waves', Academic Press, New York, 1959.
7. T.L. Cottrell, J.C. McCoubrey, 'Molecular Energy Transfer in Gases', Butterworths, London, 1961.
8. J.D. Lambert, R. Salter, Proc. Roy. Soc., 1959, 253A , 227.
9. T.L. Cottrell, A.J. Matheson, Trans. Faraday Soc., 1963, 58, 2336.
10. T.L. Cottrell, A.J. Matheson, Trans. Faraday Soc., 1963, 59, 824.
11. T.L. Cottrell, R.C. Dobbie, J. McLain, A.W. Read, Trans. Faraday Soc. 1964, 60,241
12. R.C. Millikan, L. Osburg, J. Chem. Physics, 1964, 41, 2196.
13. C.B. Moore, J. Chem. Physics, 1965, 43, 2979.
14. T.L. Cottrell, International Institute of Chemistry 12th Conference, 1962, Interscience Publications, New York, 1964.
15. A.G. Gaydon, I.R. Hurle, 8th Combustion Symposium, Williams and Wilkins Co., Baltimore, 1962.
16. T.A. Holbeche, J.G. Woodley, Royal Aircraft Establishment, Tech. Mem. No. AERO 937.
17. W.J. Hooker, R.C. Millikan, J. Chem. Physics, 1963, 38, 214.
18. P. Borrell, R. Gutteridge, Private Communication.
19. S.H. Bauer, Ann. Rev. Phys. Chem., 1965, 16, 245.
20. R.C. Millikan, J. Chem. Physics, 1963, 38, 2855.
21. R.C. Millikan, J. Chem. Physics, 1964, 40, 2594.
22. R.C. Millikan, J. Chem. Physics, 1966, 43, 1439.

23. W.E. Woodmansee, J.C. Decius, J. Chem. Physics, 1962, 36, 1831.

24. M.E. Delany, PhD. Thesis, London, 1959.

25. W. Shaefer, Zeit. für Ang. Physik, 1965, 19, 55.

26. J. Tyndall, Proc. Roy. Soc., 1881, 31, 307.

27. W.C. Röntgen, Phil. Mag., 1881, s511, 308.

28. A.G. Bell, Phil. Mag., s511, 510.

29. A.H. Pfund, Science, 1939, 90, 326.

30. M.L. Viengerov, Izvest. Akad. Nauk. USSR. (Physiks), 1940, 4, 94.

31. K.L. Luft, Zeit. für tech. Physik, 1943, 24, 97.

32. M.L. Viengerov, Comp. Rendus Docklady, 1946, 54, 779.

33. G. Gorelik, Dokl. Akad. Nauk. SSSR, 1946, 54, 7.

34. P.V. Slobodskaya, Izvest. Akad. Nauk., SSSR, 1948, 12, 656.

35. T.L. Cottrell, Trans. Faraday Soc., 1950, 46, 1025.

36. R. Kaiser, Can. J. Phys., 1959, 35, 1499.

37. P.V. Slobodskaya, E.S. Gasilevich, Opt. Spectry., 1959, 7, 58.

38. M.E. Jacox, S.H. Bauer, J. Phys. Chem., 1957, 61, 833.

39. A.W. Read, PhD. Thesis, Edinburgh, 1963.

40. I.M. Macfarlane, PhD. Thesis, Edinburgh, 1966.

41. T.L. Cottrell, I.M. Macfarlane, A.W. Read, A.H. Young, Trans. Faraday Soc., 1966, 62, 2655.

42. T.L. Cottrell, I.M. Macfarlane, A.W. Read, Trans. Faraday Soc., to be published.

43. B.J. Lavercombe, Proc. 5th Congress Intern. d'Acoustique, Liège, 1965, c 26.

44. B.J. Lavercombe, Nature, 1966, 5044, 63.

45. J.C. Decius, private communication.

46. A. van Itterbeek, P. Mariens, Physica, 1937, 4, 609.

47. D. Bender, Ann. Phys. Lpz., 1940, 38, 199.

48. G.C. Sherrat, E. Griffiths, Proc. Roy. Soc., 1934, 147A, 292.

49. M. Windsor, N. Davidson, R. Taylor, 7th Combustion Symposium, Butterworths, London, 1958.

50. D.L. Matthews, J. Chem. Physics, 1961, 34, 639.

51. P.G. Dickens, A. Ripamonti, Trans. Faraday Soc., 1961, 57, 732.

52. D.J. McCaa, D. Williams, J. Opt. Soc. Am., 1964, 54, 326.

53. S.S. Penner, 'Quantitative Molecular Spectroscopy and Gas Emissivities', Addison-Wesley, Massachussetts, 1959.

54. W.S. Benedict, R. Herman, G. Moore, S. Silverman, Astrophys. J., 1962, 135, 277.

55. L. Doyenette, L. Henry, J. de Physique, to be published.

56. L. Doyenette, M. Margottin-Maclou, L. Henry, J. de Chimie. Physique, 1967, 64, 33.

57. P. Borrell, 'Molecular Relaxation Processes', Academic Press, 1966, 263.

58. C.C. Chow, E.F. Greene, J. Chem. Physics, 1965, 43, 324.

59. L. Monchick, E.A. Mason, J. Chem. Physics., 1961, 35, 1676.

60. W.S. Benedict, R. Herman, G.E. Moore, S. Silverman, J. Chem. Physics, 1957, 26, 1671.

61. S.S. Penner, D. Weber, J. Chem. Physics, 1953, 21, 649.

62. H.J. Babrov, J. Chem. Physics, 1964, 40, 831.

63. A. de Vries, F.S. Klein, J. Chem. Physics, 1964, 41, 3428.

64. A.W. Read, Progress in Reaction Kinetics, 1965, 3, 203.

65. A.E. de Vries, private communication.

66. J.R. Airey, E.F. Greene, K. Kodera, G.P. Reck, J. Ross, J. Chem. Physics, 1967, 46, 3295.

67. P.V. Slobodskaya, Opt. Spectry, 1967, 22, 14.

PART TWO

MOLECULAR SPECTROSCOPY BY ELECTRON IMPACT

Chapter One

INTRODUCTION

1.1 General Introduction:

The electron is a particle which has played a fundamental role in our understanding of atomic and molecular structure. It provides the explanation for the occurrence of chemical bonds, and is thus the basis of the whole of chemistry. On it also rests the interpretation of the phenomena associated with metals, semi-conductors, etc.

The study of the behaviour of electrons and other charged species in solution has long formed an important branch of physical chemistry, namely electrochemistry. By contrast the behaviour of free electrons in gases has been, until recently, largely the concern of physicists. But mass spectrometry has become a very important tool in the study of chemical kinetics etc., and the diffraction effects arising in the elastic scattering of high energy electrons now provide a powerful method for the determination of the geometric configuration of polyatomic molecules. The discovery of the Ramsauer - Townsend effect in the scattering of slow electrons from gases, and more recently the observation of resonances in electron scattering - explained in terms of short-lived compound states of the electron and molecule - have also led to an increase in the interest of chemists in the field of electron impact, an increase which becomes obvious on scanning the literature. In addition electron spectroscopy provides a tool for the study of molecular states which can be studied only with difficulty, if at all, by other techniques, and this thesis is concerned with the application of electron impact to the study of electronic states of atoms and molecules.

A further factor responsible for this recent growth of interest is that modern experimental techniques make possible the measurement of quantities which could not previously be observed, and the increasing sophistication of the theory makes the significance of the experimental results more easily grasped.

The phenomena associated with electron impact therefore give new criteria against which we can test, and perhaps improve, our understanding of atomic and molecular structure.

1.2 Electron-molecule collisions:

Collisions of electrons with atoms and molecules can cause various interactions depending on the energy of the electron and the nature of the collision partner. Probably the most familiar of these interactions is ionisation:

$$e + M \longrightarrow 2e + M^+$$

which can occur when the electron has an energy at least as great as the ionisation potential of the molecule. This is the reaction taking place in the ion source of a mass spectrometer. Electrons can also cause electronic excitation of molecules:

$$e + M \longrightarrow e + M^*$$

where M^* denotes a molecule in an upper electronic state. In addition lower energy electrons may cause rotational and vibrational excitation.

Because of the wavelength of the electron and the range of electron-molecule interactions some of the concepts found useful in discussing intermolecular energy transfer must be abandoned when we come to consider electron-molecule interactions. Intermolecular forces vary rapidly with distance (typically as r^{-6}) so that it is possible to think of a fixed collision diameter for molecule-molecule impacts, independent of energy, and a property

of the molecule alone. However electron-molecule forces vary more slowly with distance (as about r^{-3}) and therefore the effective range of the interaction depends strongly on electron velocity. Neither can the wave nature of the electron be neglected. It has a de Broglie wavelength about a hundred times greater than a molecule with the same energy and diffraction and interference effects arise between the electron waves inside and outside the molecule.

In the first part of this thesis the probability of intermolecular energy transfer was discussed in terms of the average number of collisions required - a way of thinking no longer useful here because of the difficulty of deciding when a collision has occurred. A possible definition is that an electron-molecule collision has taken place if any physical change can be detected after the distance between the two particles has been first decreased and then increased. The physical change may be angular deflection, kinetic energy change, momentum change etc. detected within the limits of the uncertainty principle. The probability of electron-molecule energy transfer is then discussed in terms of an energy-dependent collision cross-section for a given process, defined as follows.

When an electron moves through a short distance x cms in a gas, density n molecules per cm^3, the probability P of making a collision is given by

$$P = n Q_T dx \qquad 1.1$$

Q_T has the dimensions of area and is known as the <u>total collision cross-section</u>. It may be split into elastic and inelastic components, similarly defined.

$$Q_T = Q_{elastic} + Q_{inelastic} \qquad 1.2$$

The difference between Q_T and the molecular collision diameter of kinetic theory is that Q is not a property of the molecule alone, but a function of the whole system: molecule, electron velocity, and type of transition.

The angular distribution of the scattered electrons is determined by a differential cross-section for the scattering of electrons into an element of solid angle $d\Omega$, making a polar angle θ, and an azimuthal angle ϕ.(see Fig.)

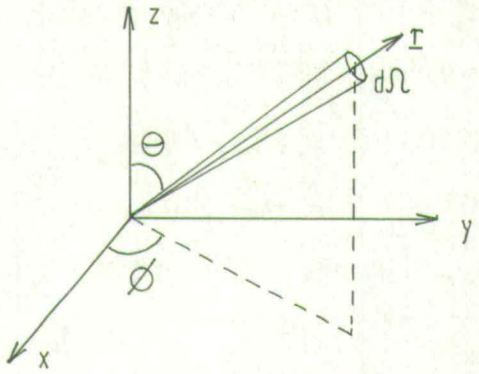

$$d\Omega = \sin\theta . d\theta . d\phi$$

The probability of scattering into this solid angle is

$$P(\theta) . \sin\theta . d\theta . d\phi$$

and the differential cross-section for scattering into $d\Omega$ is defined as

$$Q.P(\theta) \sin\theta . d\theta . d\phi = I(\theta) \sin\theta . d\theta . d\phi \qquad 1.3$$

The total cross-section is just the differential cross-section integrated over the range of solid angle

$$Q_T = \int_0^{\pi} \int_0^{2\pi} I(\theta) \sin\theta . d\theta . d\phi \qquad 1.4$$

To allow for the angular distribution of elastic scattering a momentum transfer cross-section is defined. Conservation of momentum requires that the fractional energy loss of an elastically scattered electron be about $2\, m_e/m$, where m_e is the mass of the electron, and m the mass of its collision partner. An electron scattered through an angle θ will lose approximately $2(1 - \cos\theta)m_e/m$ of its energy. The mean fractional energy loss per collision is given by

$$\frac{2m_e}{m} \times \int_0^{\pi} \int_0^{2\pi} (1 - \cos\theta)\, P(\theta) \sin\theta . d\theta . d\phi = \frac{2m_e}{m} \frac{Q_D}{Q} \qquad 1.5$$

where Q_D, the momentum transfer cross-section, is equal to

$$\int_0^{\pi}\int_0^{2\pi} Q\ P(\theta)\ \sin\theta.\ d\theta.\ d\phi \qquad 1.6$$

if the scattering is isotropic $Q_D = Q$.

These three cross-sections describe completely an electron-molecule collision.

1.3 Measurement of collision cross-sections:

Total collision cross-sections were first studied at the beginning of this century and the first quantitative results were obtained by Ramsaver (1) in an elegant electron beam experiment. His technique was used in the 1930s to study cross-sections in a wide variety of gases - see for example references (2, 3) - and has recently been employed with higher resolution by Golden and Bandel (4).

Electron swarm techniques, originally developed by Townsend (5), have been extensively utilised for the study of total collision cross-sections. They are particularly useful at very low electron energies where electron beam techniques are not applicable. A discussion of the experimental methods, results and theoretical interpretation of total collision cross-sections at low electron energies will not be given here. Accounts of the work can be found in references (6, 7, 8, 9) and references therein. Since this thesis is concerned with the inelastic scattering of electrons with sufficient energy to cause electronic excitation of atoms and molecules the measurement of cross-sections for these processes will be considered in more detail.

Measurement of inelastic collision cross-sections

We saw above that the total collision cross section can be subdivided

into a sum of the elastic collision cross-section and inelastic cross-sections for the various possible excitation processes, i.e.

$$Q_T = Q_{elastic} + \Sigma Q_{inelastic}$$

The experimental measurement of the separate inelastic collision cross-sections requires high resolution and electron beam techniques must therefore be used. Absolute measurement of collision cross-sections is very difficult and early results, obtained by indirect methods are often unreliable. However measurements of the variation of cross-sections with electron energy, and the relative magnitude of cross-sections for different transitions, are much easier.

(1) Measurement of the excitation function by optical methods:

This involves the bombardment of a gas or atomic beam with a beam of electrons, followed by measurement of the intensity of some known part of the optical radiation as a function of incident electron energy. Care must be taken in the analysis of the results to allow for population of the states by a collisional mechanism, cascading effects, and reabsorption of the emitted radiation, although these become less important at low pressures. The method is not easily applicable to the study of metastable states.

(2) Measurement of the intensity of spectral lines from a gas discharge:

The complication in the analysis of data obtained by observing the intensities of lines emitted from a gas discharge are so great that the method is very inferior to electron beam techniques. However it does permit the study of electron impact with excited atoms.

(3) The study of metastable states by detection of metastable atoms:

(a) On impact with a metal surface metastable atoms with sufficient internal energy will cause an electron to be ejected from the surface. Metastable states formed during collision with an electron beam can be detected by measuring the ejected electron current, if suitable precautions are taken. The rare gases and mercury have been studied in this way.

(b) Metastable atoms have large absorption coefficients for light of a wavelength suitable to raise them to higher states. The intensity of absorption can give a measure of the population of the metastable states.

(4) Experiments involving measurement of the kinetic energy losses of the colliding electrons:

Such experiments provide the most direct measurement of excitation cross-sections, and with modern techniques of electron energy analysis they have assumed great importance. The various methods used will be discussed in more detail in a later section.

Again accounts of the above techniques and the results obtained can be found in references (6, 7, 8).

1.4 General Features of inelastic cross-sections for atoms and molecules:

(1) Excitation of Atoms:

$$A + e \longrightarrow A^* + e \qquad (1)$$

$$A + e \longrightarrow A^+ + 2e \qquad (2)$$

We are here concerned only with process (1).

Three clearly marked types of excitation function have been observed. The first type is characteristic of excitation to states which

FIG 1 VARIATION OF COLLISION CROSS SECTIONS WITH ELECTRON ENERGY

(a) $1s \rightarrow 2p$ transition in H : ref 11

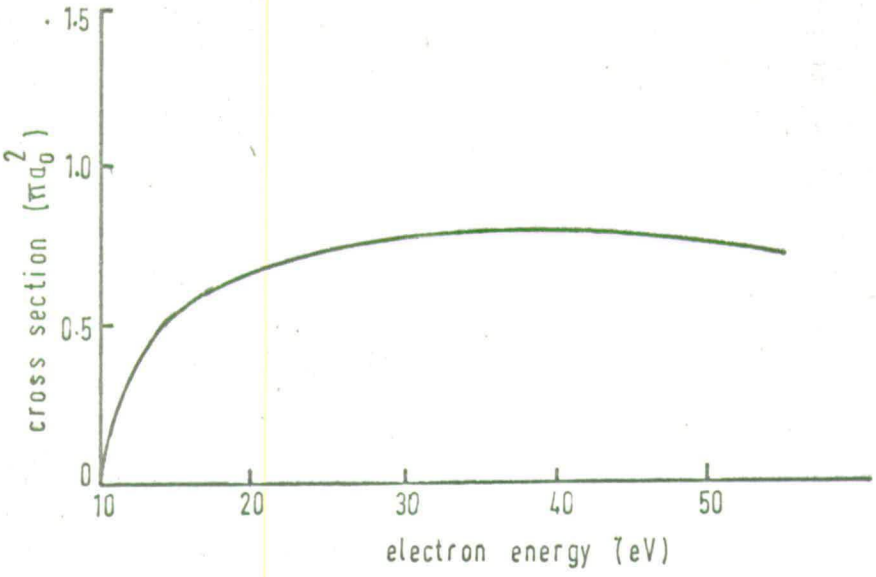

(b) $1^1S \rightarrow 3^3S$ transition in He : ref 12

(c) $1^1S \rightarrow 3^1S$ transition in He : ref 12

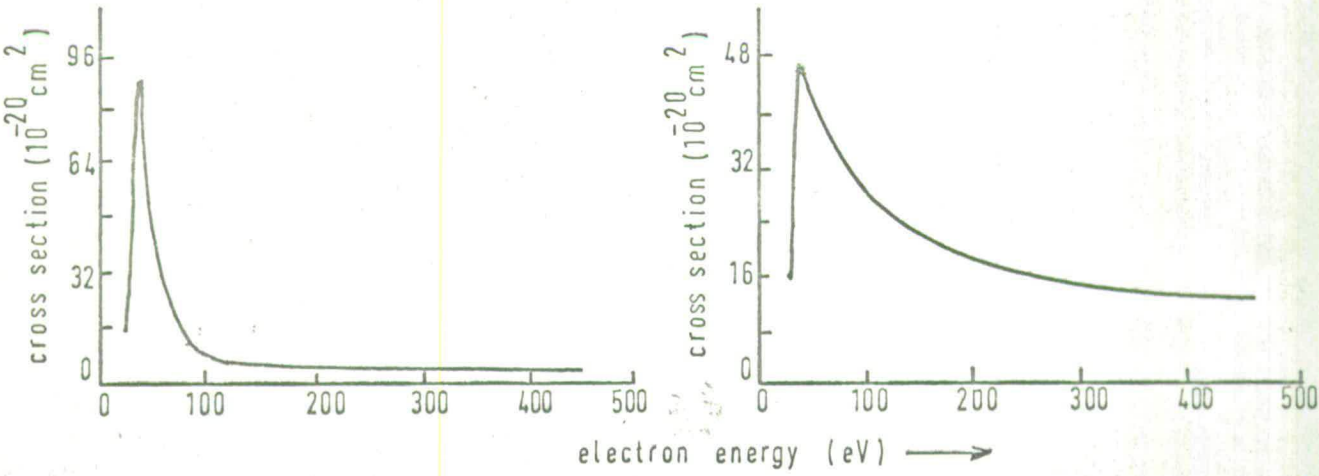

combine optically with the ground state; for example the $^1s \rightarrow 2p$ transition in hydrogen (Fig. 1a). The cross-section rises to a broad maximum at energies four to five times the threshold energy, and then decreases slowly with increasing electron energy.

Transitions involving a change in multiplicity show a different type of excitation function (Fig. 1b). The cross-section rises to a much sharper maximum just above the threshold and decreases to very small values at higher electron energies.

An intermediate type of excitation function is found for transitions which are optically 'forbidden' but involve no change in multiplicity, for example the $1^1S - 3^1S$ transition in helium (Fig. 1c).

This rather arbitrary classification of states according to the optical selection rules appears to have fairly general applicability.

A comparison of the relative probabilities of the three types of transition is shown in Fig.(2) for helium. In general high electron energies cross-sections for optically allowed transitions are larger than those for any others and cross-sections for transitions involving a change in multiplicity are large only, if at all, at energies near the threshold.

Mohr and Nicoll (10) investigated the angular distribution of electrons scattered inelastically from He, Ar, and Hg for angles between 20 and 160°, and incident energies from 23 to 196 volts. Some of their results are shown in Fig. (3). At all energies the curves fall off very rapidly with angle at small angles, but for lower energy electrons they level off at large angle.

(2) Excitation of molecules:

Inelastic collisions of electrons with molecules can lead to far more complex results than collisions with atoms. Vibrational and rotational

FIG 2 COMPARISON OF CROSS SECTIONS FOR OPTICALLY ALLOWED AND OPTICALLY FORBIDDEN TRANSITIONS IN HELIUM

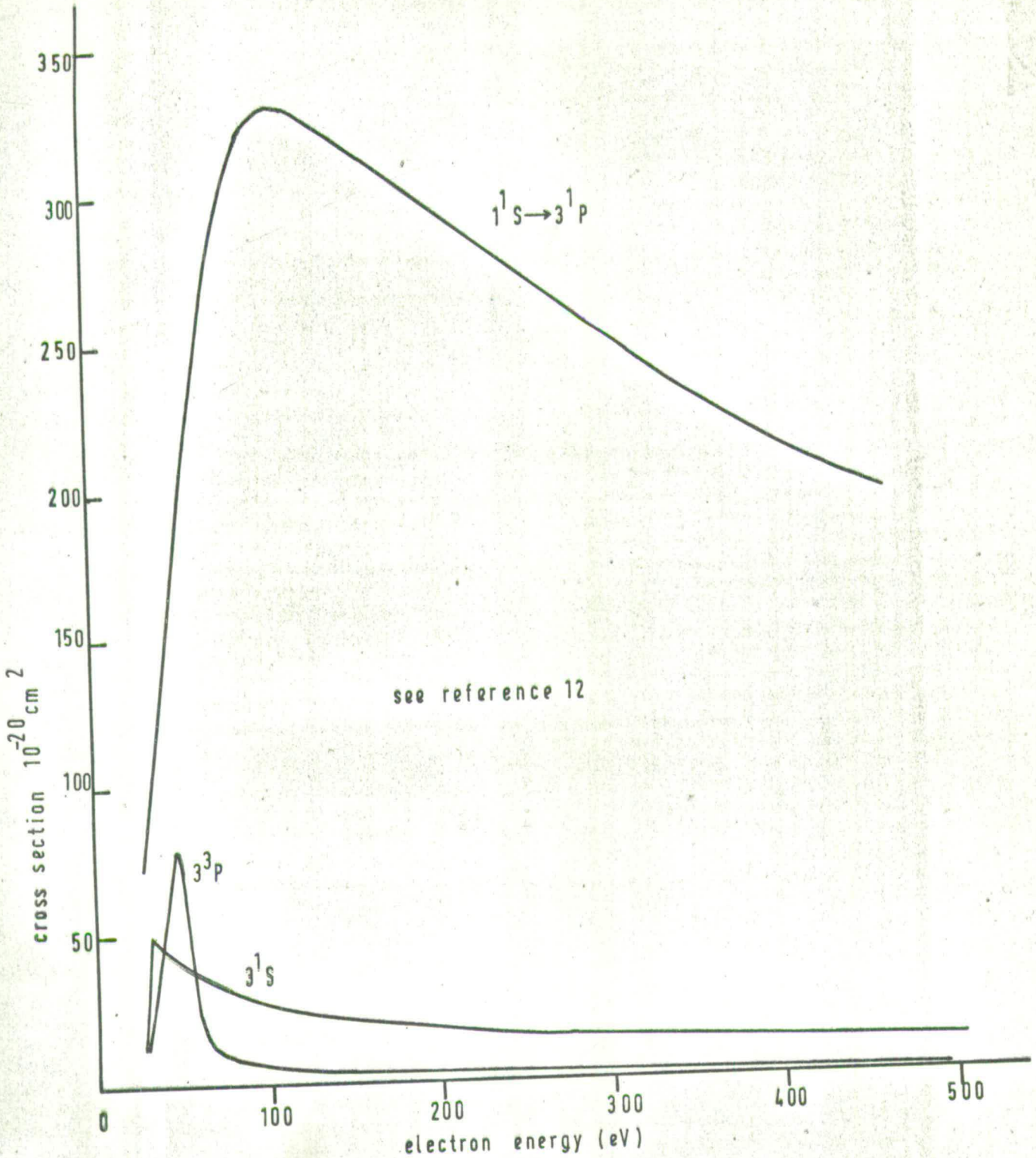

FIG 3 EXPERIMENTAL ANGULAR DISTRIBUTION OF ELECTRONS SCATTERED INELASTICALLY FROM HELIUM

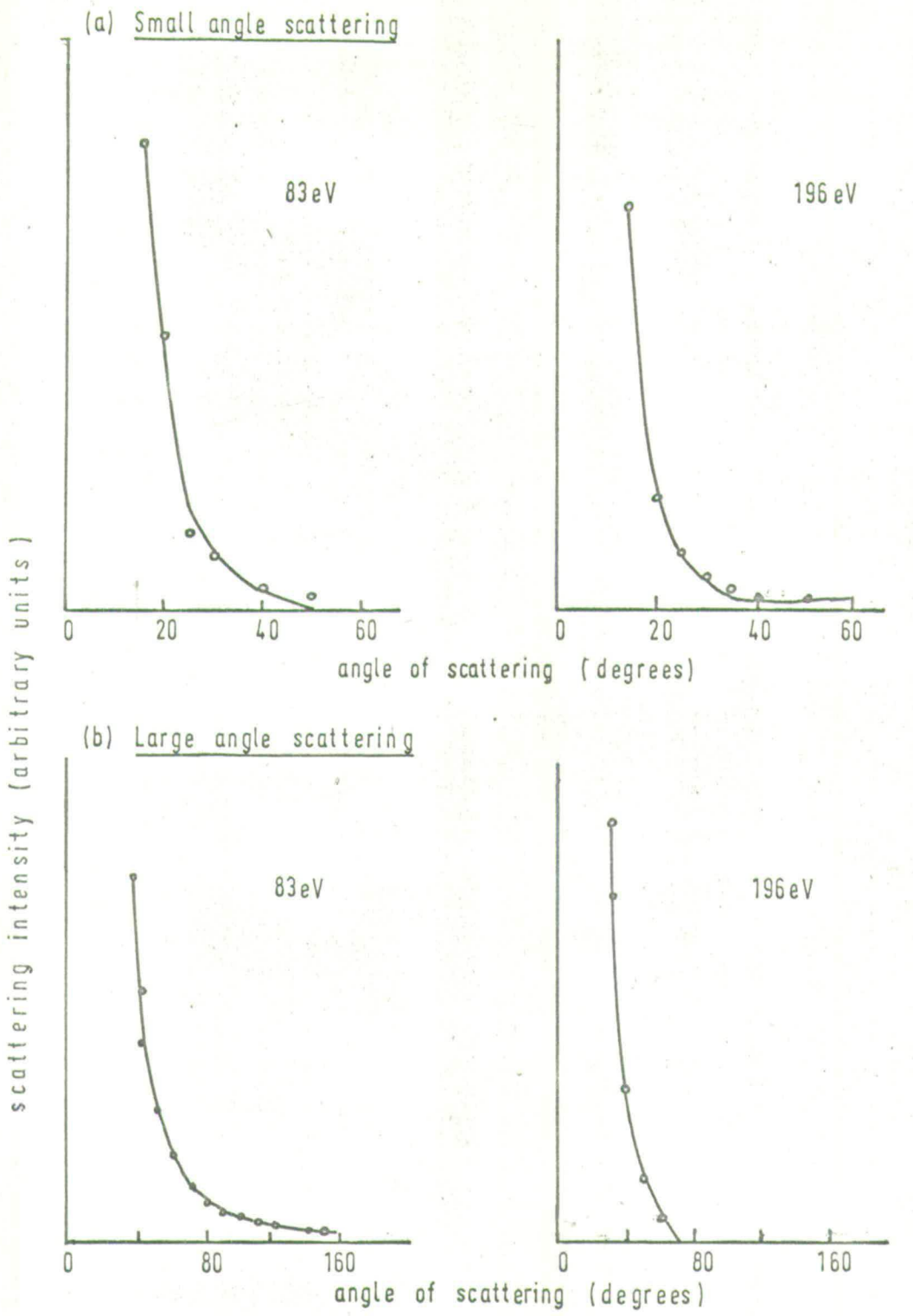

excitation can occur as well as electronic excitation, and many types of dissociative processes are possible. It is simplest to consider a diatomic molecule:

$$
\begin{aligned}
AB + e &\longrightarrow AB^{1} + e \\
&\longrightarrow AB^{*} + e \\
&\longrightarrow AB^{+} + 2e \\
&\longrightarrow A^{*} + B^{*} + e \\
&\longrightarrow A^{+} + B^{-} + e \\
&\longrightarrow A + B^{+} + 2e \qquad \text{etc.}
\end{aligned}
$$

AB^{1} denotes a vibrationally or rotationally excited molecule, AB^{*} one which is electronically excited.

Since the mass of the electron is so much smaller than that of the nucleus, and it therefore moves much faster, it is possible to neglect nuclear motion when calculating the electronic energy of a molecule (the Born-Oppenheimer approximation). Potential energy curves can then be constructed for each electronic state of the molecule, some showing a more or less deep minimum (bound molecular states) and others no minimum at all (unbound molecular states). Again based on the fact that electronic motion is so much faster than nuclear motion, the Franck - Condon principle asserts that transitions between states may be represented by vertical lines on the potential energy diagrams. Fig. (4) illustrates four possible types of transition. (1) and (2) lead to dissociation of the molecule, (3) to an upper electronic state in the ground vibrational level, and (4) to a vibrationally excited upper electronic state. The lines are drawn from the position of maximum probability for an electron in the ground state to the state for which the overlays integral - $\int \psi_1 \psi_2^{*} \, d\tau$ - is a maximum. ψ_1 and ψ_2 are the wave functions of the two states.

For polyatomic molecules no such simple geometric representation can be given.

FIG 4 FRANCK-CONDON DIAGRAMS FOR ELECTRONIC TRANSITIONS IN DIATOMIC MOLECULES

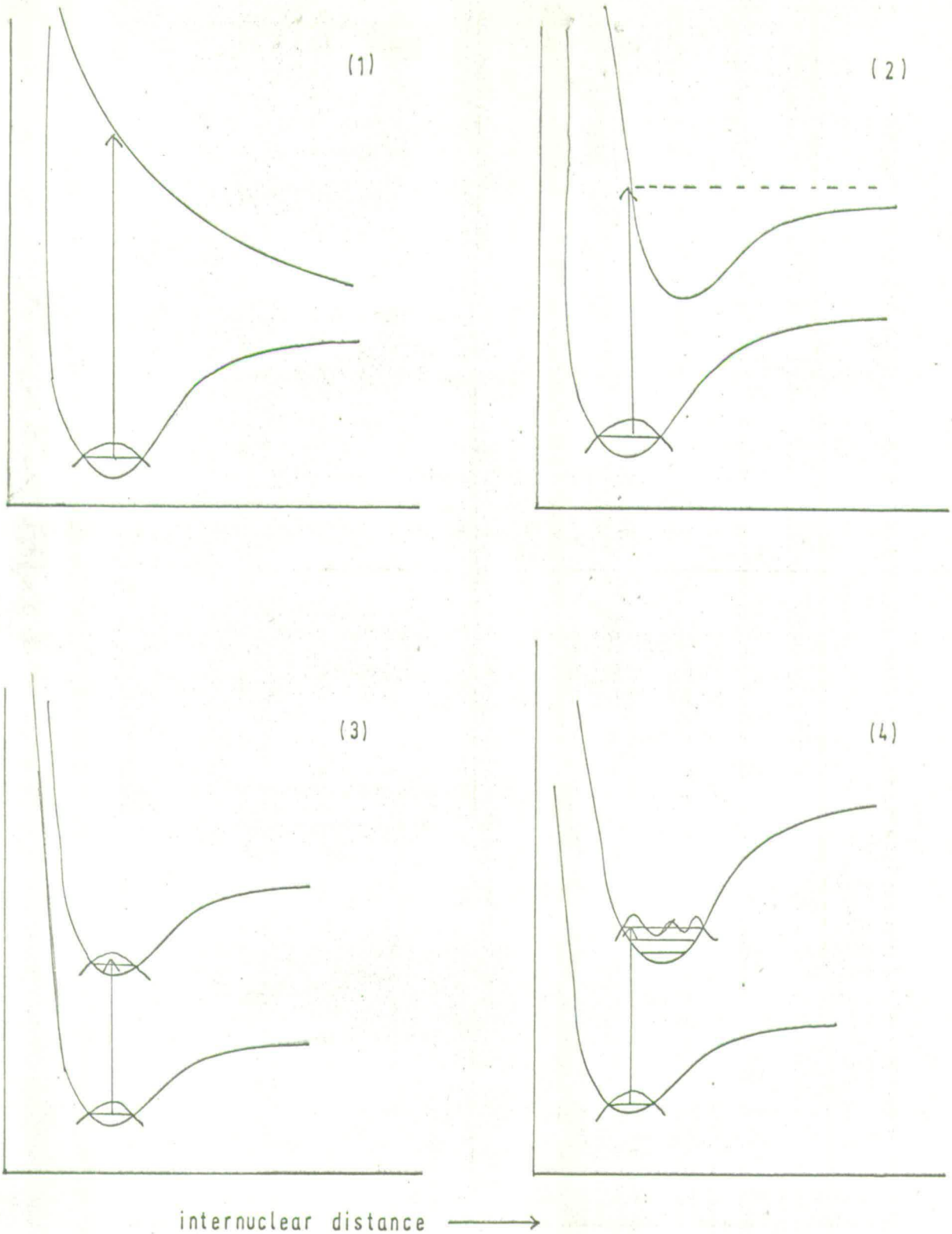

Excitation of molecules has been studied by many of the techniques used for atoms, and in general the cross-sections show the same type of behaviour. A discussion can be found in reference (14).

Rotational excitation:

Rotational excitation of molecules by electrons can occur because of the long range nature of the interaction between the electron and the molecule. Thus electrons with the necessary angular momentum can interact sufficiently strongly with dipolar or quadrupolar molecules to cause rotational excitation. Cross-sections have been deduced from electron swarm experiments but comparatively little is known about them. (7,15).

Vibrational excitation:

The 'direct' vibrational excitation of molecules by electrons is ruled out by the principle of conservation of momentum. However Haas (16) found energy losses corresponding to the vibrational excitation of N_2 and more recently Schulz (17) confirmed that vibrational excitation does occur. His results for N_2 are shown in Fig.(5). The mechanism for vibrational excitation involves the formation of a temporary negative ion state, a 'resonance' state, 2.3 eV above the ground state, which then decays to upper vibrational levels of the ground state. Many resonance states have since been observed by numerous authors in a wide variety of gases. An account of much of the work on resonances, and a rationalisation of the results can be found in reference (18).

Recently Takayanagi (19, 20) has cast some doubt on the first statement of this section that direct vibrational excitation is not possible and has shown theoretically how such a process can occur at low electron energies.

FIG 5 THE ELECTRON IMPACT SPECTRA OF NITROGEN OBTAINED BY SCHULZ

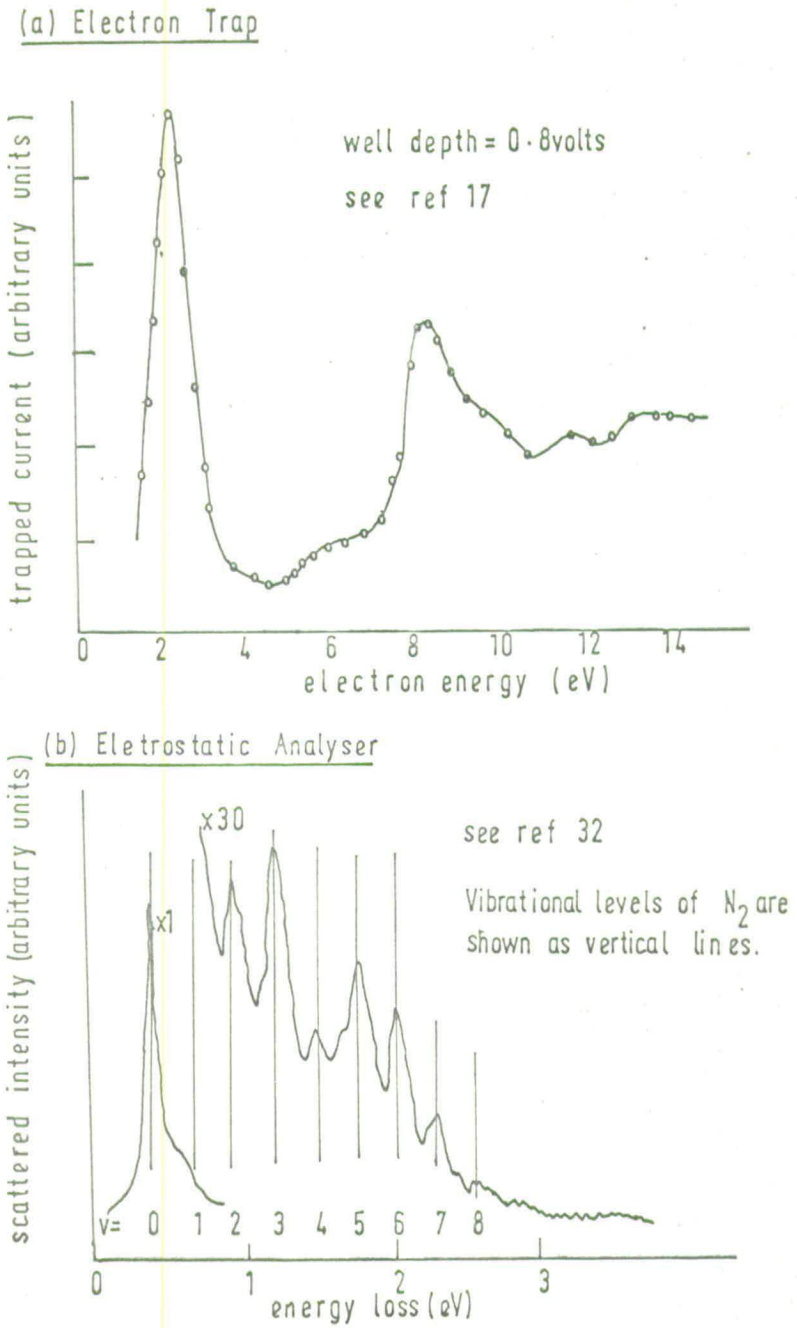

1.5 The theory of electron-molecule collisions:

The theory of electron-molecule interactions is more complicated than that of either molecule-molecule interactions, or of the interaction of molecules with radiation. In the present case both the source of excitation, the electron, and the excited species, the molecule or atom, must be treated in a fully quantum mechanical manner.

An extensive account of the theory is by Mott and Massey (21), and a very brief summary will be given here. The derivation of the exact formula for $f(\theta)$, the scattering amplitude, is given because it illustrates the manner in which the problem must be approached.

The incident stream of electrons, travelling along the z axis with velocity v is regarded as a plane wave, wavelength λ, having the form

$$e^{ikz} \quad ; \quad k = mv/\hbar \quad ; \quad \hbar = h/2\pi$$

The incident wave will be scattered by the atom or molecule giving rise to a spherical scattered wave, and the amplitude of the scattered wave at the point (r, θ, ϕ) is given by

$$f(\theta)\, e^{ikr}/r$$

Calculation of $f(0)$ gives the number of electrons scattered into a given solid angle per unit time, the differential cross-section being

$$I(\theta) = \left| f(\theta) \right|^2$$

If we consider the simplest case of scattering by a spherical potential $V(r)$, the Schrodinger equation is written

$$\nabla^2\psi + \left[k^2 - U(r)\right]\psi = 0 \qquad 1.7$$

$$U(r) = V(r).\, 2m/\hbar^2.$$

At large distances from the scattering centre the solution ψ must represent an incident plane wave and an outgoing spherical wave.

$$\psi \simeq e^{ikz} + f(\theta)\, e^{ikr}/r \qquad 1.8$$

To obtain the solution ψ is expanded in a series of Legrendre polynomials. The general solution of 1.7 having axial symmetry is

$$\psi = \frac{1}{r} \sum_{l=0}^{\infty} A_l P_l(\cos\theta) L_l(r) \qquad 1.9$$

where the A_l are arbitrary constants, and $L_l(r)$ are any solutions of the equation

$$\frac{1}{r^2} \frac{d}{dr}\left(r^2 \frac{dL_l(r)}{dr}\right) + \left\{k^2 - U(r) - \frac{l(l+1)}{r}\right\} L_l(r) = 0 \qquad 1.10$$

so chosen that ψ remains everywhere finite. The particular solution of 1.10 remaining finite at the origin is

$$(C/r) \sin\theta\, (kr - ln/2 + \eta_l) \qquad 1.11$$

C is an arbitrary constant and η_l the phase shift introduced into the spherical wave by the scattering process is dependent on k and U(r). It can be shown that

$$\psi = \sum_{l=0}^{\infty} (2l+1)\, i^l\, e^{i\eta_l} L_l(r)\, P_l(\cos\theta) \qquad 1.12$$

representing the incident and scattered wave, and since we have $f(\theta).e^{ikr}/r$ for the asymptotic form of the scattered wave, then

$$f(\theta) = \frac{1}{2ik} \sum_{l=0}^{\infty} (2l+1)(e^{2i\eta_l} - 1) P_l(\cos\theta). \qquad 1.13$$

and $$I(\theta) = \left|f(\theta)\right|^2$$

$$Q = 2\pi \int_0^{\pi} I(\theta) \sin\theta .\, d\theta$$

We have thus arrived at an expression which allows theoretical calculation of the collision cross-section. However the exact expression for $f(\theta)$ is extremely difficult to evaluate for all but the simplest systems,

and various approximations have been developed, valid under differing conditions of electron energy. The most thoroughly investigated case is that of scattering of high energy electrons where the Born approximation holds.

The Born Approximation:

The treatment is based on the assumption that the distortion of the incident wave by the atomic field is small, i.e. that all the phase shifts are small. Making use of Green's function it can be shown that

$$\psi \simeq e^{ikz} - (e^{ikr}/r) \int e^{-ik\underline{n}.\underline{r}^1} U(\underline{r}^1)\, \psi(\underline{r}^1)\, d\tau \qquad 1.14$$

where $\underline{n}$ is a unit vector in the direction $\underline{r}$ (the direction of scattering). The Born approximation says that $\psi(\underline{r}^1)$ may be replaced by the unperturbed wave function $\psi = e^{ikz}$. We then obtain for $f(\theta)$

$$f(\theta) = -(1/4\pi) \int \exp(ik(\underline{n}_o - \underline{n}).\underline{r})\, U(\underline{r})\, d\tau \qquad 1.15$$

$\underline{n}_o$ is a unit vector along the z axis such that $z = \underline{n}_o . \underline{r}$. Changing to spherical polar co-ordinates, and integrating over θ and ϕ gives

$$f(\theta) = -\frac{2m}{\hbar^2} \int_o^\infty \frac{\sin Kr}{Kr}\, V(r)\, r^2\, dr \qquad 1.16$$

$$K = k(\underline{n}_o - \underline{n})$$

This treatment is only valid for fast electrons.

Application to inelastic collisions:

Consider a collision of an electron with an atom in which the atom is raised from state m to state n by the impact. E_m and E_n are the energies of the two states, and v and v_{mn} the initial and final velocities of the colliding electron.

$$E_n - E_m = \frac{1}{2} m \left(v^2 - v^2_{mn}\right) \qquad 1.17$$

The differential cross section is

$$I_{mn}(\theta) = \frac{k_{mn}}{k} \left| f_{mn}(\theta) \right|^2 \qquad 1.18$$

Changing to momentum variables the following expression can be obtained

$$I_{mn}(K)\, dK = \frac{128 \pi^5 m^2 e^4}{k^2 h^4} \frac{dK}{K^3} \left| \int e^{ikx} \psi_m \psi^*_n \, d\tau \right|^2 \qquad 1.19$$

$$K = \left| k_{mn} \underline{n}_1 - k \underline{n}_o \right|$$

Expanding the exponential and integrating we obtain for the inelastic cross-section

$$Q_{mn} \frac{128 \pi^5 m^2 e^4}{k^2 h^4} \int_{K_{min}}^{K_{max}} \left(K^{-1} \left| x_{mn} \right|^2 + \frac{1}{4} K \left| (x^2)_{mn} \right|^2 + \cdots \right) dK \qquad 1.20$$

where $K_{min} = \left| k - k_{mn} \right|$

$K_{max} = \left| k + k_{mn} \right|$

x_{mn}, x^2_{mn} are the matrix elements of x, x^2 etc. such that

$$(x^s)_{mn} = \int \psi_m (x^s) \psi^*_n \, d\tau \qquad 1.21$$

For a transition associated with a dipole moment (optically allowed) the first term under the integral sign in 1.20 does not vanish, and is by far the greatest. Carrying out the integration gives

$$Q_{mn} \simeq \frac{64 \pi^5 m^2 e^4}{k^2 h^4} \left| x_{mn} \right|^2 \log \frac{2 mv^2}{E_n - E_m} \qquad 1.22$$

FIG 6 THEORETICAL ANGULAR DISTRIBUTION OF ELECTRONS SCATTERED ELASTICALLY AND INELASTICALLY FROM HELIUM

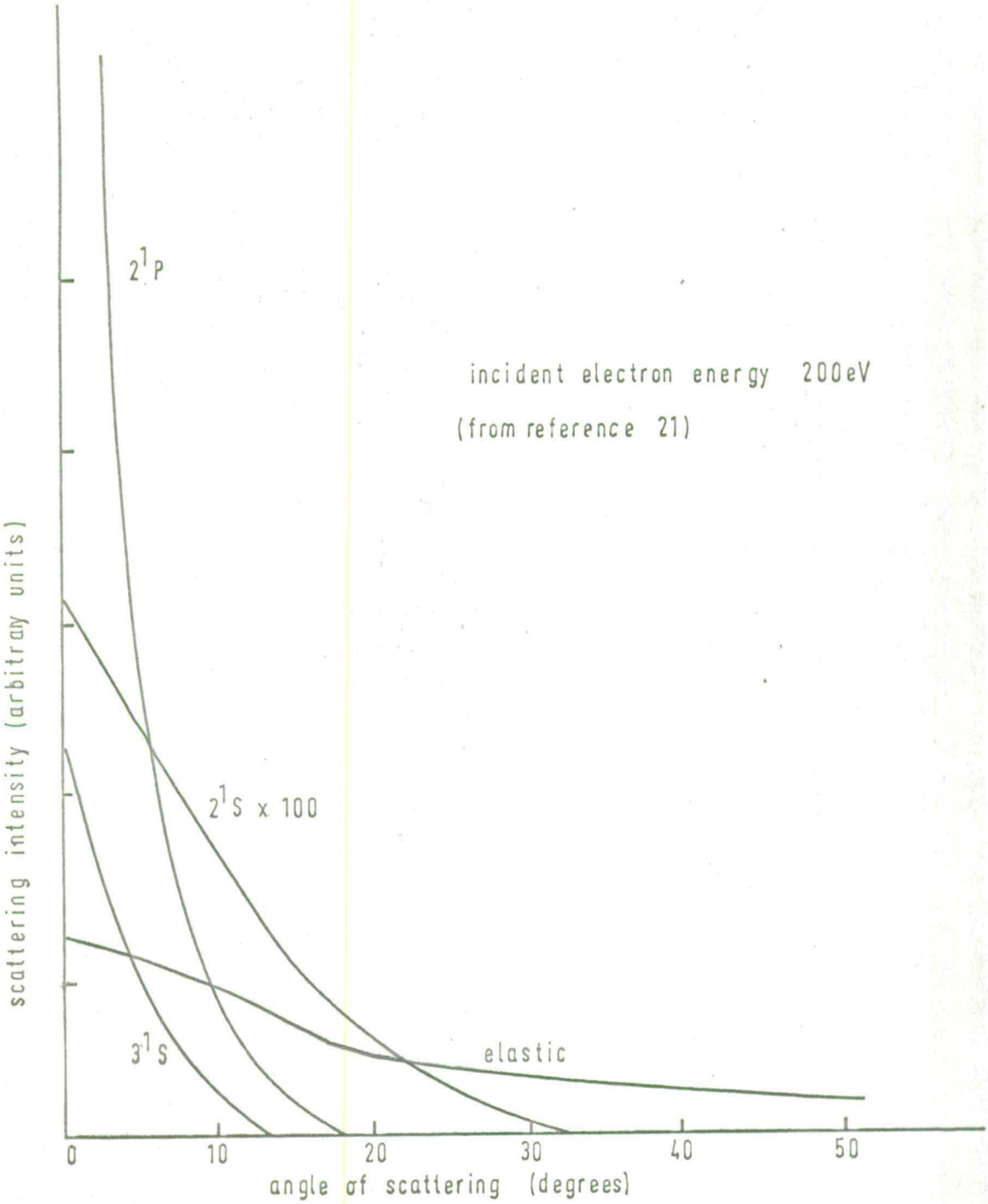

If the transition is associated with a quadruple rather than a dipole moment the first term vanishes and we obtain

$$Q_{mn} \simeq \frac{128\pi^7 m^2 e^4}{k^2 h^4} \left|(x^2)_{mn}\right|^2 \left|E_m\right| \qquad 1.23$$

Thus we can see that owing to the logarithmic term in 1.22 the cross-sections for optically allowed transitions fall off less rapidly with increasing electron energy than do those for optically forbidden transitions. The theory can therefore explain satisfactorily the observed variation with electron energy at relatively high energies. The predicted angular distribution of electrons scattered inelastically from helium is shown in Fig. (6) - of Fig. (3). Again the agreement with experiment is good at high energies.

In the above theory the probability of a transition involving a change in multiplicity is zero. Mathematically this is due to the symmetry properties of the wave function corresponding to states of different multiplicity so that the integral 1.21 always vanishes; physically to the impossibility of changing the total electron spin on impact. But it is the total spin of the atom or molecule plus the incident electron which must now be conserved. The possibility of electron exchange is neglected in the above treatment. Suppose the initial molecular electron spin is $s\hbar$, so that the multiplicity is $2s + 1$, the total spin of incident electron plus molecule is $(s \pm \frac{1}{2})\hbar$. If the excited state has spin $s^1\hbar$, making the total electron spin after collision $(s^1 \pm \frac{1}{2})\hbar$, then to conserve spin $s^1 \pm \frac{1}{2}$ must lie within $s \pm \frac{1}{2}$ i.e. $s^1 = s + 1$, or $s^1 = s - 1$. Thus when electron exchange is involved the multiplicity can change by ± 2. Exchange can of course occur without a change in multiplicity.

Electron exchange can be accounted for at high energies by the Born-Oppenheimer approximation (not to be confused with the previously mentioned Born-Oppenheimer approximation for neglect of nuclear motion). In a manner

similar to the Born approximation for the calculation of $f_{mn}(\theta)$, a scattering amplitude $g_{mn}(\theta)$ is calculated for the case when electron exchange takes place. The differential cross-section is then given by

$$I_{mn}(\theta) = \frac{k_n}{k_m} \left(\tfrac{1}{2} \left| f \right|^2 + \tfrac{1}{2} \left| g \right|^2 + \tfrac{1}{2} \left| f - g \right|^2 \right) \qquad 1.24$$

The agreement between theory and experiment has been most extensively studied for scattering from H and H_e for which good approximate wave functions are available, and therefore any errors in the predictions arise from failure of the scattering approximations and not from inadequate wave functions.

At low electron energies neither of the above approximations is valid and the theoretical treatment becomes much more complex. * Among the approximate methods which have been used are the distorted wave approximation, semi-classical approximations, effective range theory, and increasingly in recent years variational methods have been employed.* No general method of practical usefulness can be developed when the Born approximation is not valid*. The most successful treatments, such as variational methods, are too complex to discuss in detail here but a full account can be found in reference (21).

We will now summarise those properties of inelastic cross-sections which are well established on both theoretical and experimental grounds.

(1) At electron energies far above the threshold all inelastic cross-sections decrease with increasing electron energy. For optically allowed transitions this decrease is slower than for optically forbidden ones, and for transitions involving a change in multiplicity it is very rapid indeed.

(2) At electron energies where exchange is unimportant the cross-sections for optically allowed transitions are much greater than those for any others. Less information is available in the region where exchange is important.

(3) In the energy range where exchange is unimportant the differential cross-sections decrease very rapidly with increasing angle.

(4) When exchange is important the angular distribution is much more uniform.

One of the most interesting properties for the chemist of excitation by electron impact is the possibility of causing transitions to states of different multiplicity. As we have seen, at high energies the probability of such excitation is negligible, except where spin orbit coupling is significant. But at lower energies transitions involving changes in multiplicity may take place quite readily, and at some energies may occur with greater probability than excitation to a level of the same term series. For light atoms electron exchange is the only mechanism by which transitions between states of different multiplicity can occur.

Exchange will be predominant under conditions for which the Born approximation is least likely to hold. These are conditions of low electron energy (<100 eV.) and high scattering angle. It was decided to investigate the scattering of electrons under such conditions with the hope that spin forbidden transitions would be seen.

As we saw before the most satisfactory methods for studying optically forbidden transitions involve the measurement of the kinetic energy losses of the scattered electrons. The various techniques which have been employed will now be reviewed in more detail.

FIG 7 SCHEMATIC DIAGRAM OF A TYPICAL ELECTRON TRAP (a), AND THE POTENTIAL DISTRIBUTION AT THE AXIS OF THE TUBE, (b).

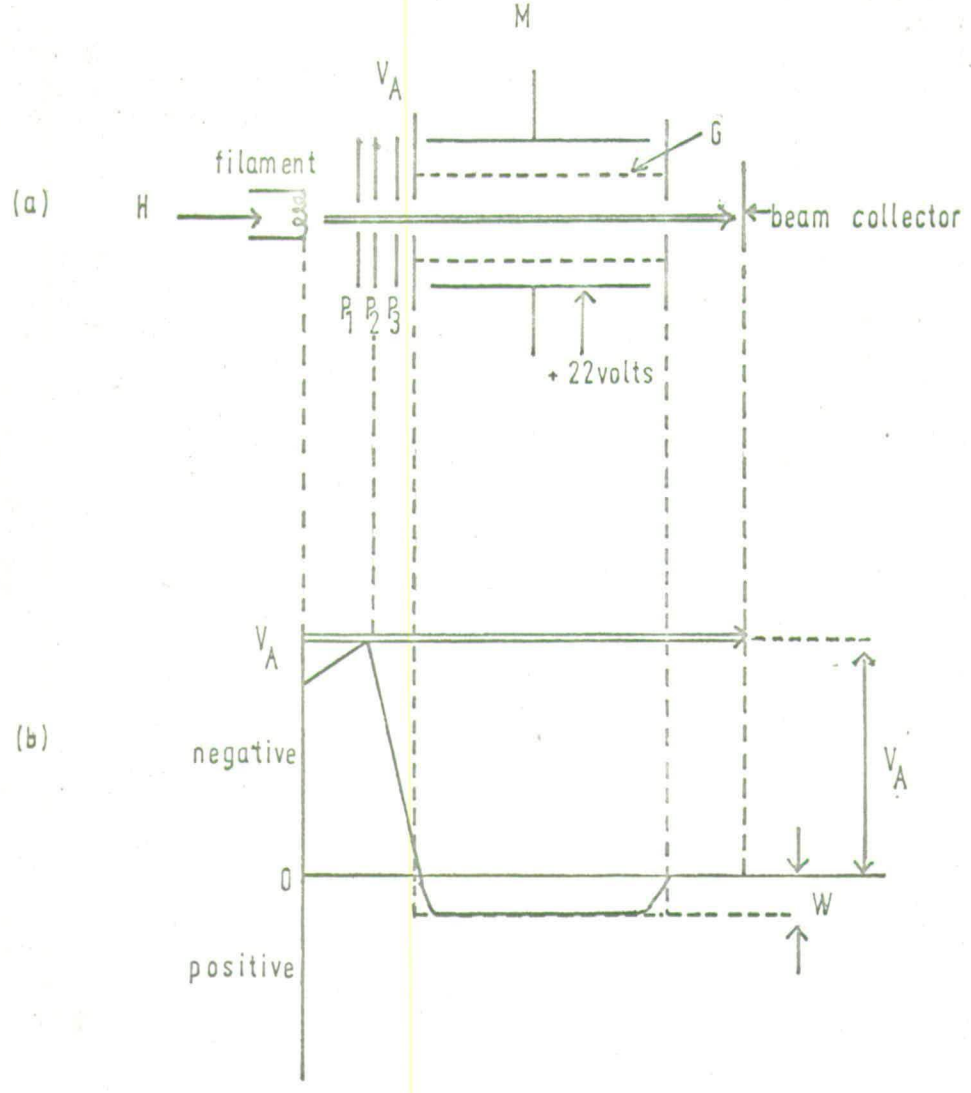

1.6 Electron beam experiments:

In electron beam experiments a monoenergetic beam of electrons is passed through a gas under such conditions of gas pressure and electron path length that no electron makes more than one collision with a gas molecule. Under these conditions of course most electrons make no collisions at all, and the observable effects are small. Maiér-Liebnitz (22) conducted one of the first of such experiments, in which electrons were accelerated from a filament and allowed to diffuse outwards through a gas in cylindrical symmetry. After passing through a grid the electrons were collected at a cylindrical collector to which was applied a potential sufficient to repel those electrons which had suffered inelastic losses. He obtained cross-sections for electronic excitation in the inert gases and observed vibrational excitation in N_2 and H_2.

A more refined technique has been developed by Schulz in his 'trapped electron' experiment.

The Electron Trap:

A typical electron trap is shown in Fig. (7). Electrons from the filament, aligned by the magnetic field H, traverse the electron gun into the collision chamber. The cylindrical grid G is surrounded by a cylindrical collector M. To M is applied a potential 22 volts positive with respect to G, of which 0.3 volts penetrate to the axis of the tube. Thus the well depth is 0.3 volts. Electrons in the beam making inelastic collisions and losing all but 0.3 volts or less of their energy are trapped in the well and reach the collector M. The incident electron energy is selected by a retarding potential difference method. Electrodes P_1 and P_3 are at a potential positive with respect to the filament and draw current from it. P_2 is at a potential V_A negative with respect to the filament, providing a potential barrier

surmountable only by the higher energy electrons. If V_A is increased to $V_A + \Delta V_A$ the difference in the trapped current results from electrons in the voltage interval ΔV_A. By measuring the trapped current at different electron energies one can estimate the probabilities of inelastic losses as a function of energy.

In addition to the inelastically scattered electrons, there are two other contributions to the trapped current.

(1) Negative ion formation:

This can be accounted for since the negative ion current can be measured separately by reducing the potential between M and G so that no electron trapping occurs.

(2) Elastically scattered electrons:

At near zero accelerating voltages elastically scattered electrons have an isotropic angular distribution. Thus the scattered electrons may have insufficient axial velocity to escape from the trap. At these voltages it requires a very improbable subsequent collision to direct the electrons out of the trap, but at higher energies escape becomes more probable and the elastic contribution to the trapped current disappears. Schulz therefore does not measure trapped currents below 1 eV.

Using the electron trap he has investigated inelastic processes in N_2 (23, 24), O_2 (25), CO(23, 24), N_2O (26), H_2O (27) and H_2 (24).

The Double Electrostatic Analyser:

Electrons of velocity u entering a radial, inverse first power, electrostatic field describe circular orbits of radius r provided that they enter perpendicular to the lines of force, and that u is related to the field strength x at each point of the orbit by

$$m_e u^2 / r = - x_e$$

Electrons of the same velocity entering at $\pm \alpha$ degrees to the lines force describe non circular orbits which recross the circular arc at

$$\Phi = \pi/\sqrt{2} = 127^\circ 17^1 \quad \text{(Fig.)}$$

A focussing electron energy selector may therefore be built with entrance and exit slits separated by the angle Φ. A treatment of the focussing properties is given by Hughes and Rojansky (28). More recently the 127° analyser has been investigated by Clarke (29) and Marmet and Kerwin (30).

Schulz (31, 32) has used two 127° analysers in an S configuration to study the vibrational excitation of N_2. The energy-selected beam from the first analyser passes through a gas filled collision chamber and electrons scattered in a given direction, after traversing the second analyser, are collected at a shielded electron collector. This technique, although more refined in that it enables electron energy losses to be measured directly, is less sensitive than the electron trap and can only be used when the inelastic cross sections are high. His study of the vibrational excitation of N_2 showed that this involves the formation of a temporary negative ion state.

Simpson (33) and other workers (34, 35) have used velocity analysers of the hemispherical and 127° variety. Much of their work has been devoted to the study of the sharp resonance peaks which occur in the collision cross-sections. These are thought to be due to the formation of unstable compound states of the atoms or molecules and electrons, and as stated above, are important in the excitation of vibrational states of molecules by electron impact.

FIG 8 DIAGRAM OF LASSETTRE'S APPARATUS

For full details see ref 45

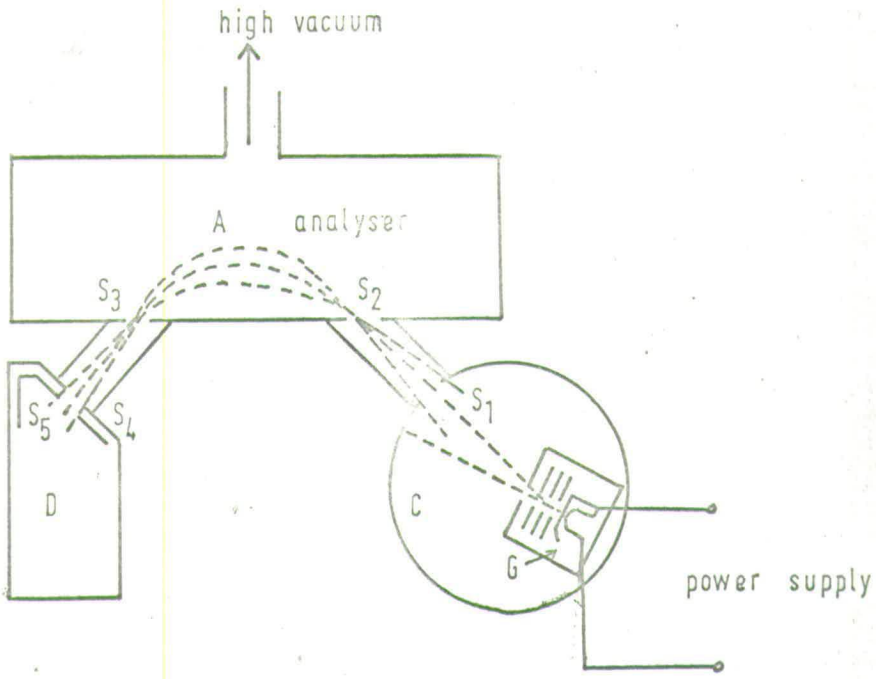

C — collision chamber

G — electron gun

A — 127° electrostatic analyser

D — detector

Electron Impact Spectroscopy:

At high incident electron energies and low scattering angle, where the Born approximation, is obeyed, electron impact spectra should correspond with optical spectra (ref. 21, chapter 16). Van Atta (36) working in the energy range 100 - 300 e.V. found no evidence of optically forbidden transition in He, Ne and Ar. Other early studies of H_2 (37, 38), N_2 (39, 40), CO (41), CO_2 (41) and H_2O (42) conducted by a variety of techniques, revealed no evidence of excitation of optically forbidden transitions at kinetic energies greater than 100 e.V.

Recently Lassettre and his collaborators, in an elegant series of experiments, used an electron impact spectrometer to study electronic excitation cross-sections for electrons in the energy range 300 - 600 e.V. Their apparatus, Fig. (8), consists of an electron gun G, producing an electron beam of variable energy, and a collision chamber C with a pair of slits S_1 and S_2 determining the direction of the scattered electrons reaching the detector. This is a 127° analyser followed by an electron multiplier. For full details see reference (45). Lassettre and co-workers have used this apparatus to study scattering at zero degrees, and in some cases up to angles of 15°, enabling them to test the theoretical predictions over a wide range of conditions. The substances which they have studied are listed: helium (43, 45, 46, 50, 51, 68), hydrogen (43, 44), methane (43), ethane (43), cyclohexane (43), ethylene (43, 67), water (43, 54, 62, 65), carbon monoxide (45, 48, 53, 66), nitrogen (47, 54, 55, 56, 57, 63, 64, 69), ammonia (54), benzene (54), carbon dioxide (58, 60), acetone (59) and 2-butanone (59). This is the most extensive study of inelastic losses of high energy electrons, and the results obtained are in good agreement with theoretical predictions. Lassetre's work was restricted to high electron

energies, and because of intensity problems he could not study scattering at angles above 15°.

At lower electron energies (less than 100 e.V.) singlet-triplet transitions can be observed in electron impact spectroscopy because of electron exchange. The scattering of low energy electrons (4 to 180 e.V.) was studied by Arnot and Baines (70) who obtained total, elastic, and inelastic cross-sections for Hg. Womer (71) observed the $2^1S - 2^3S$ transition in helium. The method of Arnot and Baines has recently been further developed by Kuppermann and Raff (72, 73, 74).

The Kuppermann and Raff experiment:

Their apparatus is shown in Fig. (9). Electrons from the cathode C are accelerated by the gun through the pinhole P into the collision area. The scattered electrons are energy analysed by a retarding potential difference method using a series of cylindrical grids coaxial with the electron beam. The current at the cylindrical collector S is measured as a function of the maximum energy loss E of the scattered electrons. Differentiation of this curve gives a series of peaks corresponding to electronic transitions in the atoms or molecules. Electrons scattered through angles from 22 to 112° reach the collector, 90° scattering being favoured. Kuppermann and Raff obtained spectra for He and Ar in the electron energy range 25 to 50 e.V. They also studied H_2 at 60 e.V., H_2O at 30 e.V. and ethylene at 40. 50, and 75 e.V. In many of these spectra spin forbidden transitions, and dipole forbidden transitions appeared with equal prominence to optically allowed transitions,

Since it appears that interesting and new information which would increase our understanding of molecular structure can be obtained by the study of low energy electron impact it was decided to start work at Edinburgh on

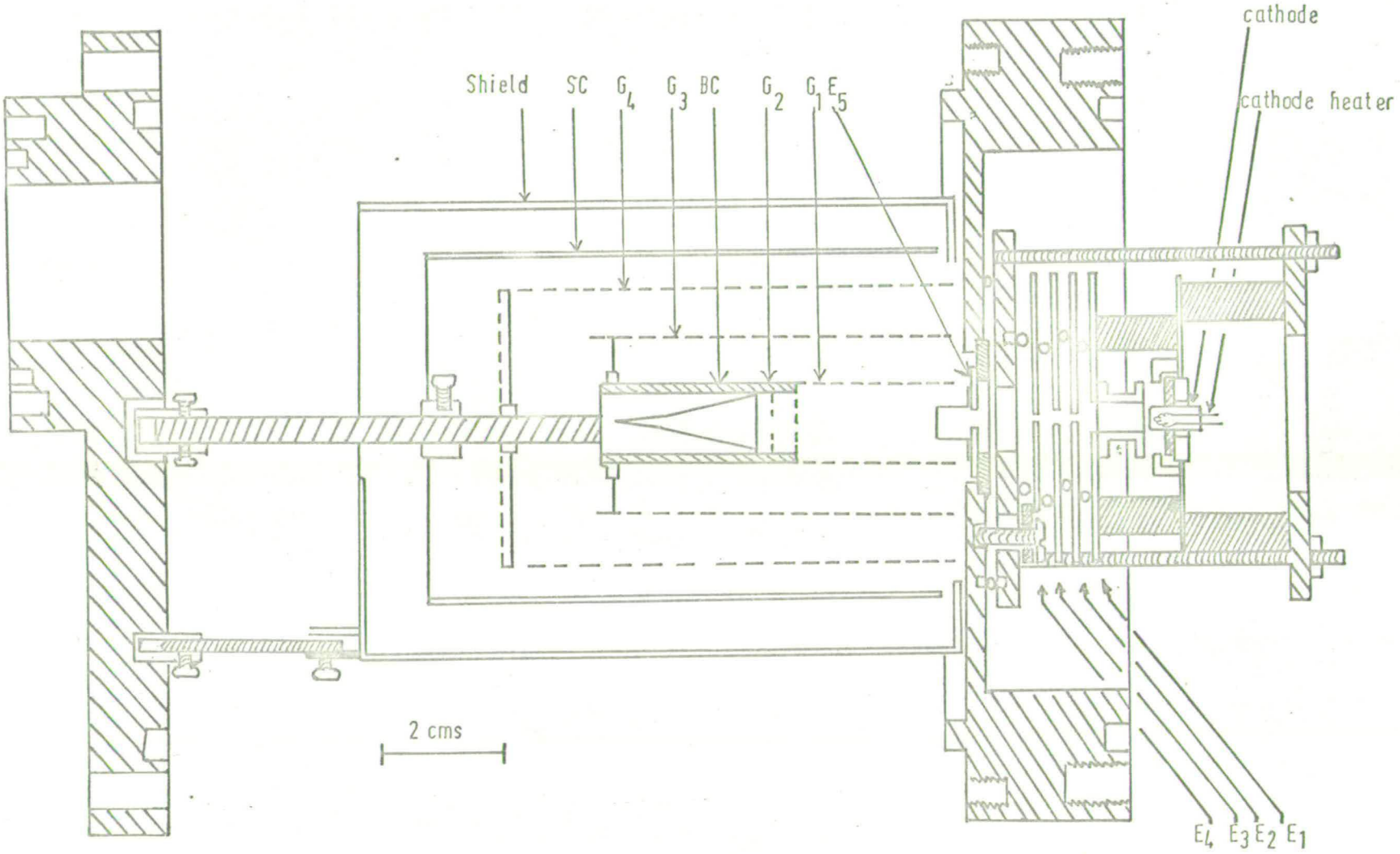

FIG 9. DIAGRAM OF THE KUPPERMANN AND RAFF APPARATUS : ELECTRON GUN AND COLLISION CHAMBER

both the electron trap, and an electron impact spectrometer of the Kuppermann and Raff type (75). The present work concerns the development of the electron impact spectrometer.

Chapter Two

EXPERIMENTAL

2.1 Description of Apparatus:

The apparatus, based on that of Kuppermann and Raff, was designed and tested by Dr. A.W. Read (76). It consists of two evacuated chambers connected by a small diameter pinhole. Electrons produced from an oxide coated cathode in one chamber are energy selected and focussed by the gun, pass through the pinhole, and collide with gas molecules flowing through the other chamber at pressures between 10^{-3} and 10^{-5} torr. The unscattered beam is collected at a Faraday cup. Electrons scattered through large angles pass through a series of cylindrical grids, are energy analysed by a retarding potential difference method, and collected at a cylindrical collector,

Previous experience with electron swarm devices at Edinburgh had shown that the better the ultimate vacuum before the gas flow is started, then the more reliable the results. This is because of the elimination of absorbed gases from the electrodes and grids. The vacuum system was therefore designed with the aim of achieving a rather better ultimate vacuum than the 3×10^{-7} torr obtained by Kuppermann and Raff. The stringent vacuum requirements demanded the exclusion of all materials unstable at high temperatures or low pressures, and for this reason no resins etc. were used in the support system for the electrode assembly. Also, in order to obtain the best possible ratio of scattered to background current, all magnetic materials were excluded from the system. The detailed design and construction of the electrode assembly was carried out by 20th Century Electronics. The general layout of the apparatus is shown in Fig.(10).

FIG 10 SCHEMATIC DIAGRAM OF THE APPARATUS

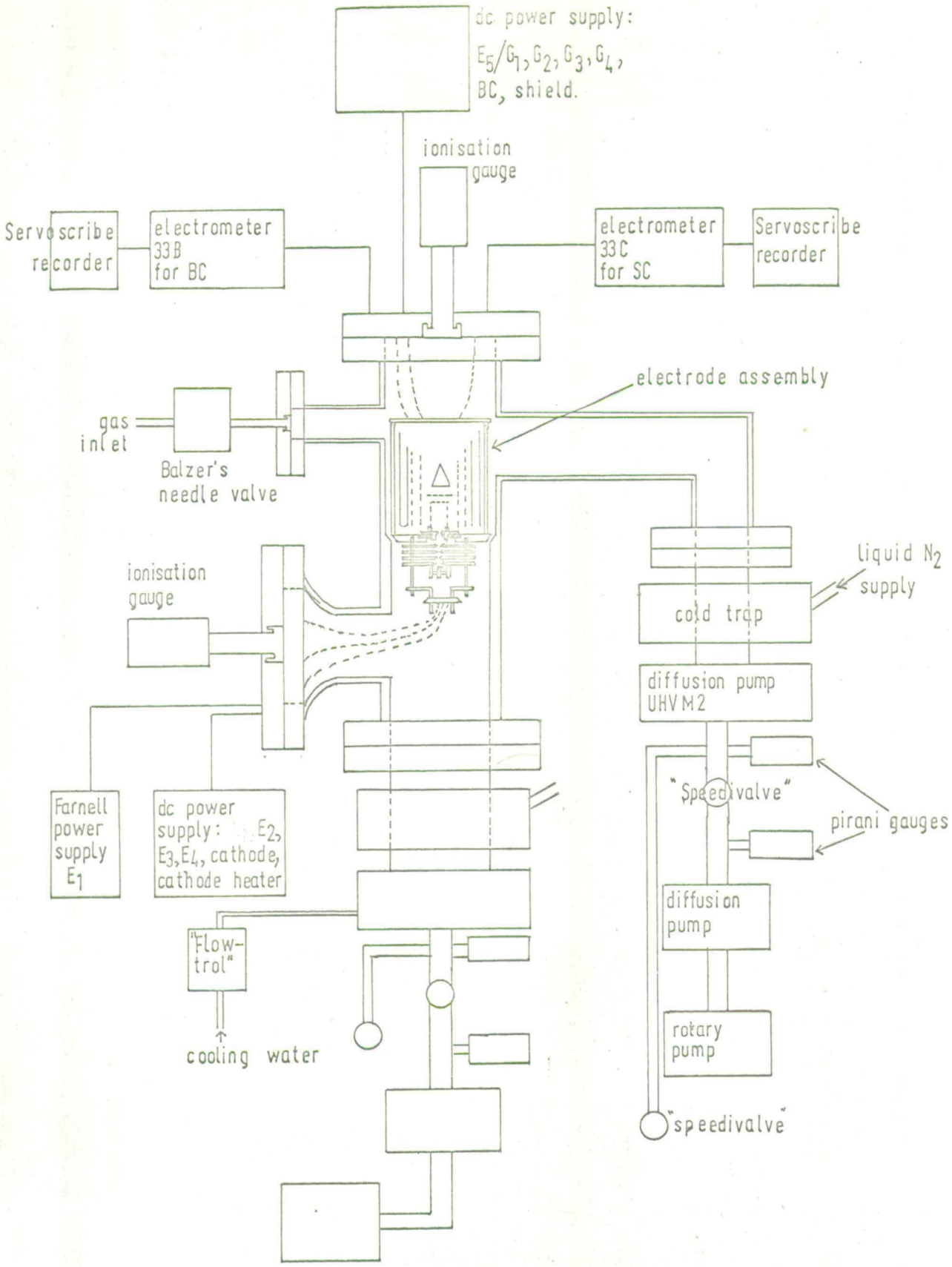

2.1.1. The Vacuum System:

The vacuum chamber is constructed from non-magnetic stainless steel of overall wall thickness $^1/_4$" , and internal diameter 4". The central steel plate of the electrode assembly (Fig. 11) rests on a small shelf in the centre of the chamber and separates the electron gun from the collision chamber, a connection being provided by the 1.5 m.m. diameter pinhole in E_5. Differential pumping of the two chambers is achieved by means of two Edwards U.H.V.M.2 pump groups, each consisting of a three stage mercury diffusion pump and trapping system. The trapping system is a lower chevron baffle, kept cool by a water-cooled thermoelectric element, and a Z baffle in contact with an annular N_2 reservoir which was filled by an automatic liquid N_2 dispensing system. This pumping system has a quoted maximum pumping speed at the inlet of 70 l/sec. for air. An interlock system provided protection against failure of the water or liquid N_2 supply, and against vacuum failure.

The backing line for each pump consists of a cold trap, single stage mercury diffusion pump, and a rotary pump. Two Edwards 'Speedivalves' connect the backing lines to the ultrahigh vacuum system and a further two inlets, also sealed by 'speedivalves', are provided for convenient leak testing of the system.

The collision chamber is connected via a right-angled stainless steel tube to a 5" diameter flange bolted to the inlet flange of one diffusion pump. The other pump is attached to the bottom of the gun chamber by a 7" diameter flange. Each chamber is fitted with a further 7" flange through which all the electrical connections are made, and the pressure is monitored by two ion gauge heads (Edwards Type IG3) at the centres of these flanges.

A conventional glass inlet line is connected to the ultra-high vacuum system through a Balzer's needle valve (Type U.V.8H). The differential screw mechanism of this valve allows fine adjustment of the gas flow rate through

the system. Gold 'O' rings were used for all vacuum seals in the ultra-high vacuum part of the assembly.

The main chamber and the upper parts of the diffusion pumps could be baked to about 250°C, although later in the experiment facilities were installed which allowed the chamber to be baked to 400°C. An ultimate vacuum of 2×10^{-8} torr was attained in both chambers; and the differential pumping arrangement permitted the pressure in the gun chamber to be kept at about 10^{-6} torr during measurements, when the pressure in the collision chamber rose to about 10^{-3} torr, successfully preventing contamination of the cathode.

2.1.2 The Electrode Assembly (Fig.11)

1. The Electron Gun:

The cathode and its heating element along with five planar electrodes constitute the electron gun. The cathode used is a modified 20th Century oxide coated cathode-grid assembly, indirectly heated by means of a filament rated at 6.3 volts, 0.5 amps. E_1 is constructed from 0.010" Ferry, the diameter of the central hole being 5 m.m., this relatively large hole allowing many electrons to reach the lens. E_2, E_3, and E_4 are of 0.040" Ferry having central holes 0.5 m.m. in diameter in the case of E_2 and E_4, and 1 m.m. for E_3. All four electrodes are 2" in diameter. E_5 is made of molybdenum with a central hole 1.5 m.m. in diameter through which the electron beam enters the collision chamber. It is mounted on the centre non-magnetic stainless steel plate from which it is insulated by a silica disc. The other electrodes are supported by alumina rods attached to the steel plate and separated from one another by ceramic spacers. The distances between the centres are: cathode - E_1 = 2 m.m., $E_1 - E_2$ = 3 m.m., $E_2 - E_3 = E_3 - E_4$ = 1.5 m.m., $E_4 - E_5$ = 7 m.m.

FIG 11 ELECTRODE ASSEMBLY

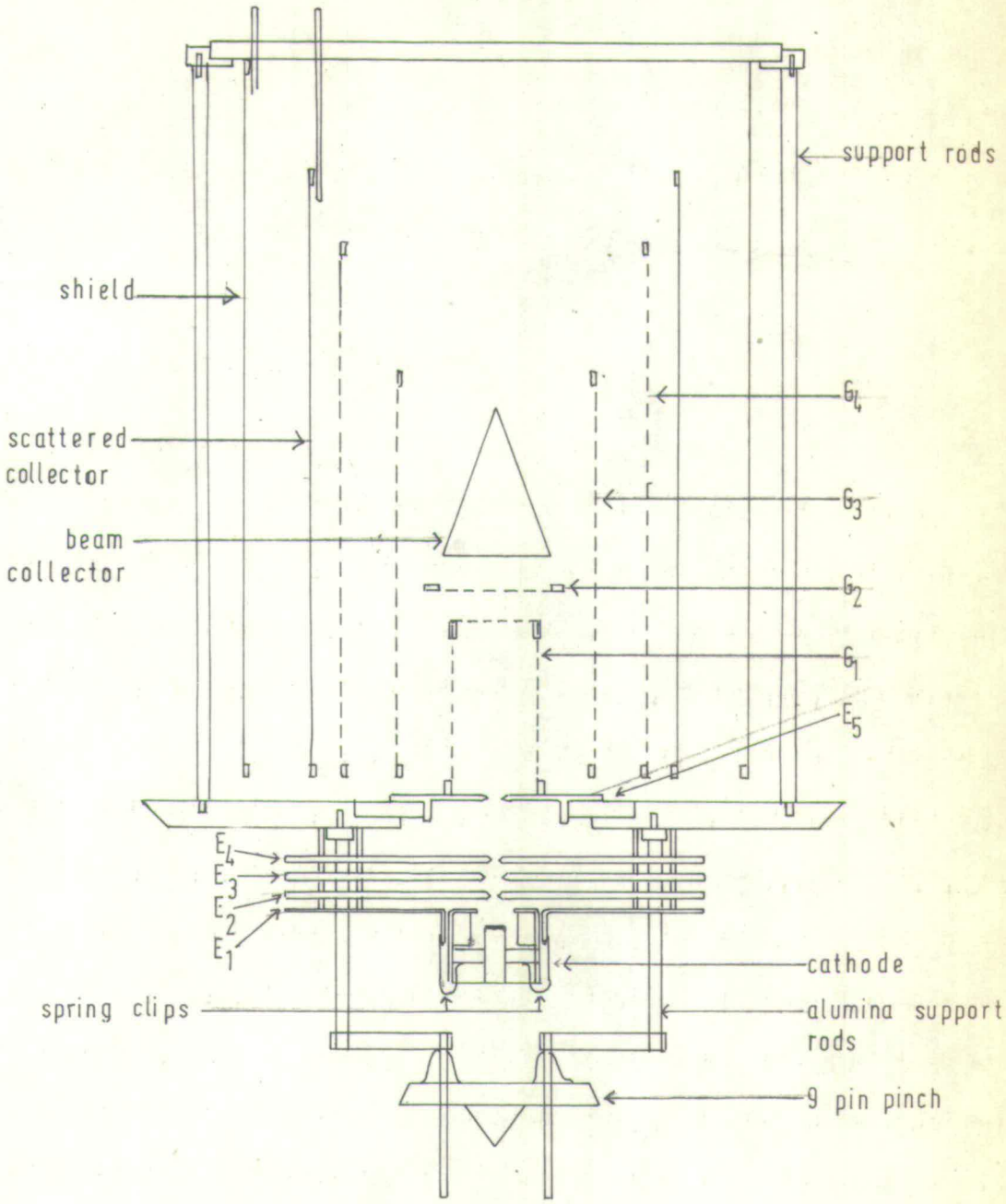

Scale :- 1:1 approx

To facilitate replacement the cathode assembly is a press fit held in position by spring clips. Electrical leads for the cathode, cathode heater, and electrodes E_1 - E_4 are brought through a 9 pin pinch below the gun and thence connected to the ceramic seals in the side flange (Fig.10). Glass insulation is used.

In operation E_1 is run at a potential positive to the cathode and draws electrons from it. E_2, E_3 and E_4 are used as an Einzel lens : E_2 and E_4 are placed at the same potential so that electrons suffer no energy change in traversing the gun. E_3 is placed at a potential lower than E_2 and E_4 and has the effect of filtering out from the beam those electrons which have relatively high components of velocity perpendicular to the beam axis, thus collimating the beam and reducing the background current in the collision chamber. In practice the potential on E_3 is usually varied until the ratio of scattered electron current to beam current in the empty cell is at a minimum. As well as optical collimation of the beam the electrodes E_2 and E_4, by virtue of their small central holes, introduce a high degree of mechanical collimation.

The potential on E_5 determines the energy of the beam entering the collision chamber and is normally set at the same value as the potential on E_2 and E_4. With this system currents measured at the beam collector were typically of the order of 10^{-8} amps.

2. The Collision Chamber:

(1) Grid G_1: This is a cylinder 25 m.m. long and 12.5 m.m. in diameter with sides of 70% transparency molybdenum mesh and a top of 90% transparency tungsten mesh, supported by a cage of 0.020" diameter molybdenum wire. Its purpose is to provide a field free region in which the only electron energy losses arise from collisions with the gas. The bottom end of G_1 is mechanically

connected to E_5 and the electrical lead, insulated by glass, runs along the steel plate and up the outside of the shield electrode to the top plate.

(2) Grid G_2: is placed 4 m.m. in front of G_1. It is a circle of 90% transparency tungsten mesh 14 m.m. in diameter, mounted on a molybdenum ring. During operation it prevents penetration of the field of the beam collector into the region of G_1. It is also used for energy analysis of the beam. If the current reaching the beam collector is plotted against the potential on G_2, the curve falls off rapidly as the repelling potential on G_2 reaches numerically the energy of the beam since the electrons do not then have sufficient energy to pass through the grid and reach the collector.

(3) The beam collector (BC) is a cone of 0.020" tantalum sheet 20 m.m. long with a base opening 15 m.m. in diameter situated 5 m.m. from G_2. The shape means that electrons entering the collector make many collisions with the surface, hence reducing the probability of their being reflected out of the collector. To reduce the probability of reflection further a holding voltage of about 50 volts with respect to E_5 is applied to the beam collector.

(4) Grid G_3: Surrounding G_1 is the grid G_3 made of 70% transparency molybdenum mesh supported on 0.020" diameter tungsten rods. It is 30 m.m. in diameter and 57 m.m. long. The purpose of this grid is to stop the passage of positive ions. To it is applied a potential a few volts positive with respect to E_5, and since any positive ions formed will have a low kinetic energy this potential is sufficient to prevent them penetrating to G_4 and the scattered collector.

(5) Grid G_4: This is the key grid for successful operation of the spectrometer. It is a cylinder of 70% transparency molybdenum mesh 75 m.m. long and 40 m.m. in diameter mounted on 0.020" tungsten wire. At the beginning

of the measurement of a spectrum it is set at a potential negative with respect to the cathode, so that no scattered electrons have sufficient energy to pass through it to the scattered electron collector. The potential is then gradually increased until elastically scattered electrons can reach the collector, whereupon a rapid rise in scattered current is obtained. As the potential is further increased electrons which have made inelastic collisions are able to penetrate to the scattered electron collector, causing similar sharp rises in the current. The points at which these sharp rises are observed correspond to the various excitation processes occurring in the atoms or molecules of the gas. A more detailed discussion of the variation of scattered current with the potential on G_4 will be given later.

(6) The scattered electron collector (SC) is made from 0.020" tantalum sheet, 54 m.m. in diameter and 85 m.m. long, supported by 0.020" tungsten rods. To ensure efficient collection of the electrons reaching it a constant holding voltage is applied between the scattered electron collector and G_4. In practice the scattered collector is held at earth potential and all other potentials set accordingly.

(7) The shield is a further tantalum cylinder 73 m.m. in diameter and 100 m.m. long. In spite of the precautions taken, a number of electrons are reflected from the surfaces in the collision chamber. Since some of these electrons, after successive collisions with the walls of the apparatus might reach the scattered electron collector this second tantalum cylinder is placed around it, and held at a potential some 40 volts positive with respect to the cathode. Some of the reflected electrons are thus prevented from reaching the scattered collector.

All the collision chamber electrodes are suspended from a second non-magnetic stainless steel plate, attached to the central plate by three stainless steel rods, 2 m.m. in diameter, placed outside the shield electrode. Electrical connections from the electrodes to the ceramic-metal seals in the top flange are made through the top stainless steel plate, from which they are insulated by quartz discs.

2.1.3 Electronics:

The Potential Circuits:

A diagram of the potential circuits is given in Fig. (12). The potentials on E_2, E_3, E_4, E_5/G_1, G_2, BC, G_3 and the shield are, applied relative to the cathode, by means of circuits each consisting of two 90 volt batteries connected across a Beckmann 300 K helipot, Type A. The variable posts of the helipots are connected to the appropriate grid or electrode, and the centre points of the batteries, via a switching arrangement, to the cathode. The switching arrangement allows any of the electrode or grid circuits to be connected to a Vibron vibrating reed electrometer (Model 33-B), so that the current reaching any one of them be measured. The potential between G_4 and the scattered electron collector is applied by the same type of circuit. Since the currents reaching E_1 would cause rapid decay of the batteries, the potential on it is applied,relative to the cathode, by a Farnell stabilised voltage supply Type E 350, rated 0-350 volts, 0 - 100 milliamps output. The potential on G_4 relative to the cathode is applied by means of a circuit consisting of a 45 volt battery and a 100 K helipot (Beckmann Type A), and a second switching arrangement allows the battery voltages to be checked at any time. A Solartron digital voltmeter, Type LM 1010 2, is used to measure the potentials on all the electrodes and grids.

FIG 12 POTENTIAL CIRCUITS

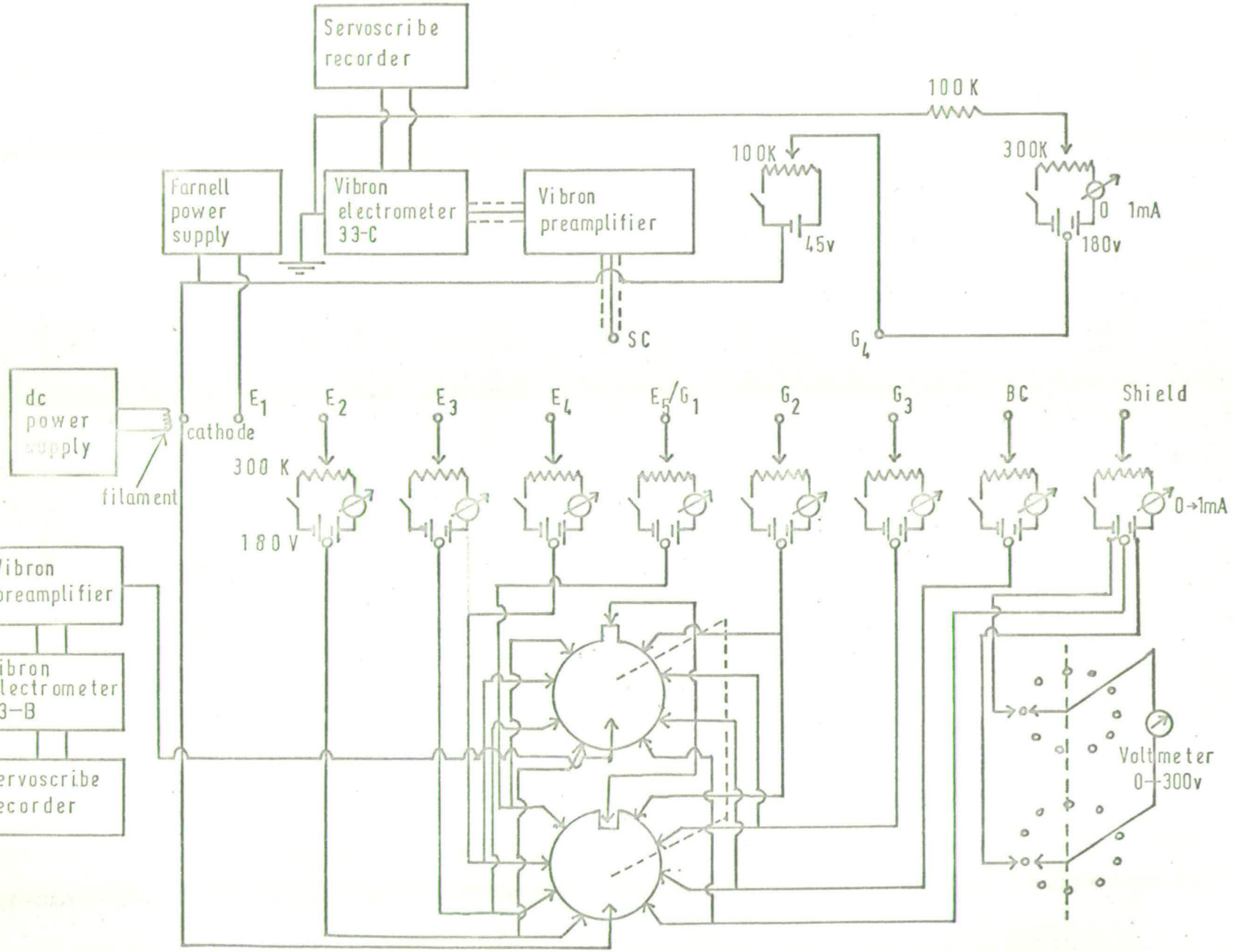

Current Measurement:

The currents reaching all the electrodes and grids, except the scattered electron collector, are measured on the Model 33 B Vibron vibrating reed electrometer, while the scattered electron current is measured on a Vibron vibrating reed electrometer Model 33 C, which is capable of measuring currents down to 10^{-14} amps. Two 'Servoscribe' potentiometric recorders (Type RE 511) are used to make continuous recordings of the scattered electron current, and the current reaching any other grid or electrode, usually the beam collector.

2.2 Experimental Procedure and Behaviour of the Apparatus:

After assembly the apparatus was leak tested using a 20th Century mass spectrometer leak detector. When the system was vacuum tight the diffusion pumps were started, reducing the pressure to less than 10^{-6} torr within a few hours. The vacuum chamber and upper parts of the diffusion pumps were than baked for 12 - 24 hours, after which the pressure in both gun and collision chambers was normally about 2×10^{-8} torr.

Once satisfactory vacuum conditions had been achieved the heating element for the cathode was switched on and the voltage slowly raised, degassing the emitter at such a rate that the pressure in the gun chamber never rose above 1×10^{-6} torr. Conversion of the cathode coating from carbonate to oxide was effected by raising the voltage to a high value (maximum 12 volts) for a short time before reducing it to the rated 6.3 volts, 0.5 amps. The relatively low operating temperature ($\sim 1000^{\circ}K$) of this type of cathode means that the resultant electron beam has a smaller energy spread than one from a directly heated cathode - such as tungsten, which has an operating temperature of $\sim 2500^{\circ}K$.

2.2.1. Adjustment of the Gun Electrodes:

The ratio of scattered electron current to beam current:

Since the scattered signal will be small it is necessary that the ratio of scattered current, I (SC), to beam current, I (BC), in the empty cell be small. The potentials on the lens electrodes were varied until, for a given beam energy this ratio was minimised. Typical results are shown in Table 1.

Table 1.

Potential settings of the lens electrodes

Potential (volts)					I (SC) / I (BC)
E_2	E_3	E_4	E_5/G_1	G_4	
30	4.2	30	30	13	1×10^{-2}
75	15.8	75	75	13	6.5×10^{-4}

These may be compared with the results obtained by Raff (74) who found that, in order to achieve the desired small background current, he had to incorporate a small magnet in the electron gun.

Table 2.

Comparison with Raff's results

Beam Energy (volts)	I (SC) / I (BC)		
	A	B	C
40	--	1.62×10^{-3}	3.6×10^{-3}
43	2.39×10^{-1}	--	--
50	--	5.57×10^{-4}	2.6×10^{-3}
65	4.12×10^{-1}	1.47×10^{-3}	1.3×10^{-3}

A - Raff without magnet
B - Raff with magnet
C - Present work

Since the present results are comparable with those obtained by Raff after incorporating a magnet, and because there is a danger that the magnetic field might penetrate into the collision chamber, altering the trajectories of the scattered electrons, it was decided to omit the magnet in the present

FIG 13 ENERGY ANALYSIS OF INCIDENT BEAM

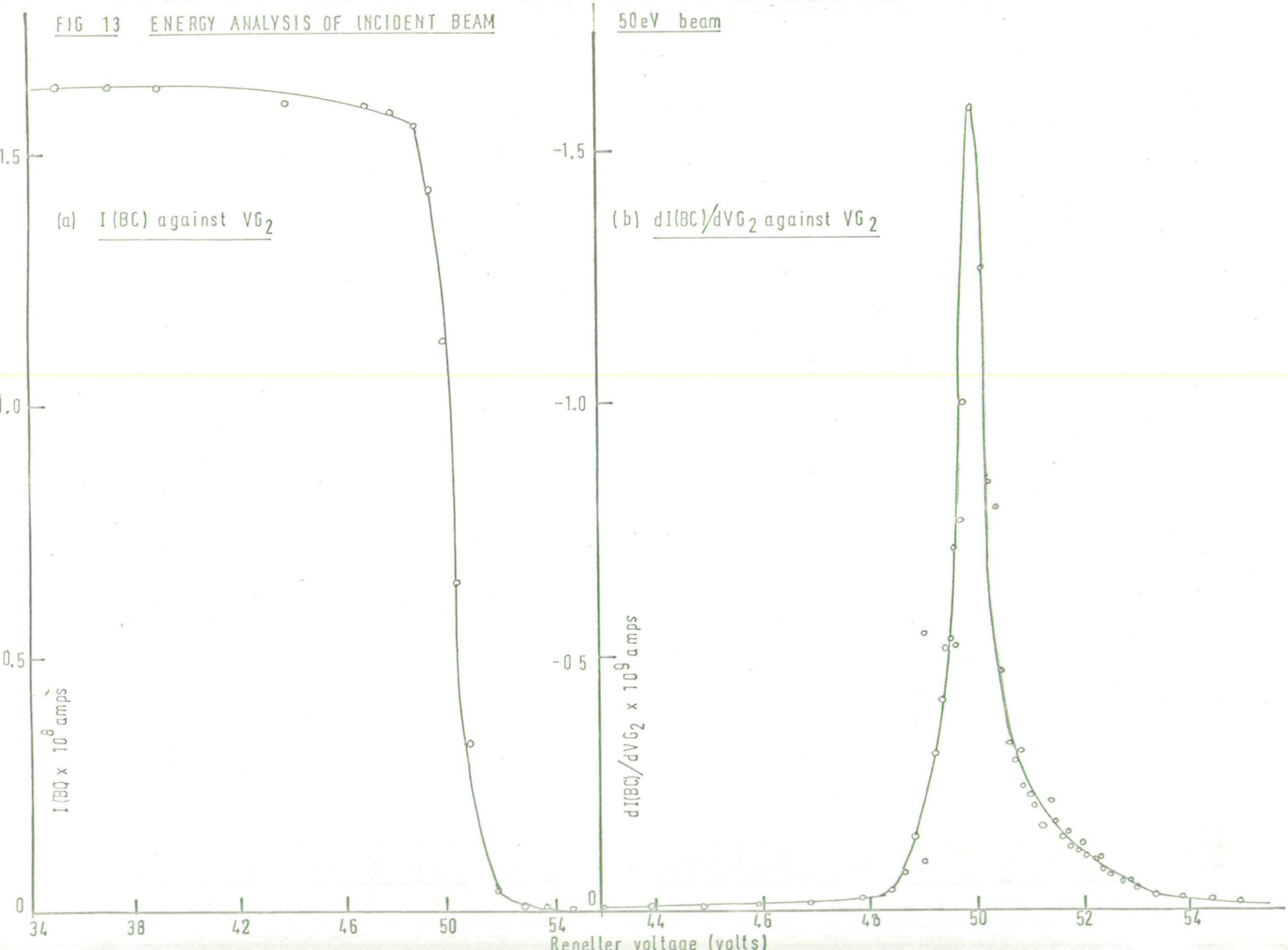

experiment. Also obvious from Tables 1 and 2 is the fact that as the beam energy is decreased to 30 eV the background scattering increases. For this reason most measurements were made using beams of energies around 50 eV.

2.2.2. Energy Analysis of the Incident Beam:

It is possible to obtain an indication of the energy spread of the incident beam by using G_2 as an energy analyser. As the potential on G_2 is gradually reduced until the repelling potential reaches a value numerically equal to the beam energy, the current reaching the beam collector drops sharply. If the curve of beam current against the voltage on G_2 (VG_2) is then differentiated a sharp peak is obtained whose half width, i.e. its width at half height, can be taken as a measure of the energy spread of the beam. On the basis of this definition the expected energy spread from the cathode being used is 0.15 eV. Unfortunately, the method of analysis will give a value which is too large (74) because

(a) Not all the electrons in the beam approach the collector in a direction perpendicular to G_2, and

(b) Field penetration effects into the region between G_1 and G_2 distort the beam as the potential difference between G_1 and G_2 is changed.

Analysis using G_2 as a retarding potential therefore gives an upper limit to the actual energy spread. Results for a 50 eV incident beam are shown in Fig. (13 a) and (13 b). The experimental conditions were : $VE_2 = VE_4 = VE_5/G_1 = 50$ volts, $VG_3 = 52$ volts, VBC = 90 volts, $VG_4 = 5$ volts, V Shield = 70 volts, and the holding voltage = 18 volts.

The half width of the peak is 0.7eV instead of the expected 0.15eV. Raff's results are somewhat similar: for an incident beam of 40eV the measured energy spread was 1eV. However possible reasons for this are given above,

FIG 14 VARIATION OF SCATTERED ELECTRON CURRENT WITH VG_3

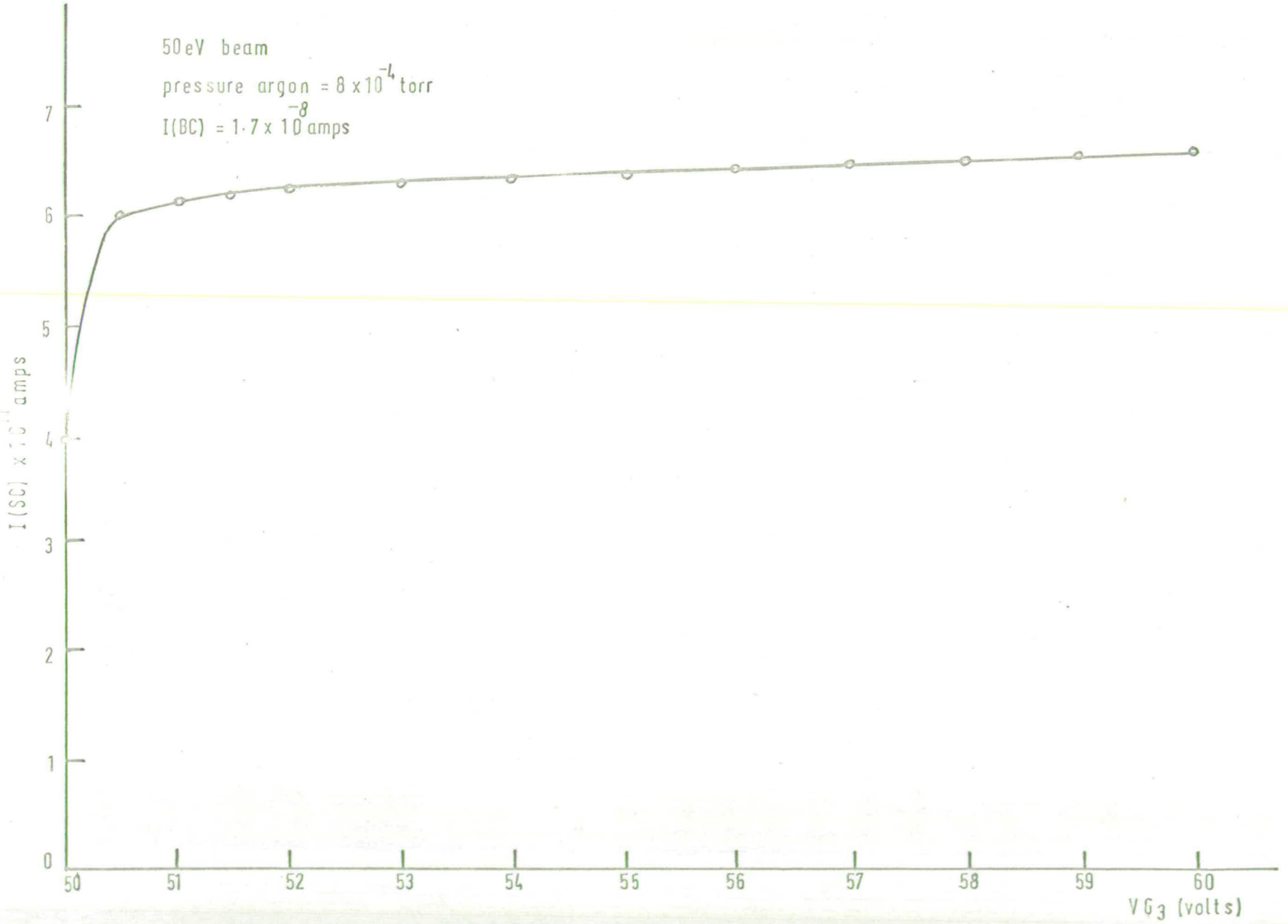

and spectra obtained indicate that, in both cases, the actual energy spread of the beam is close to the predicted 0.15eV.

2.2.3. Positive Ion Current:

The purpose of the grid G_3 is to prevent positive ions, formed during the collision process, from reaching the scattered electron collector. Fig. (14) shows a plot of the scattered electron current against VG_3 with argon in the collision chamber. The conditions were: $VE_2 = VE_4 = VE_5/G_1 = 50$ volts, $VG_2 = 50$ volts, VBC = 85 volts, $VG_4 = 10$ volts, holding voltage = 15 volts, and the pressure of argon was 8×10^{-4} torr. It can be seen that when G_3 becomes slightly positive with respect to E_5/G_1 there is a sharp rise in the measured scattered electron current, which then continues to rise slowly because of field penetration effects. The magnitude of the sharp rise is equal to the magnitude of the positive ion current reaching the scattered electron collector when G_3 is at the same potential as E_5/G_1. In operation a potential about 2 volts positive with respect to E_5/G_1 is always applied to G_3.

2.2.4. Scattered Electron Collector Efficiency:

To prevent electrons being reflected from the surface of the scattered electron collector, a holding voltage is applied between it and G_4. The value of the holding voltage is quite critical since it determines the efficiency of the collector, and its effect is illustrated in Fig. (15) where the current measured at the collector is plotted against the holding voltage.

The conditions were: $VE_2 = VE_4 = VE_5/G_1 = 50$ volts, $VG_2 = 60$ volts, VBC = 85 volts, $VG_3 = 52$ volts, V shield = 70 volts; and the pressure of argon = 5.5×10^{-4} torr.

FIG 15 VARIATION OF SCATTERED ELECTRON CURRENT WITH HOLDING VOLTAGE

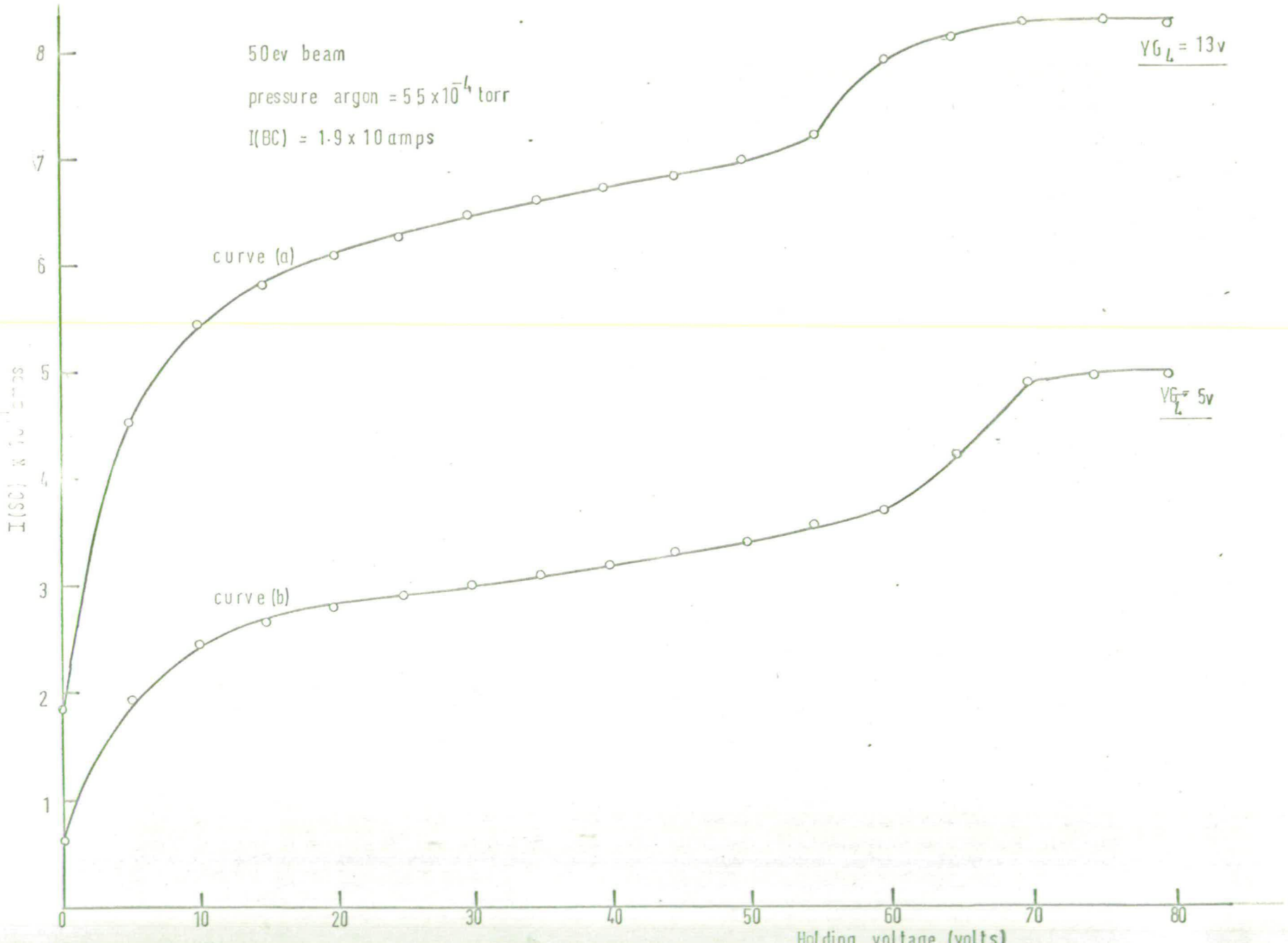

Consider curve (a). Below 15 volts the current drops off rapidly indicating a large increase in the number of reflected electrons, but above this voltage the current increases only slowly with holding voltage, showing that most of the electrons are now being collected rather than reflected. A second sharp rise is seen starting at 55 volts. It was thought that the second rise might be caused by field penetration into the region between G_3 and G_4. If this is so, then at a higher repelling potential on G_4 the effect should not be noticed until a higher holding voltage is reached. Confirmation comes from curve (b): the second rise does not now start until the holding voltage reaches 60 volts.

In practice a holding voltage of around 20 - 30 volts was normally applied, minimising field penetration effects while simultaneously operating the scattered collector at high efficiency.

2.2.5 Variation of Scattered Electron Current with pressure:

In Chapter One we saw that, when a single particle moves through a short distance dx cms in a gas, density n molecules per cm^3, the probability of making a collision is given by

$$P = n.\,Q.\,dx \qquad 2.1$$

A flux of N particles per cm^2 moving at velocity v, is reduced in this distance by a number

$$dN = n\,N\,Q\,dx \qquad 2.2$$

Integrating we obtain

$$N = N_o \exp(-n\,Q\,x) \qquad 2.3$$

For electrons, which carry a single charge, the current I_o equal to $N_o v$ is reduced after travelling x cms through the gas to

$$I = I_o \exp(-nQx) \qquad 2.4$$

FIG 16 VARIATION OF SCATTERED ELECTRON CURRENT WITH PRESSURE

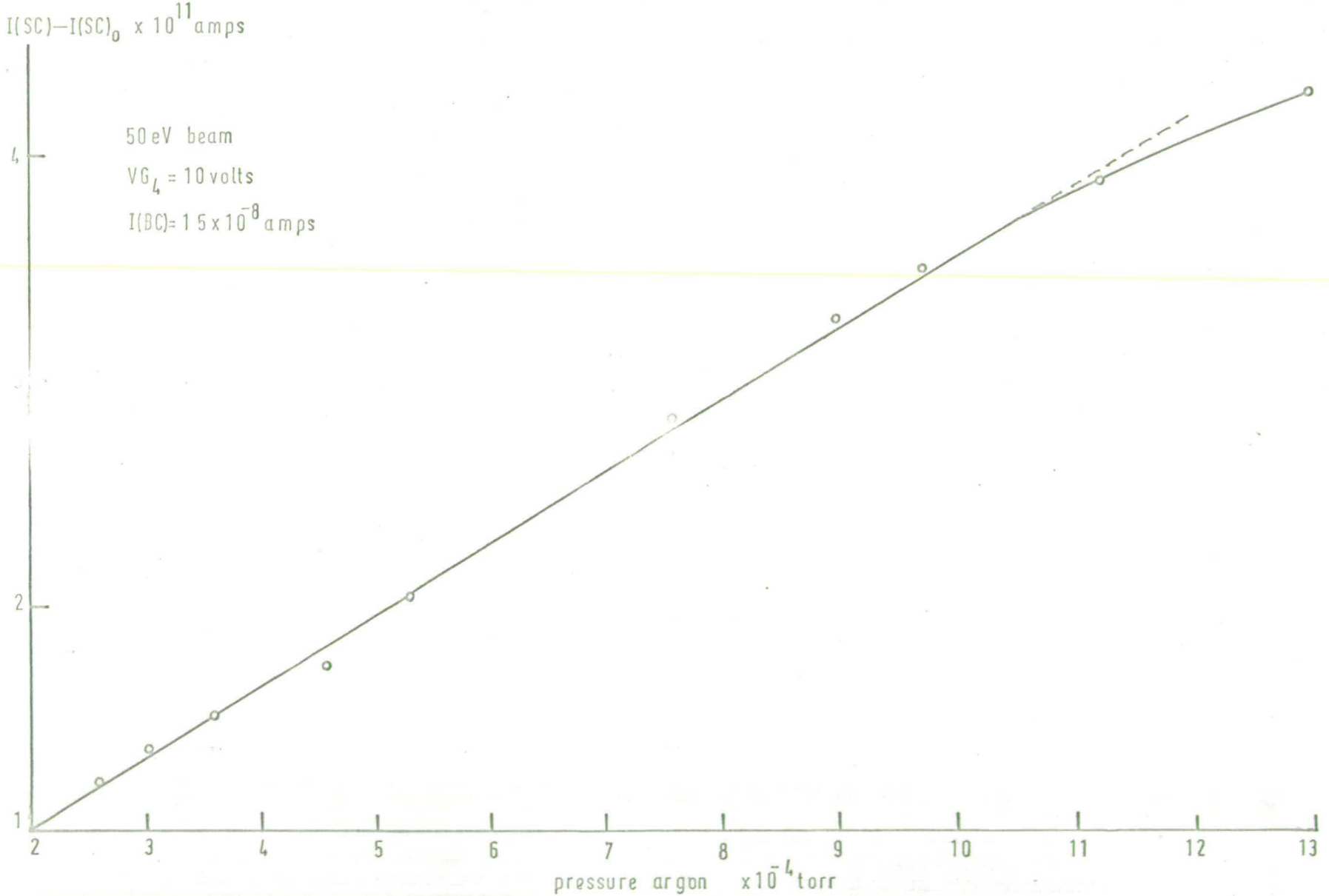

In the present experiment we have

$$I(BC) = I_o \exp(-nQx) \qquad 2.5$$

where I_o is the current entering the collision chamber, I(BC) the current reaching the beam collector, and x the distance between these two points.

I(SC), the current reaching the scattered collector, is given by

$$I(SC) = a(I_o - I(BC)) \qquad 2.6$$

a being that fraction of the scattered electrons which is collected.

For single collision conditions

$$I(BC) = I_o (1 - nQx)$$
$$I(SC) = aI_o nQx \qquad 2.7$$

and under these conditions $I_o \simeq I(BC)$, so that

$$I/SC) / I(BC) = I(SC) / I_o = anQx \qquad 2.8$$

The scattered current is therefore directly proportional to the pressure for fixed beam current, collision cross-section and path length. In Fig.(16) the current at the scattered electron collector, minus the background current $I(SC)_o$ in the empty chamber, is plotted against the ionization gauge reading with argon in the chamber. The conditions were : $VE_2 = VE_4 = VE_5/G_1 = 50$ volts, $VG_2 = 55$ volts, $VG_3 = 52$ volts, VBC = 84 volts, $VG_4 = 10$ volts, holding voltage = 15 volts, and V shield = 60 volts. The relation is linear up to pressures of 1×10^{-3} torr, whereupon double scattering sets in and equation 2.8 no longer holds. An operating pressure was always chosen to lie somewhere in the linear portion of the curve, which of course may differ from gas to gas.

2.2.6 Variation of Scattered Electron Current with Beam Current:

From equation 2.8 it can be seen that, just as the signal should show a linear variation with pressure, so should it show a linear variation with beam current, since doubling the beam current effectively doubles the number

FIG 17 VARIATION OF SCATTERED ELECTRON CURRENT WITH BEAM CURRENT

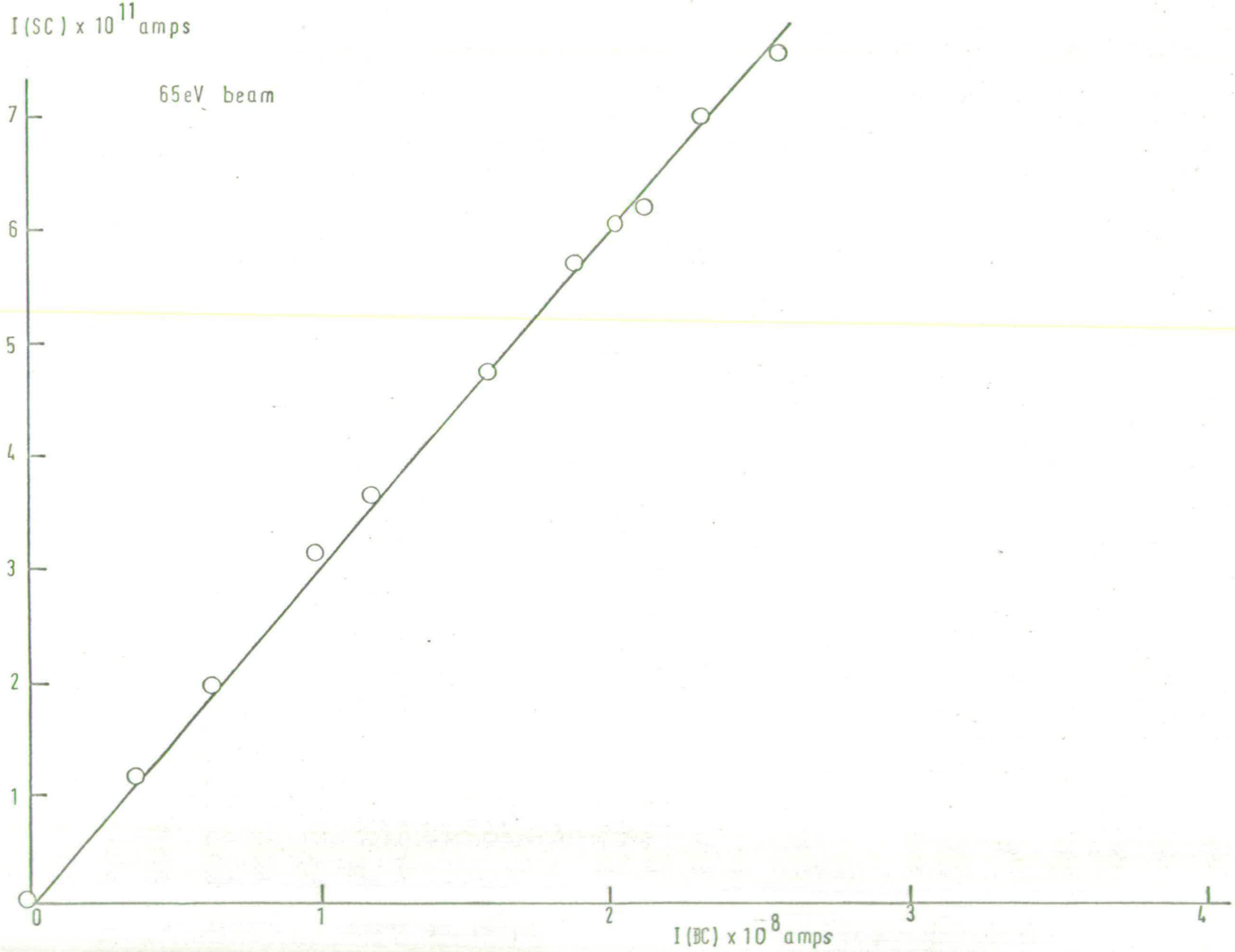

of collisions taking place. If the beam current is varied by changing the potential on one of the gun electrodes then the electron optics will be slightly altered, and two factors will contribute to the change in scattered electron current. To avoid this complication the beam current was varied by varying the cathode-heater current, and hence the cathode emission. Results are shown in Fig. (17) for a 65 eV beam with 2.5×10^{-4} torr of argon in the collision chamber. The electrode settings were $VE_2 = VE_4 = VE_5/G_1 = 65$ volts, $VG_2 = 70$ volts, $VG_3 = 66$ volts, VBC = 90 volts, V shield = 70 volts, $VG_4 = 10$ volts, and holding voltage = 30 volts. Linear behaviour is observed, as predicted.

2.2.7. Variation of Scattered Current with Repelling Potential:

Electron impact spectra are obtained by varying the voltage on G_4 relative to the cathode, and measuring the current reaching the scattered electron collector for each value of this potential. In order to analyse the data correctly and to obtain from it the electronic excitation energies of the gas under study, Raff determined the functional relationship between I (SC) and VG_4. A brief account of his calculation will be given.

Consider a hypothetical apparatus in which only electrons scattered through $90 \pm y$ degrees can reach the collector, where y is a small angle, and in which the repelling field between G_3 and G_4 is perpendicular to the beam axis at all points. When the repelling field is numerically greater than the beam energy no electrons can pass through G_4, and the current at the collector will be zero; but as the repelling field is reduced to a value numerically less than the beam energy, there will be a sudden rise in scattered electron current due to elastically scattered electrons reaching the collector. The current then levels off as the repelling field is further reduced, until the first inelastically scattered electrons have sufficient energy to overcome

FIG 18 THEORETICAL 90° IMPACT SPECTRUM OF AN ATOM — FROM REF. 74

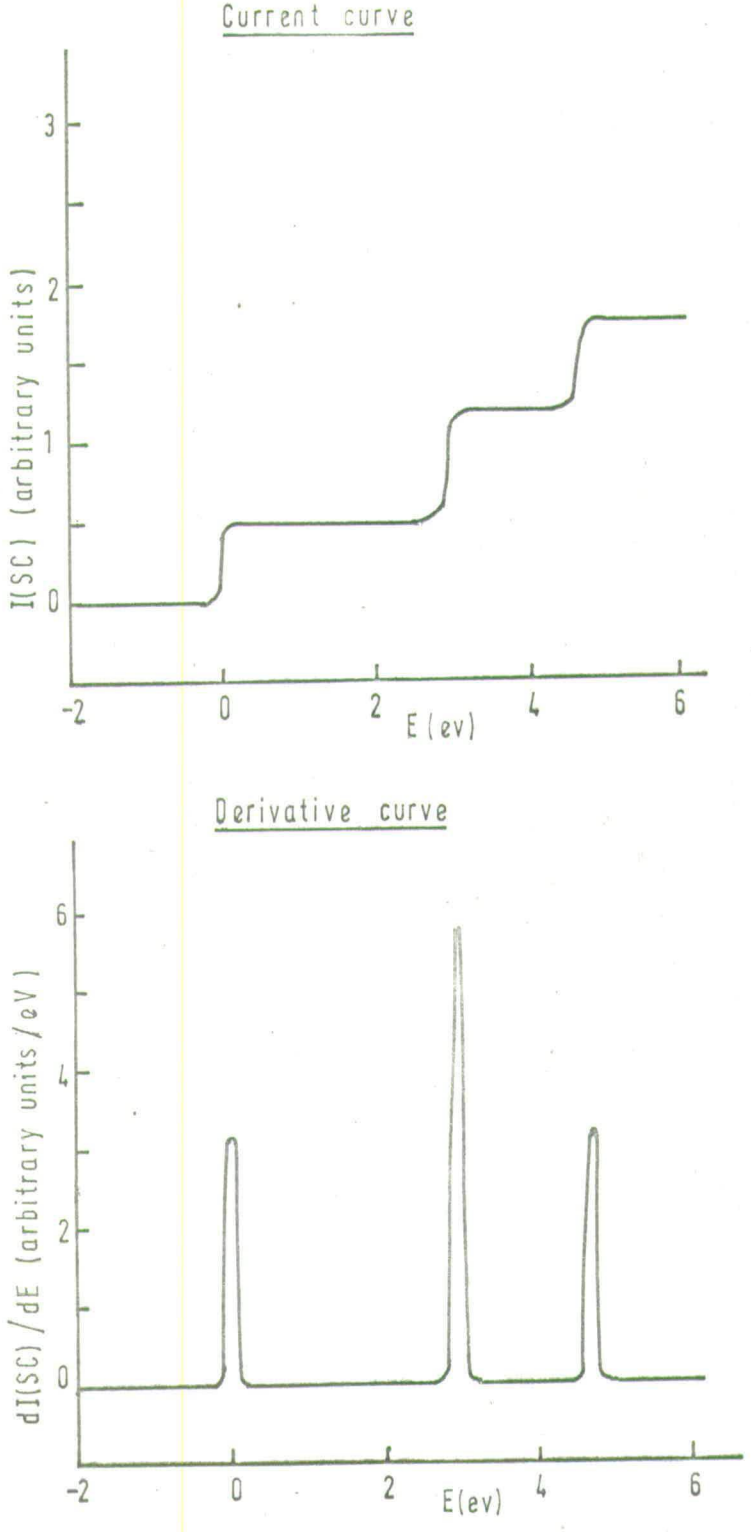

it, whereupon there is another sudden rise in scattered electron current.

Differentiation of the plot of scattered electron current against VG_4 would give a series of infinitely high spikes at the excitation points, were it not for limitations of apparatus resolution and energy spread of the incident beam. These tend to lower and broaden the spikes - Fig.(18). In this hypothetical experiment the transition energies in the gas would be given by the positions of the peak maxima.

The actual experiment differs from the one just described in several important respects.

(1) Electrons are being collected over angles other than 90° so that the repelling field is not always perpendicular to the velocity vector of the scattered electron. For an electron of energy E, scattered through an angle θ, the energy effective in overcoming the repelling field is $E \sin^2 \theta$. Thus in the actual experiment not all electrons losing the same amount of energy to the gas will be collected at the same value of VG_4, the effect being to lower and broaden the peaks.

(2) Electrons scattered through small angles will 'see' grids which are less transparent than do those which are scattered through large angles.

(3) It was assumed that the lines of force between G_3 and G_4 were perpendicular to the beam axis at all points. This will not be so near the top edge of G_3, where G_4 protrudes above it.

Continuing the analysis of the actual experiment for atoms, Raff obtained the following expression for the derivative:

$$\frac{dI(SC)}{dV} = \sum_i \frac{A \pi Q_i}{E_i} \left[\frac{V}{E_i - V}\right]^{\frac{1}{2}} g_i(\theta,\phi) \left[\sin^{-1}\left(\frac{V}{E_i}\right)^{\frac{1}{2}}\right] f(\theta)^3 \left[\sin^{-1}\left(\frac{V}{E_i}\right)^{\frac{1}{2}}\right] \qquad 2.9$$

where V(volts) is the potential on grid E_5 relative to $G_4 = VE_5 - VG_4$,

Q_i is the total collision cross section for process i,

FIG 19

(a) Electron impact spectrum of an atom with one electronic level 10 volts above the ground state —— for calculation see ref 74

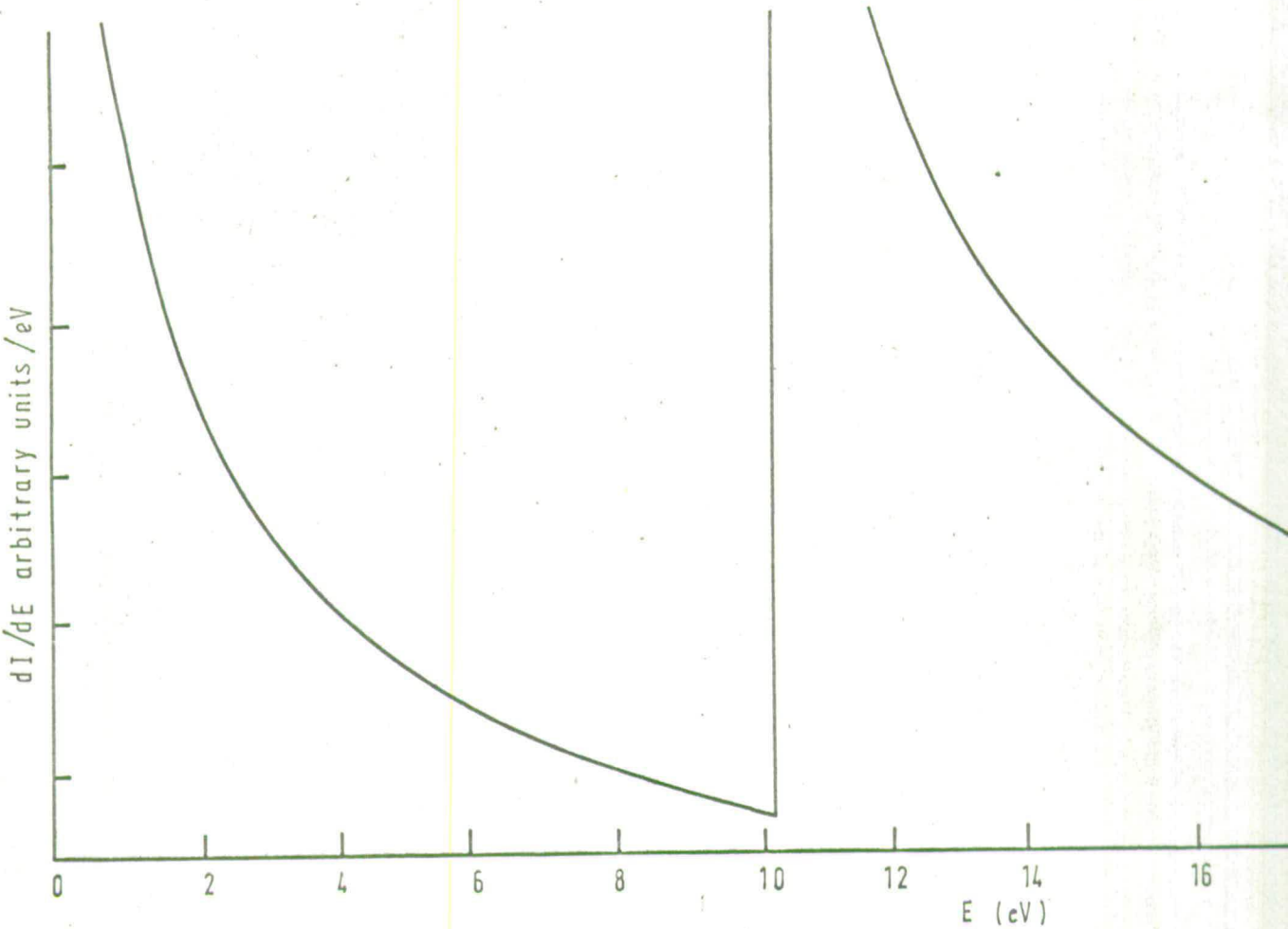

(b) Assumed form of the the angular distribution function giving the above spectrum

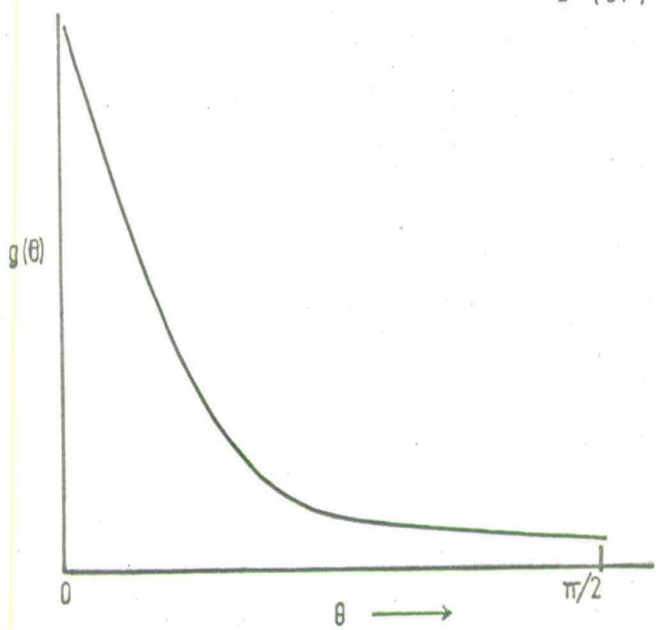

A is a normalisation constant depending on the beam current and pressure in the collision chamber $= nI(BC)x$ (see equation 2.3),

$g_i(\theta,\phi)$ is the normalised angular distribution function of scattered electrons for process i,

$f(\theta)$ is the grid transparency function for a single grid, and

E_i (eV) is the energy of the scattered electron.

Fig.(19 a) shows the electron impact spectrum calculated by Raff for an atom with one electronic state 10eV above the ground state. The incident beam energy was 50eV and he assumed that the cross sections for the elastic and inelastic processes were the same. The form of $g(\theta,\phi)$ used is shown in Fig. (19 b). The exact form of the spectrum obtained is very dependent on $g(\theta,\phi)$, which of course varies from gas to gas and transition to transition - see Fig.(3). Raff concludes that for atoms transition energies should be taken from the onset values rather than the peak maxima.

A similar calculation was conducted for molecules. Fig. (20 a) shows one possible set of transitions for a diatomic molecule. Any number of transitions between E_1 and E_2 may occur, the probability depending on their individual cross-sections, and the probability density of the ground state vibrational wave function; therefore as V is varied, one is running over a continuous set of transitions. The value of dI/SC)/dV as V is varied from $(E^* - E_1)$ to $(E^* - E_2)$ is given by

$$\frac{dI(SC)}{dV} = \int_{-\infty}^{h(V)} \frac{Q(x).A}{(E - E_x)} \left[\frac{V}{E - E_x}\right]^{\frac{1}{2}} g\left[\sin^{-1}\left(\frac{V}{E - E_x}\right)^{\frac{1}{2}}\right] f^3\left[\sin^{-1}\left(\frac{V}{E - E_x}\right)^{\frac{1}{2}}\right] n(x)dx \qquad 2.10$$

where E^* is the energy of the incident beam, n(x) represents the probability density of the vibrational ground state, and the upper limit h(V) depends on V. The result of a much simplified calculation is shown in Fig. (20 b). In this case onset is at E_1 and no infinite spikes appear.

FIG 20

(a) ELECTRONIC TRANSITIONS IN A DIATOMIC MOLECULE

(b) THEORETICAL ELETRON IMPACT OF A DIATOMIC MOLECULE

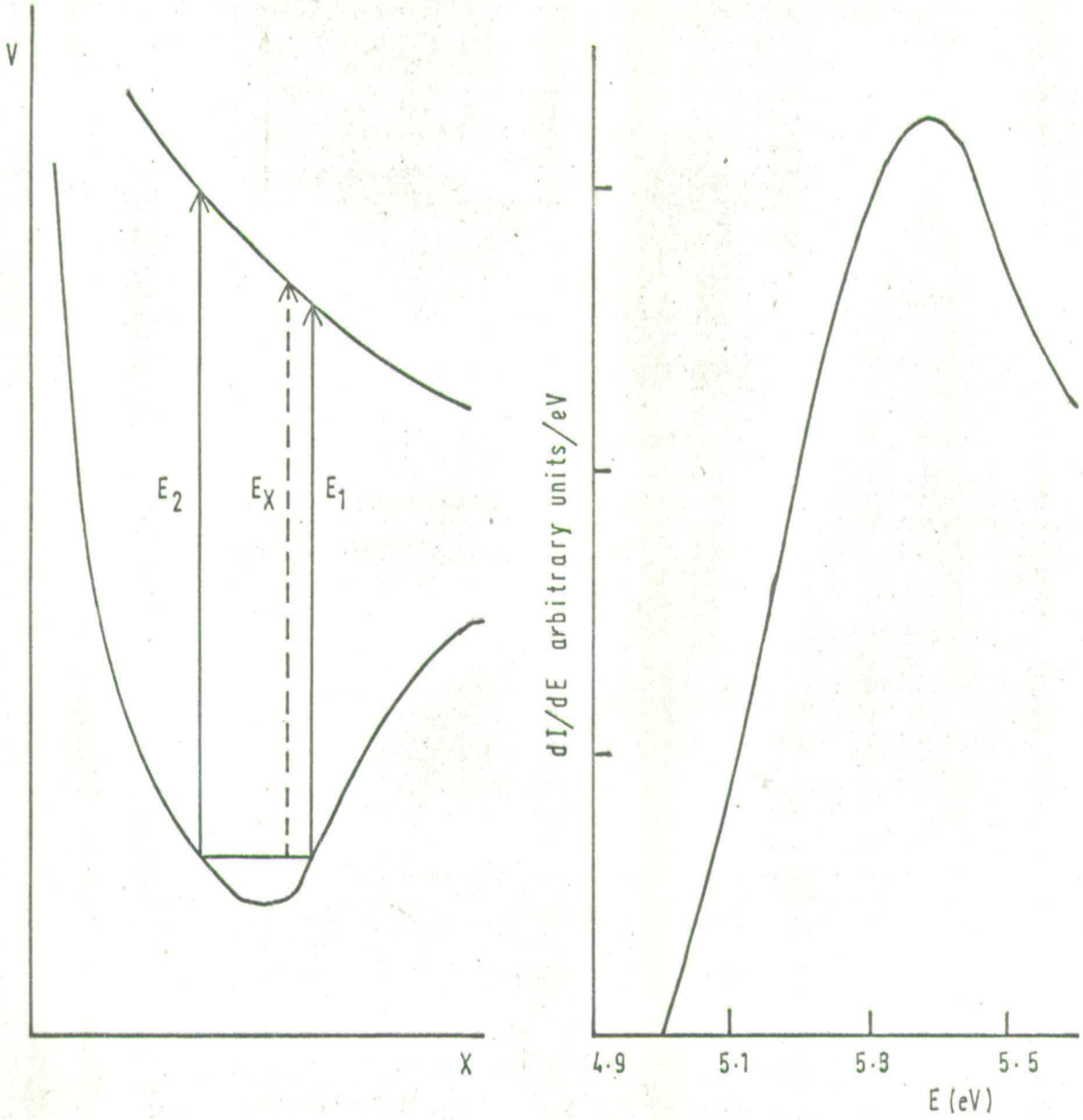

The spectrum was calculated assuming that $E_1 = 5$ volts and $E_2 = 5.5$ volts

The calculations indicate that the apparatus will produce peaks at values which correspond closely to the energy loss for a vertical transition from the centre of the ground state to the excited electronic state.

Some doubt had, however, been cast on the results obtained by Kuppermann and Raff - see reference 77 -, and it was therefore decided to repeat their experiments in helium and argon.

2.3 Electron Impact Spectra of Helium and Argon:

2.3.1. Materials:

Both argon and helium were obtained from cylinders (British Oxygen Co.Ltd.), and used without further purification.

2.3.2. Elastic Scattering:

Being the easiest to detect the elastic peaks were studied first. The apparatus was baked for a short time before any measurements were taken, and the gas flow rate was then adjusted, by means of the needle valve, until the desired pressure was obtained. After setting up a beam of the chosen energy, the variation of scattered electron current with VG_4 was measured, while simultaneous records of beam current were taken on the second recorder in order to correct for any minor fluctuations. The curves obtained are shown in Figs.(21) and (22). Values were interpolated at small, equally spaced intervals on these curves and used as input data for a computer program which calculated the derivative numerically. The method used for numerical differentiation was originally developed by Rutledge (79), and in the present case a sixth degree polynomial was fitted to seven successive points. Figs.(23) and (24) show the resulting plots of $dI(SC)/dVG_4$ against VG_4, the vertical line in the bottom left hand corner representing the scatter in the derivative introduced by the differentiation procedure.

FIG 21 I(SC) AGAINST VG_4 — ELASTIC SCATTERING IN ARGON

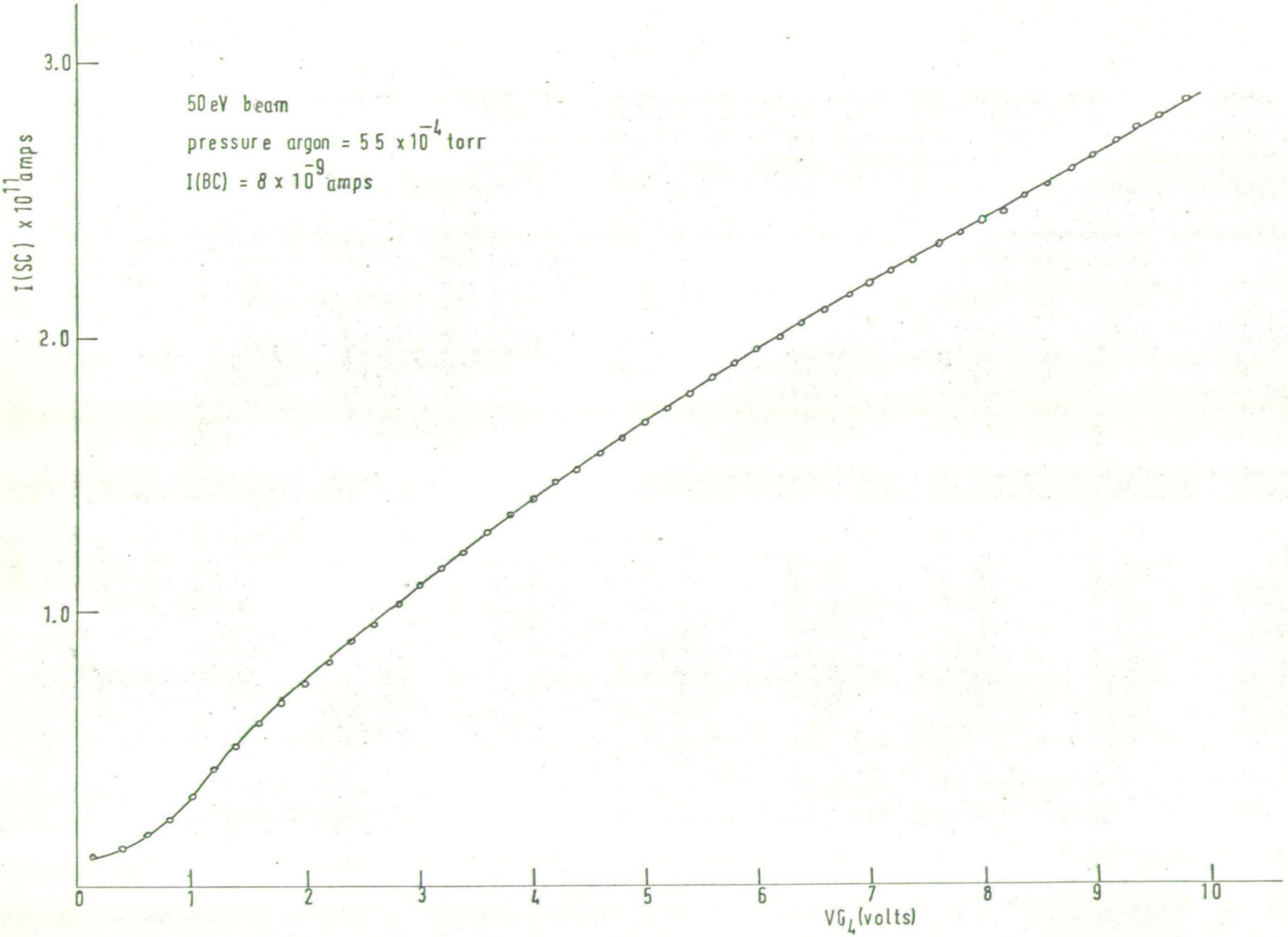

FIG 22 I(SC) AGAINST VG_4 — ELASTIC SCATTERING IN HELIUM

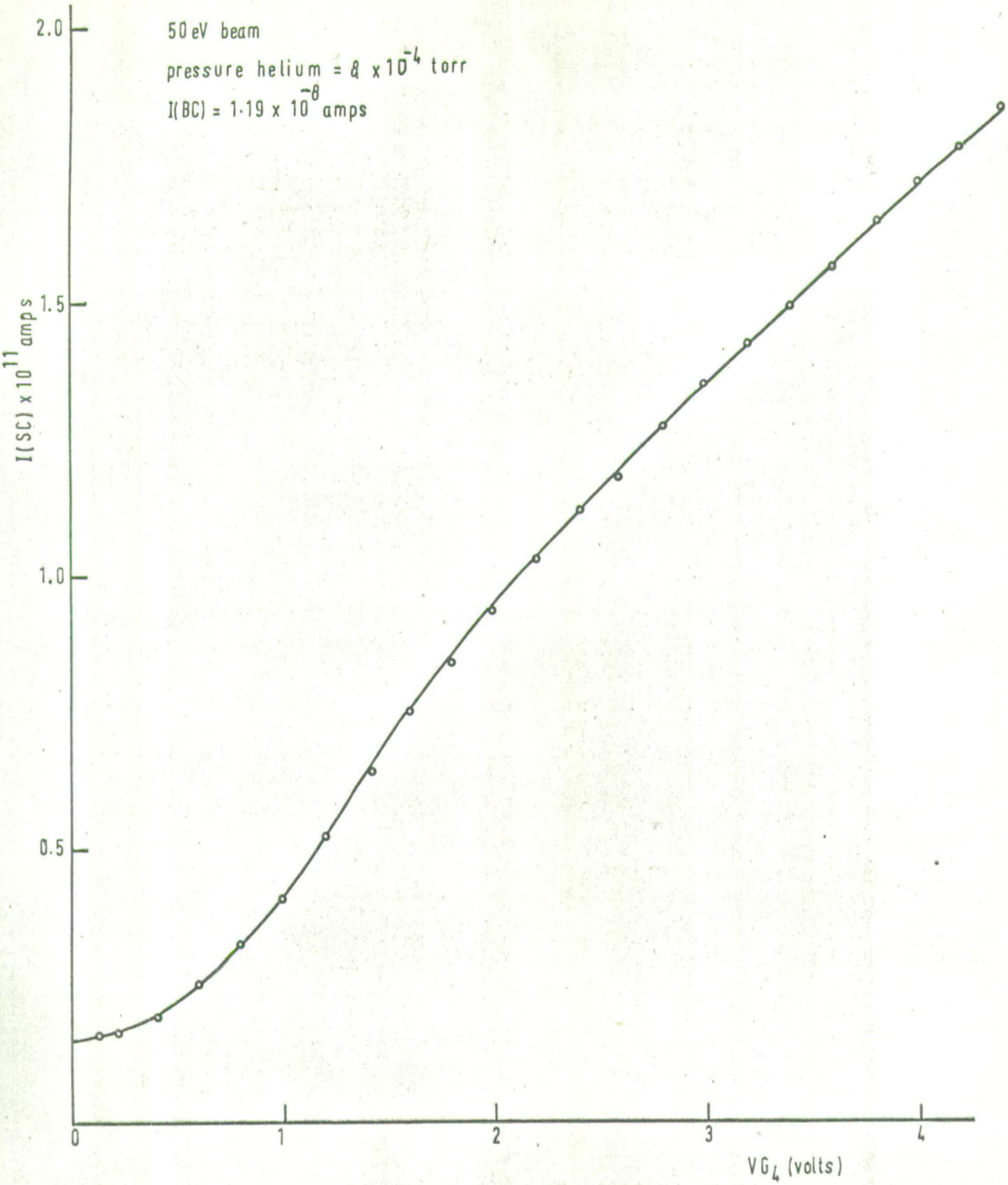

FIG 23 $d(I(SC) - I(SC)_0)/dVG_4$ AGAINST VG_4 — ELASTIC PEAK IN ARGON

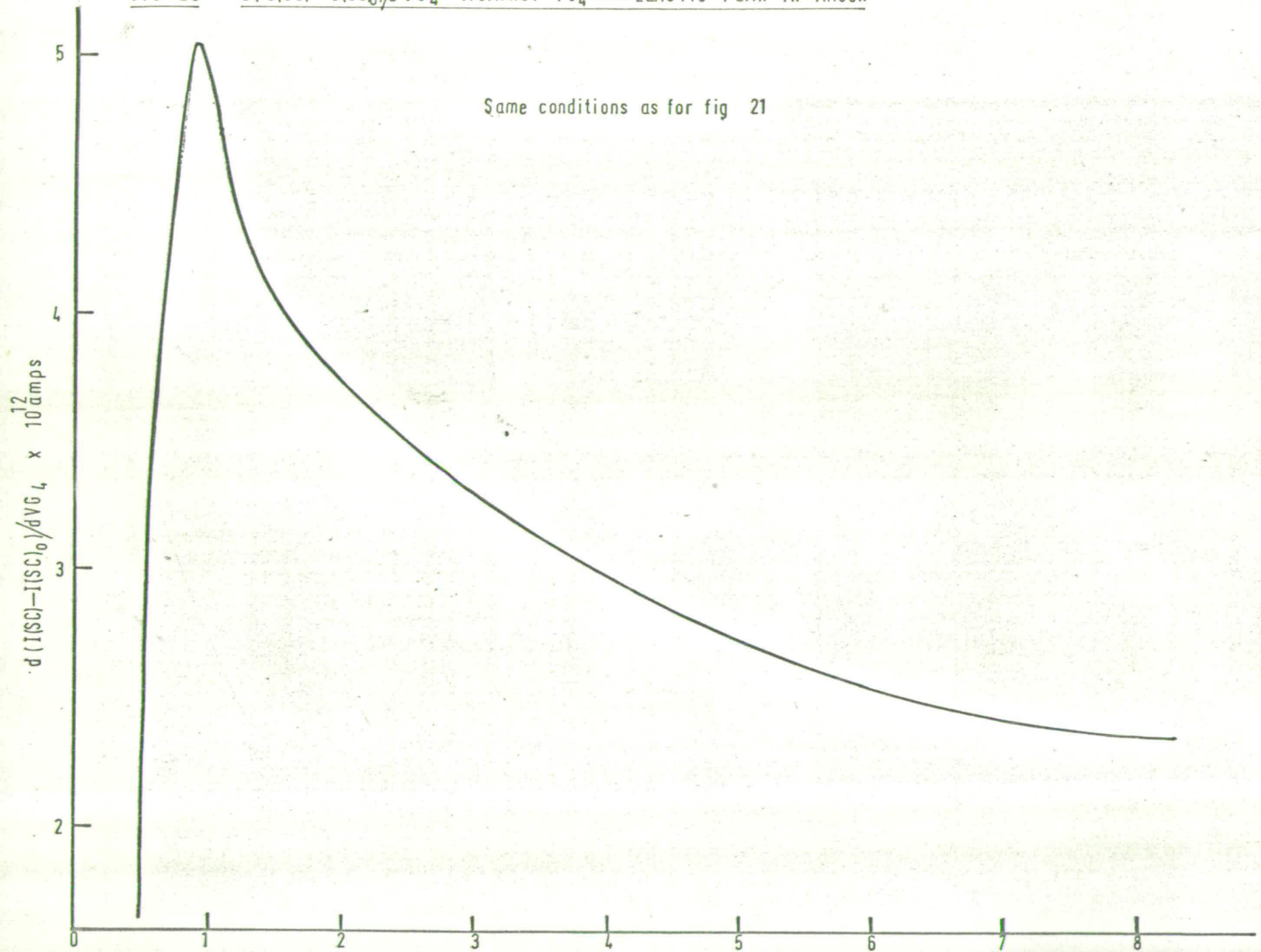

FIG 24 $d(I(SC)-I(SC)_0)/dVG_4$ AGAINST VG_4: ELASTIC PEAK IN HELIUM

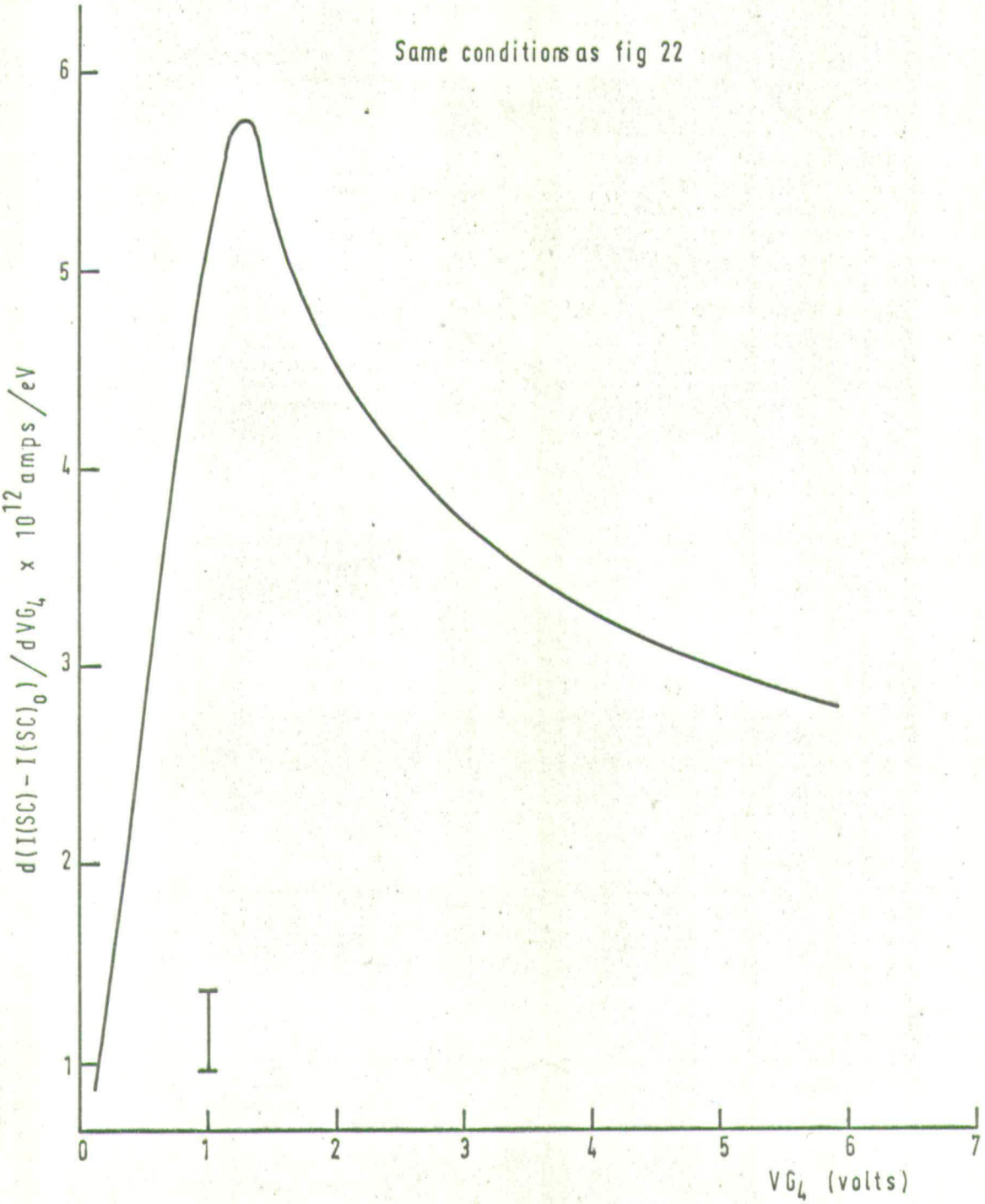

FIG 25 ANGULAR DISTRIBUTION FUNCTION IN ARGON

(a) function assumed by Raff (ref 74)

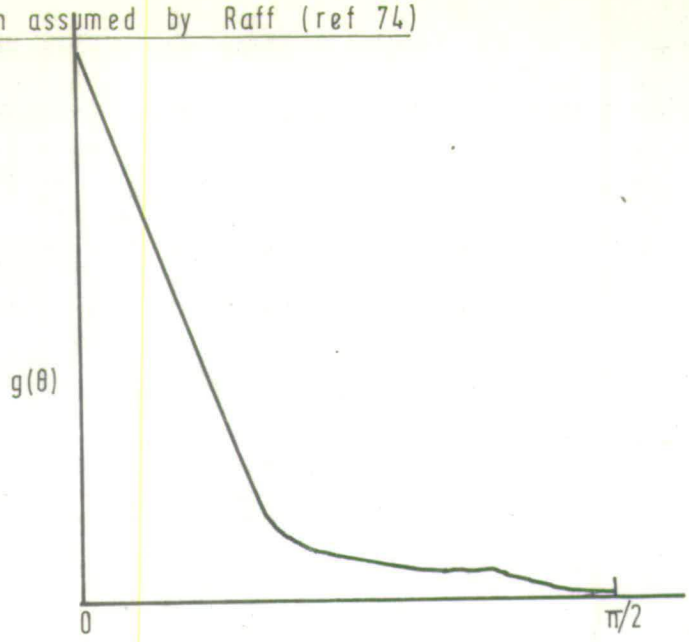

(b) function measured by Mohr and Nicoll (ref 10)

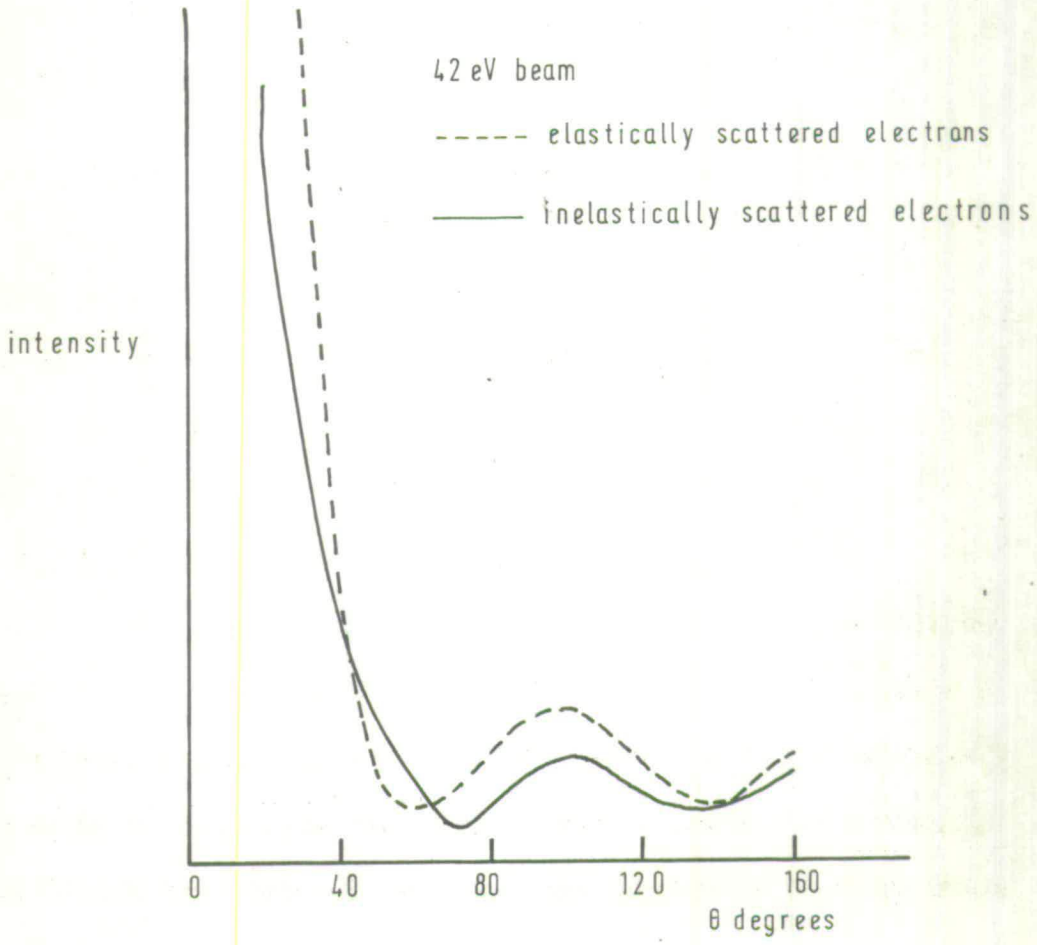

One puzzling observation is that the peaks occur at about 1.5eV above zero, an effect also noted by Kuppermann and Raff (72). Since there is no similar shift in the inelastic peaks the effect cannot be explained in terms of contact potentials (the contact potential correction found necessary by Kuppermann and Raff was only about $\pm$ 0,2eV). Raff's calculations indicate that apparent shifts in the measured peaks can be caused by the shape of angular distribution function of the scattered electrons. Maxima in the function can introduce subsidiary peaks, or dips, in the derivative, too narrow to be resolved in this apparatus. The experimental angular distribution function for electrons scattered elastically and inelastically from argon are shown in Fig. (25) along with the function used by Raff in his calculations. Since the elastic shift is observed in this work and in Raff's, it does not appear to be a random shift, and the answer may lie with the above type of effect, although the situation is by no means clear.

2.3.3. Inelastic Scattering:

The Spectrum of Helium:

A 50eV beam was set up and, after obtaining the current against voltage curve in the empty cell, the curve with 8×10^{-4} torr of helium in the chamber was obtained (Fig. 26). The conditions were: $VE_2 = VE_4 = VE_5/G_1 =$ 50 volts, $VG_2 = 60$ volts, VBC = 90 volts, $VG_3 = 52$ volts, holding voltage = 20 volts.

The difference between these two curves is shown in Fig. (27), and the derivative of this, obtained in the same manner as for the elastic peaks, is shown in Fig. (28). Raff's procedure was then to shift the peaks until the ionisation peak corresponded with the optically determined value of the ionisation potential, a contact potential correction of about 0.2eV. However, since there is some doubt about whether the peak near 24.6eV is in fact due

FIG 26 I(SC) AND $I(SC)_0$ AGAINST VG_4—INELASTIC SCATTERING IN HELIUM

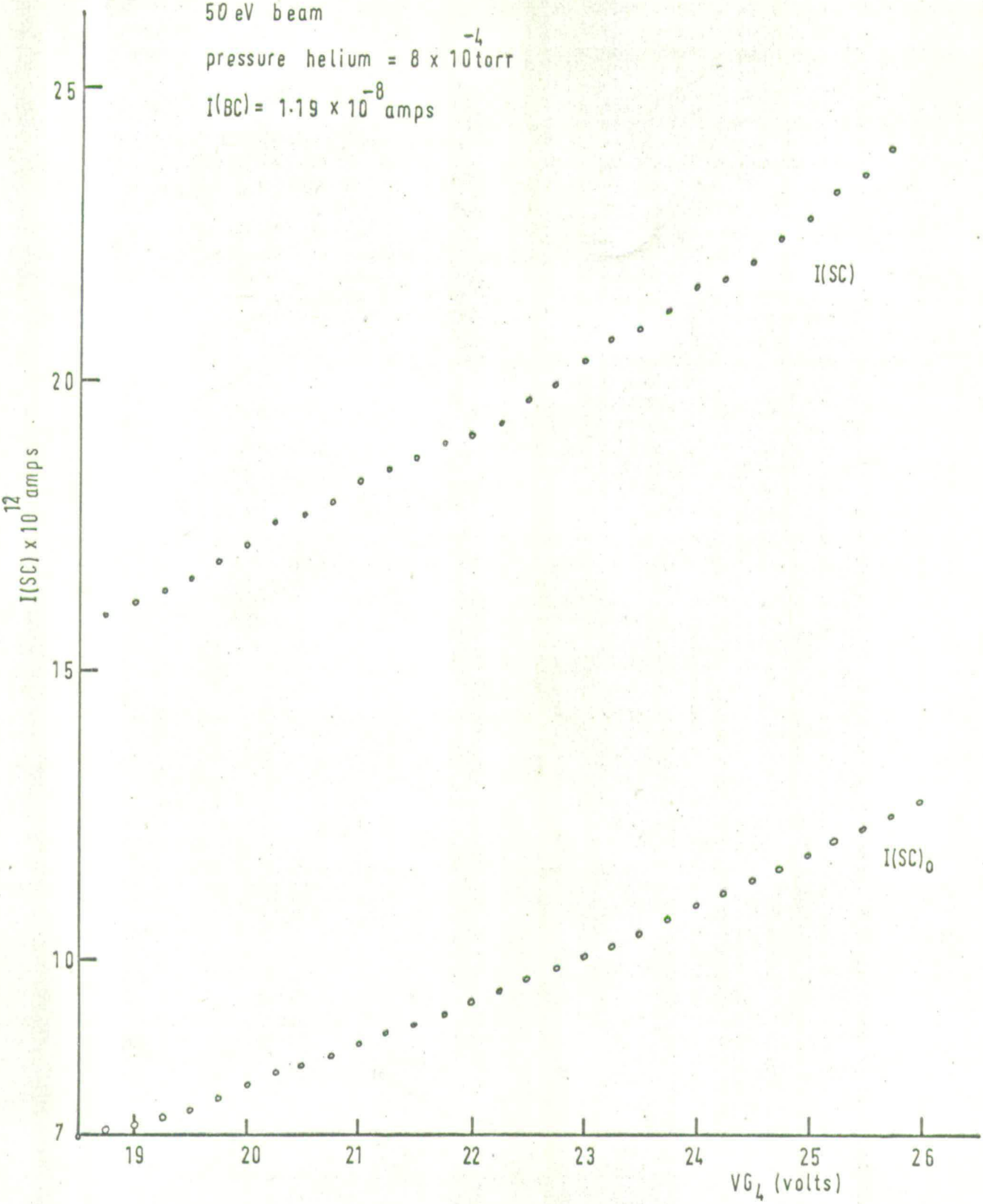

FIG 27 $I(SC) - I(SC)_0$ AGAINST $V G_4$—INELASTIC SCATTERING IN HELIUM

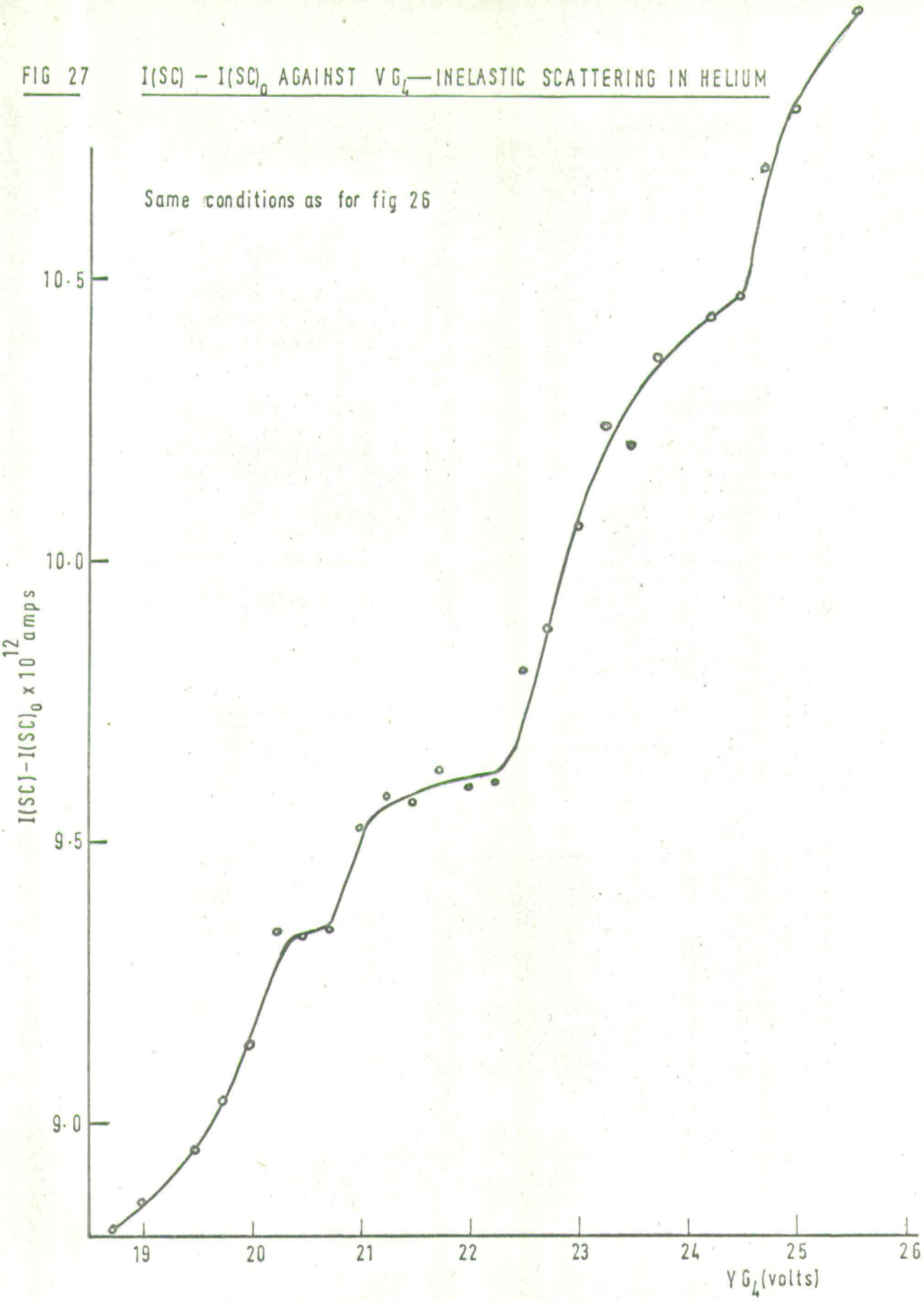

FIG 28 ELECTRON IMPACT SPECTRUM OF HELIUM

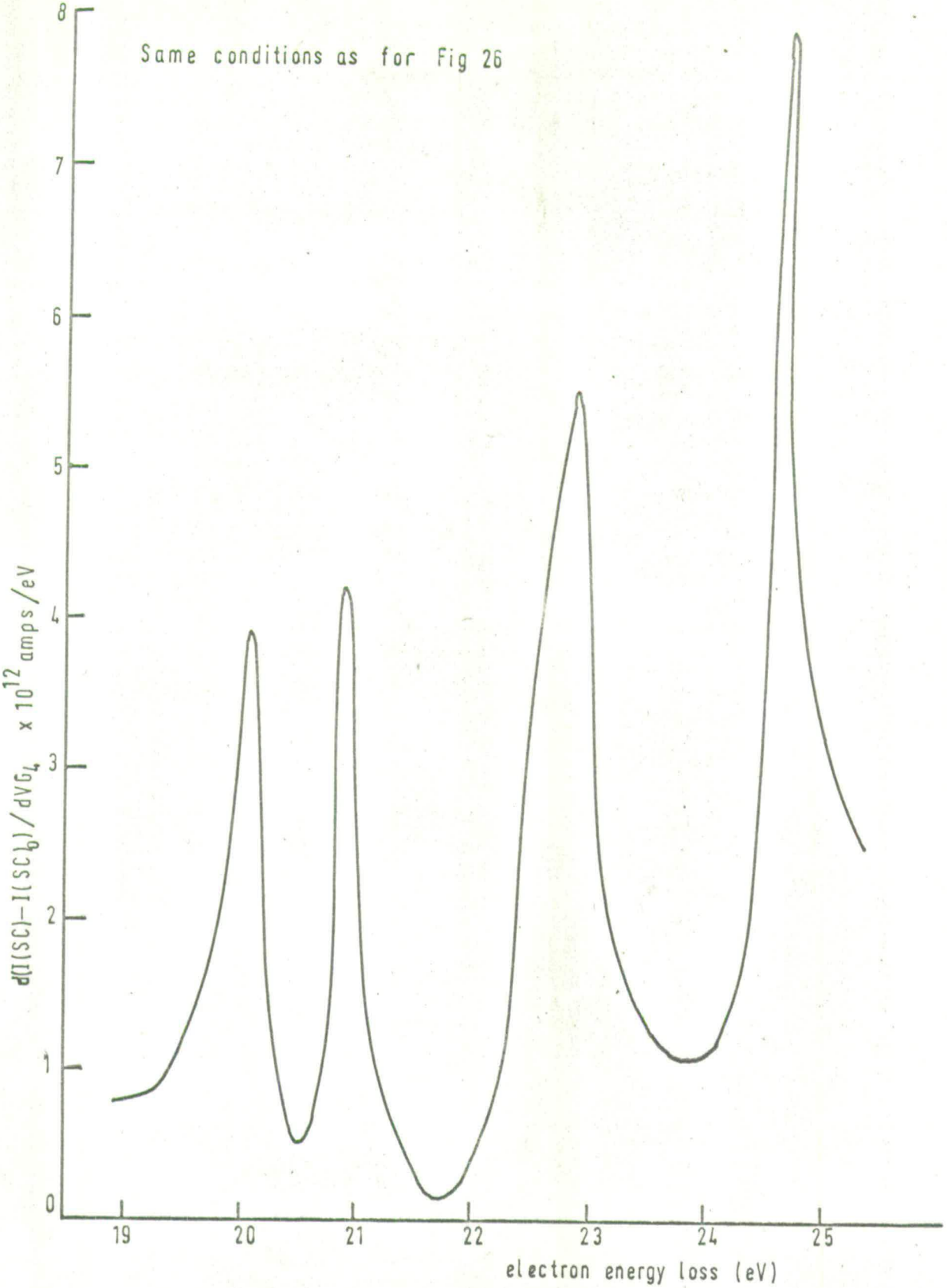

FIG 29 ELECTRON IMPACT SPECTRUM OF HELIUM

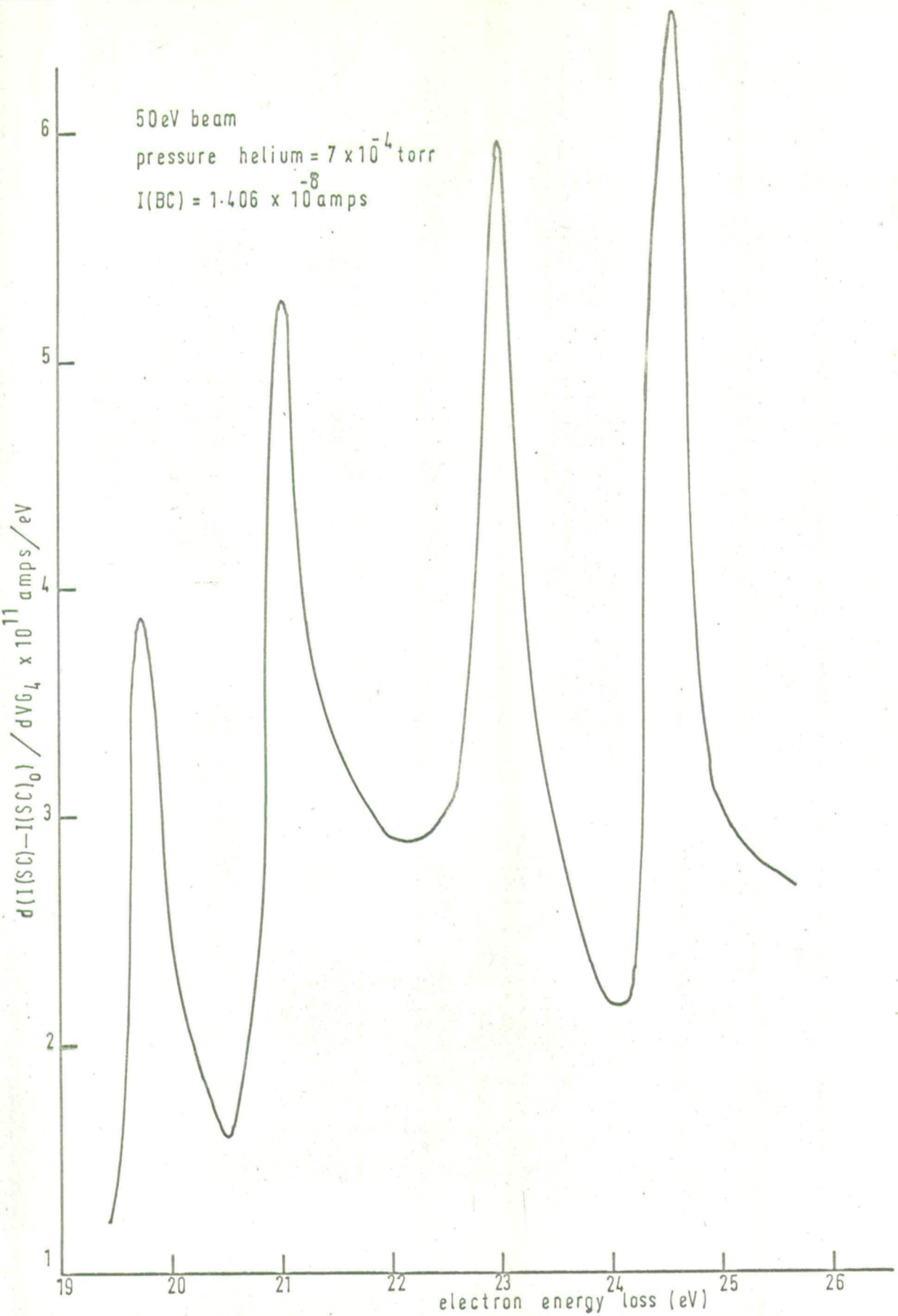

to ionisation (see next chapter), this procedure was not adopted here; the peak values quoted are unshifted.

Peaks are seen at 20.1, 20.9, 22.9 and 24.7eV. The peak at 20.1 agrees fairly well with the known value of 19.8eV for the 2^3S state. The 2^1S, 2^3P, and 2^1P states are seen as one peak at 20.9eV, their optical values being 20.6, 20.95 and 21.2eV respectively. The 3^1S state is seen at 22.9eV, in exact agreement with the optically determined value. The large number of states lying between the 3^1S state and the ionisation limit are not resolved in this instrument. To illustrate the reproducibility of the results a second helium spectrum is shown in Fig.(29). Here the peaks occur at 19.8, 21.0, 23.0 and 24.5eV, again in good agreement with known optical values.

The Spectrum of Argon:

The spectrum obtained with a 50eV beam is shown in Figs. (30 - 32). Peaks occur at 11.8, 13.0 and 15.5eV. Since L-S coupling is not a good approximation in argon, L-S notation will not be used to describe the states. The first peak at 11.8 corresponds to the excitation of a p electron to the 4s orbital, the singlet being at 11.6 and the triplet at 11.8eV, in good agreement with the above observations. The next set of argon levels lies between 12.9 and 13.25eV, in agreement with the second peak seen here at 13.0eV. The levels between this and ionisation are not resolved. In many of the argon spectra obtained the ionisation potential was not clearly marked.

The above results are in excellent agreement with those of Kuppermann and Raff, and indicate the same degree of accuracy, about $\pm$ 0.2eV, for the spectrometer. The variation of relative peak heights with incident beam energy should give information on the type of transition involved. As we saw in the introduction, the cross sections for spin forbidden transitions

FIG 30 I(SC) AND $I(SC)_0$ AGAINST VG_4 — INELASTIC SCATTERING IN ARGON

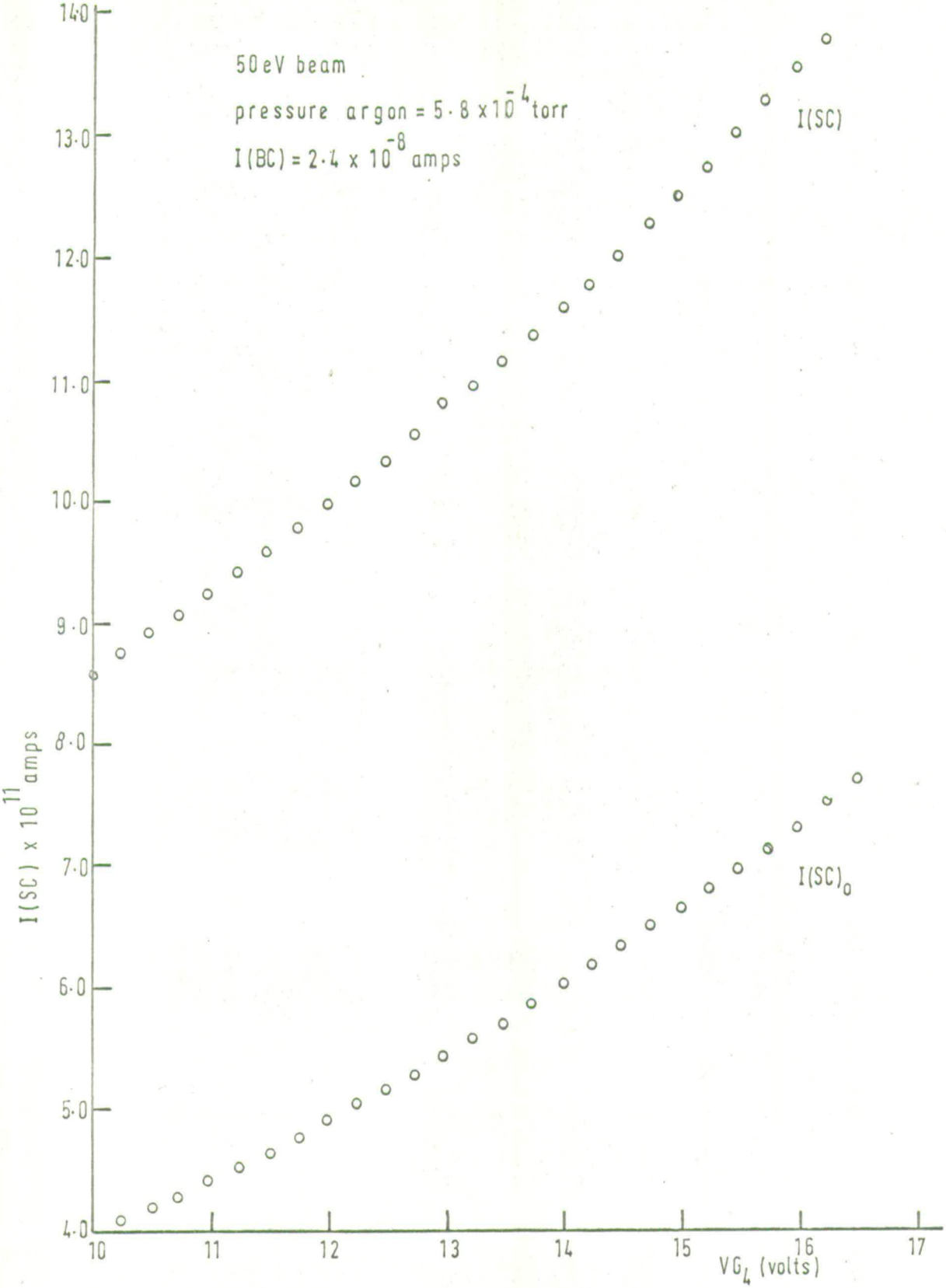

FIG 31 $I(SC) - I(SC)_0$ AGAINST VG_4 — INELASTIC SCATTERING IN ARGON

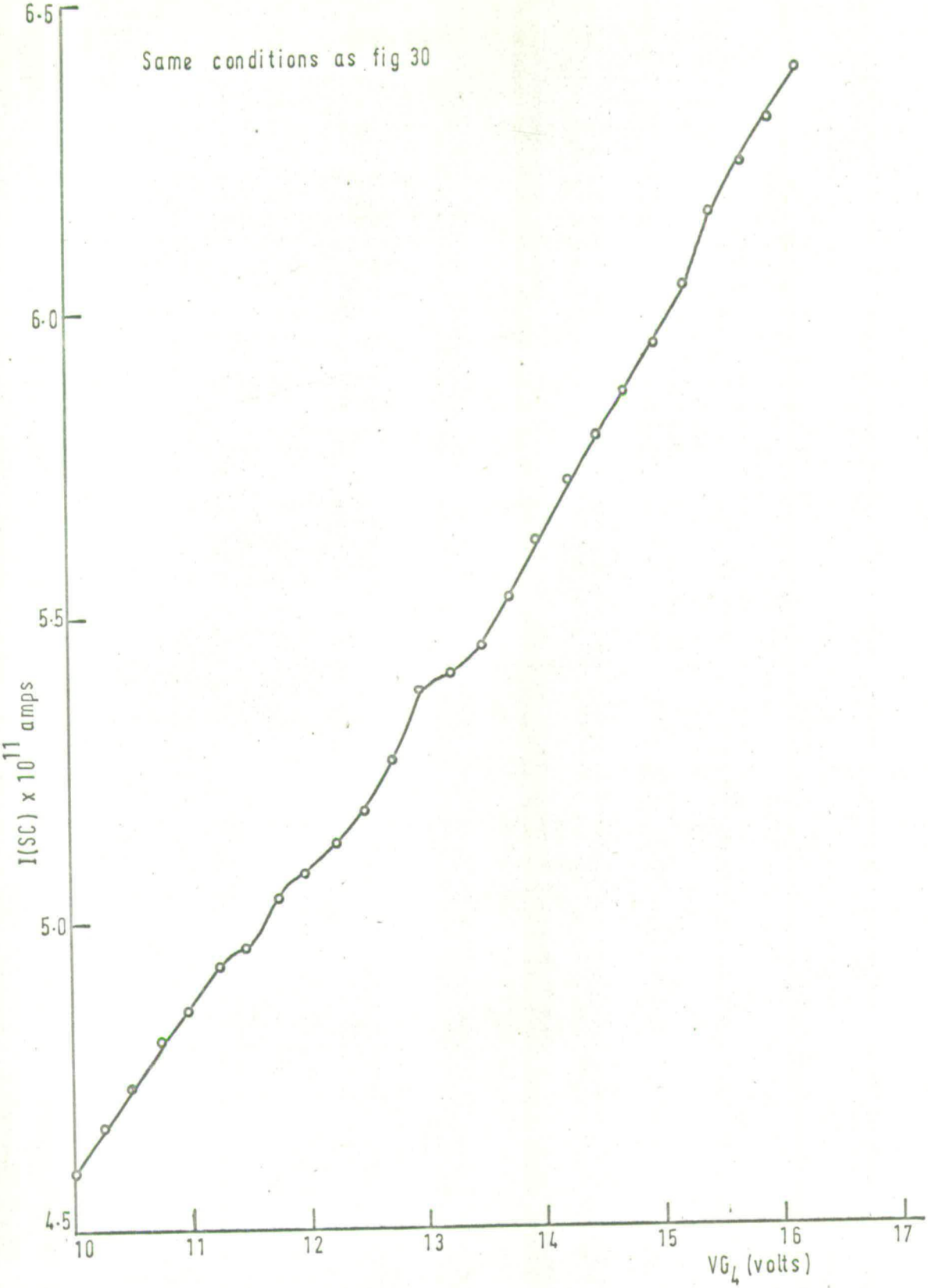

FIG 32 ELECTRON IMPACT SPECTRUM OF ARGON

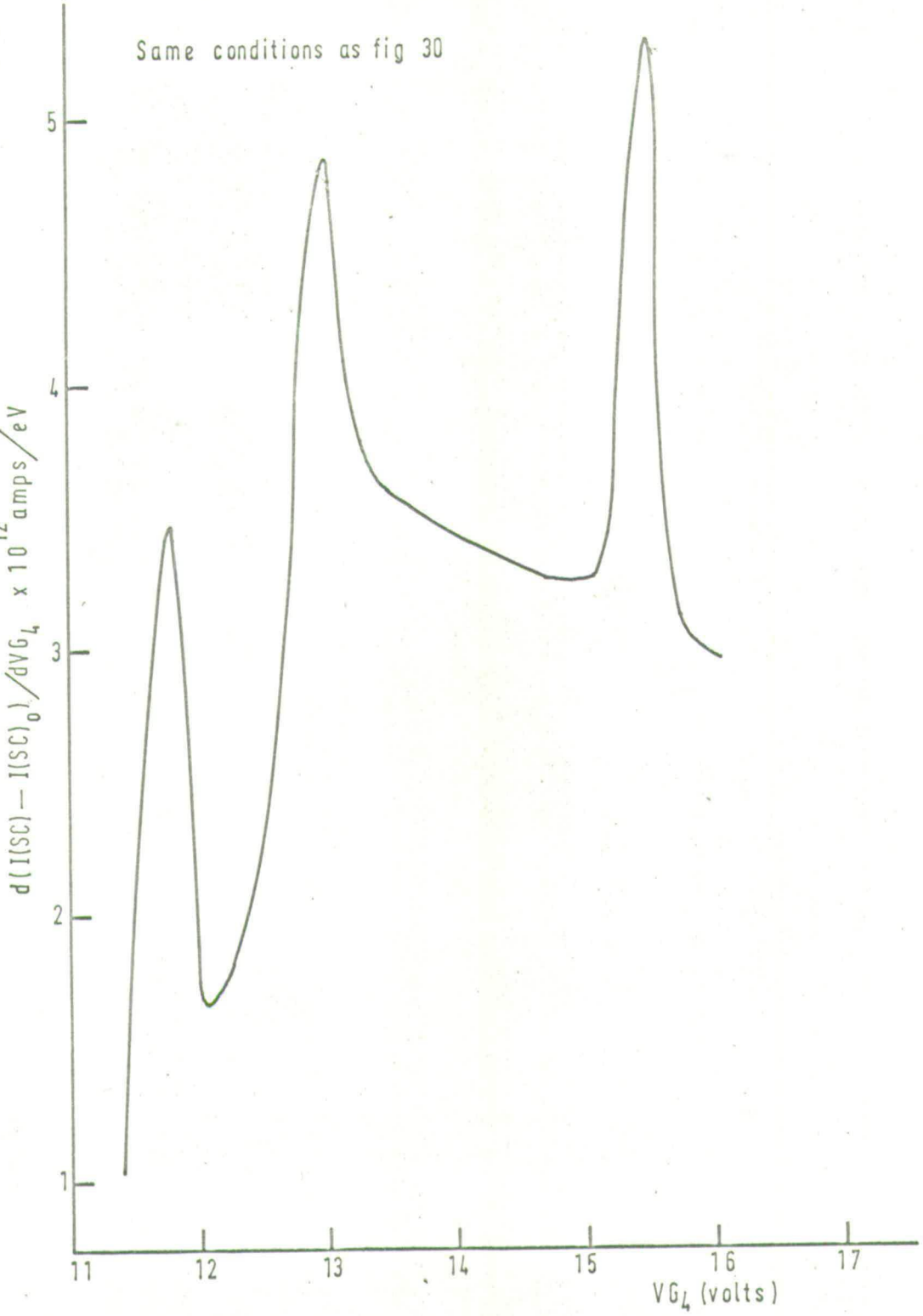

decrease much more rapidly with increasing electron energy than do those for optically allowed transitions. However, the error introduced by the differentiation procedure used here makes the comparison of peak heights a rather dubious procedure.

The results appear to indicate that states inaccessible by optical techniques can be studied by low energy, high angle electron impact spectroscopy. However, these results were obtained only with great difficulty. Random fluctuations in, for example, pressure and beam current can, and do, introduce spurious peaks. Many spectra must therefore be taken before spurious effects can be identified, and in fact most of the results must be discarded. The main causes of instability are the two mentioned above: fluctuations in beam current, and fluctuations in pressure. These could be removed by introducing servo controlled systems but during the course of the present research other workers have obtained results which appear to contradict those of Kuppermann and Raff in some respects, and cast some suspicion on the technique. Before going on to discuss possible improvements in any more detail, we will therefore pause and compare the results obtained by the various methods in order to evaluate the usefulness, or otherwise, of the one employed here.

FIG 33 ELECTRON IMPACT SPECTRA OF HELIUM AT HIGH ENERGIES

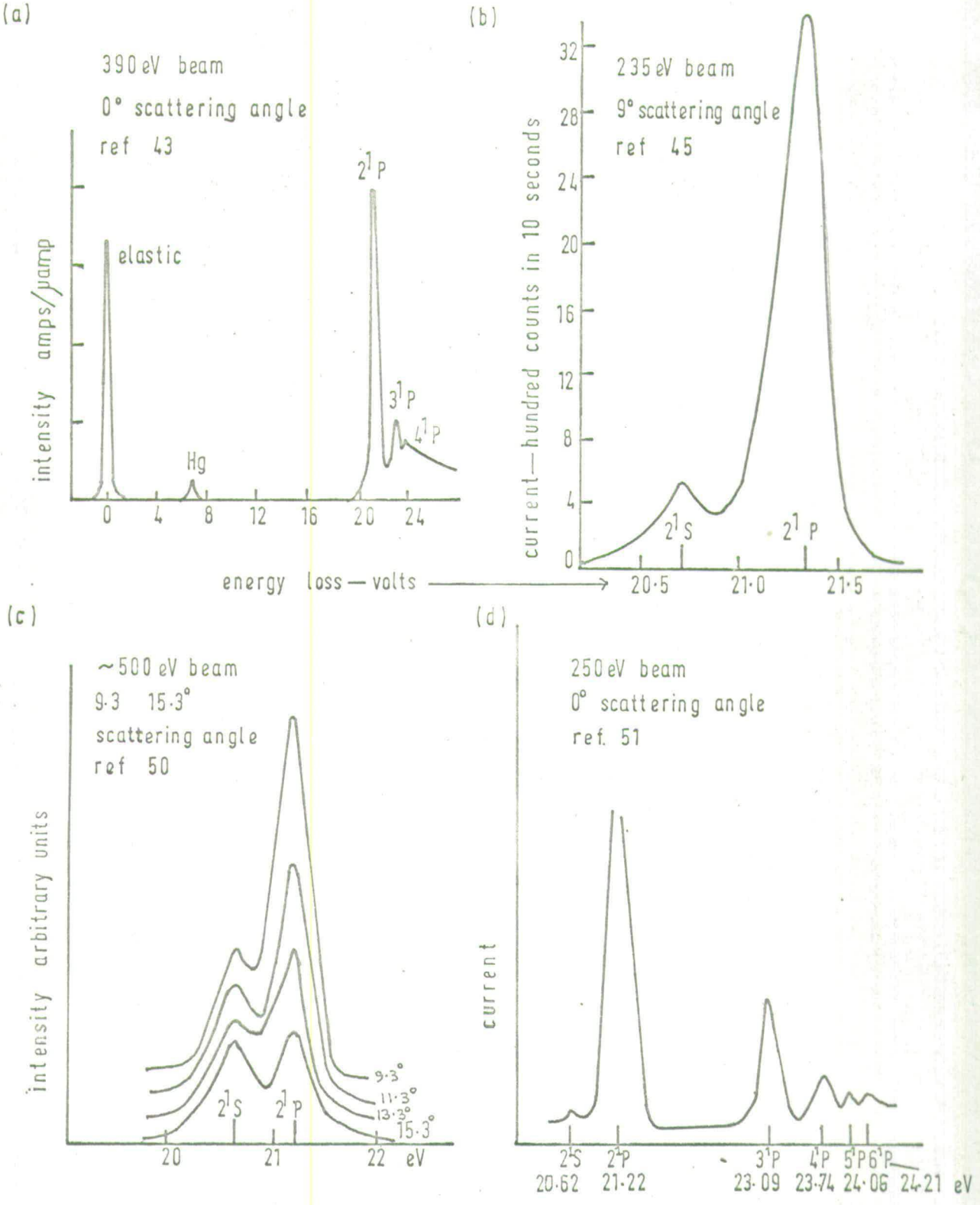

Chapter Three

DISCUSSION

3.1. Comparison with other work:

The two substances whose electron impact spectra may be most usefully discussed here are helium and ethylene, which have been studied by various workers over a wide range of energies and angles.

The electron impact spectrum of helium:

Lassettre and co-workers (see Chapter One) have made an extensive study of the electron impact spectrum of helium at high energies and low scattering angle, conditions under which the Born approximation is valid. There should therefore be an exact correspondence, within the limits of the resolution of the apparatus, between electron impact and ultraviolet spectra, a prediction which was confirmed by Lassettre's work. His first results, for 390 eV electrons and zero scattering angle, are shown in Fig. (33a) where the most prominent feature of the spectrum is the 2^1P transition at 21.2eV (43). Using lower energy electrons, and looking at 9° scattering, the angular momentum forbidden 2^1S transition was resolved - Fig.(33b)-, some at least of the increased resolution being due to greater dispersion of the analyser at lower kinetic energies (45). The variation with angle was further investigated for angles up to 15° (46,50) and some of the results are shown in Fig.(33c).

Lassettre found that at low angles only one peak around 21eV was visible, the 2^1P peak, but as the angle was increased a second peak corresponding to the 2^1S was resolved. Although the scattering intensity for both transitions decreased steadily with increasing angle, the intensity for the optically allowed $1^1S - 2^1P$ transition decreased more rapidly than that for the optically forbidden $1^1S - 2^1S$ transition, until by 15° the transitions occurred with equal probability. This is exactly the type of behaviour predicted by the

FIG 34 ELECTRON IMPACT SPECTRA OF HELIUM AT LOW ENERGIES

(a)

50eV beam
large angle scattering
ref. 72

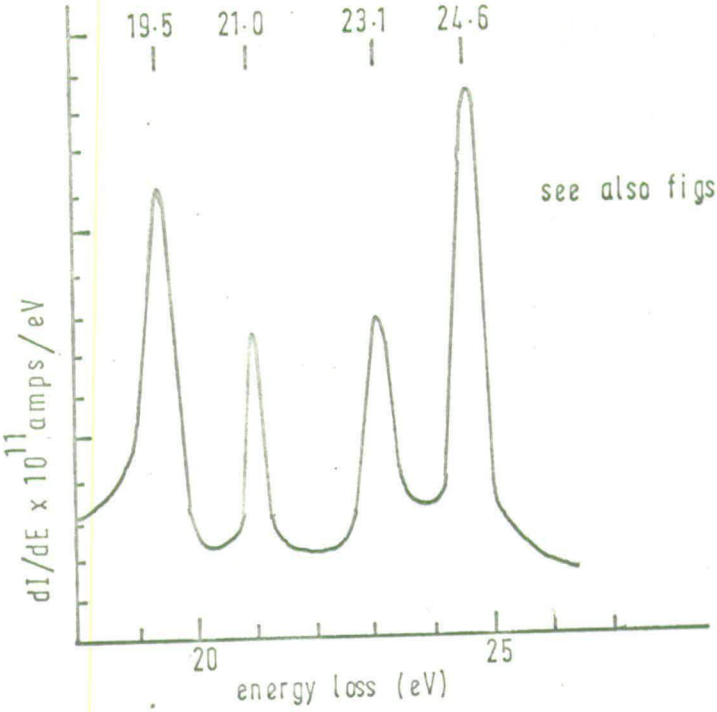

see also figs (28) and (29)

(b)

50eV beam
scattering angle < 20mrad
ref. 77

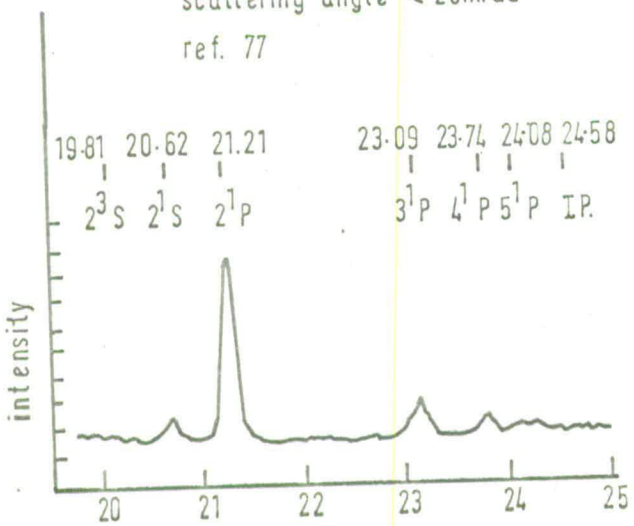

(c)

60eV beam
90° scattering angle
ref. 78

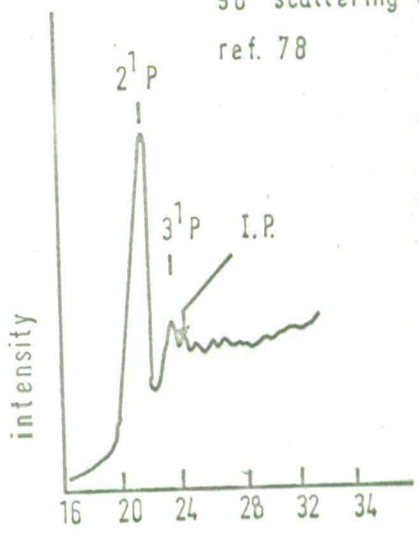

energy loss (eV)

the theory (see Chapter 1). The expected variation of relative intensity with electron energy was also observed: at 600eV the 2^1S state was not clearly resolved, but for a fixed scattering angle the intensity relative to the 2^1P state increased steadily as the energy was decreased to 232eV (46).

In a later experiment an electrostatic analyser was installed in the electron source (51). Much higher resolution was then achieved, but at the expense of intensity, which meant that only zero angle scattering could be studied. Fig.(33d) shows a typical spectrum obtained with 250eV electrons, the 5^1P and 6^1P states now being resolved. Using the same apparatus he was later able to resolve the 3^1S angular momentum forbidden transition.

The helium spectrum obtained by Kuppermann and Raff is shown in Fig.(34a), very similar to the ones obtained in the present work - Figs.(28,29). The most striking differences between these and the spectra of Lassettre and co-workers are the prominent peaks for the 2^3S state and the first ionisation potential. In no other electron impact work is ionisation clearly marked. Lassettre studied the region around 24.6eV carefully and found "no indication whatsoever of a peak at this voltage, of a discontinuity of slope, or of any departure from a continuous curve with continuously changing slope". He states that the reason that no peak is seen at the ionisation potential is the low resolution of the spectrometer, and its absence is not fundamentally related to the scattering process, or to the energy states of the scatterer (43). Since the resolution achieved by Kuppermann and Raff is lower than Lassettre's one would not expect them to observe any peak at the ionisation potential, but the peaks were systematically present in all their experiments, as indeed they are in the present work on helium.

In the light of other work it seems unlikely that ionisation is being observed. Doering (82) has suggested that the peaks may correspond to transitions to a bound state near the ionisation limit.

The prominence of the 2^3S and 3^1S states might be explained by the failure of the Born approximation at low energies. To determine whether the deviations from optical spectra observed by Raff are a consequence of the low electron energy Simpson and Mielczarek investigated the forward scattering of 50eV electrons (77). Their apparatus consisted of two hemispherical electrostatic analysers. The filtering analyser produced an electron beam of half width 0.1eV, and electrons scattered into an angle 0 20 mrad were energy analysed in the second analyser by determining the amount of energy required to restore them to the primary beam value. However the spectra they obtained - Fig.(34b)- resemble Lassettre's rather than the present one and those of Kuppermann and Raff. Neither the 2^3S state nor the ionisation limit were prominent, leading Simpson and Mielczarek to conclude that the deviations observed by Raff are a consequence of the high angular scattering, rather than of the low electron energy. A discussion was given by Kuppermann and Raff (81) who reached the same conclusion.

An experiment designed to clarify the situation was recently carried out by Doering (78). In his apparatus electrons from a thoria coated iridium filament were accelerated through a slit into the collision chamber, the unscattered beam was collected at a Faraday cup isolated from the collision chamber by an 86% transparency grid, and electrons scattered through 90° left the collision chamber via a second slit, were retarded to 3eV in order to increase the dispersion at the exit slit of the 127° analyser, and collected at a shielded collector. The limiting factor in the resolution was the energy spread of the beam from the filament: 0.7eV. Spectra were obtained for electrons in the energy range 40 - 100eV, but in no case was the 2^3S state observed, from which Doering concludes that the $1^1S - 2^3S$ transition must be at least a factor of 5 less intense than the $1^1S - 2^1P$ transition, and that there is no great variation of the spectrum with scattering angle. A typical spectrum is shown in Fig.(34c).

FIG 37 RELATIVE CROSS SECTIONS FOR HELIUM

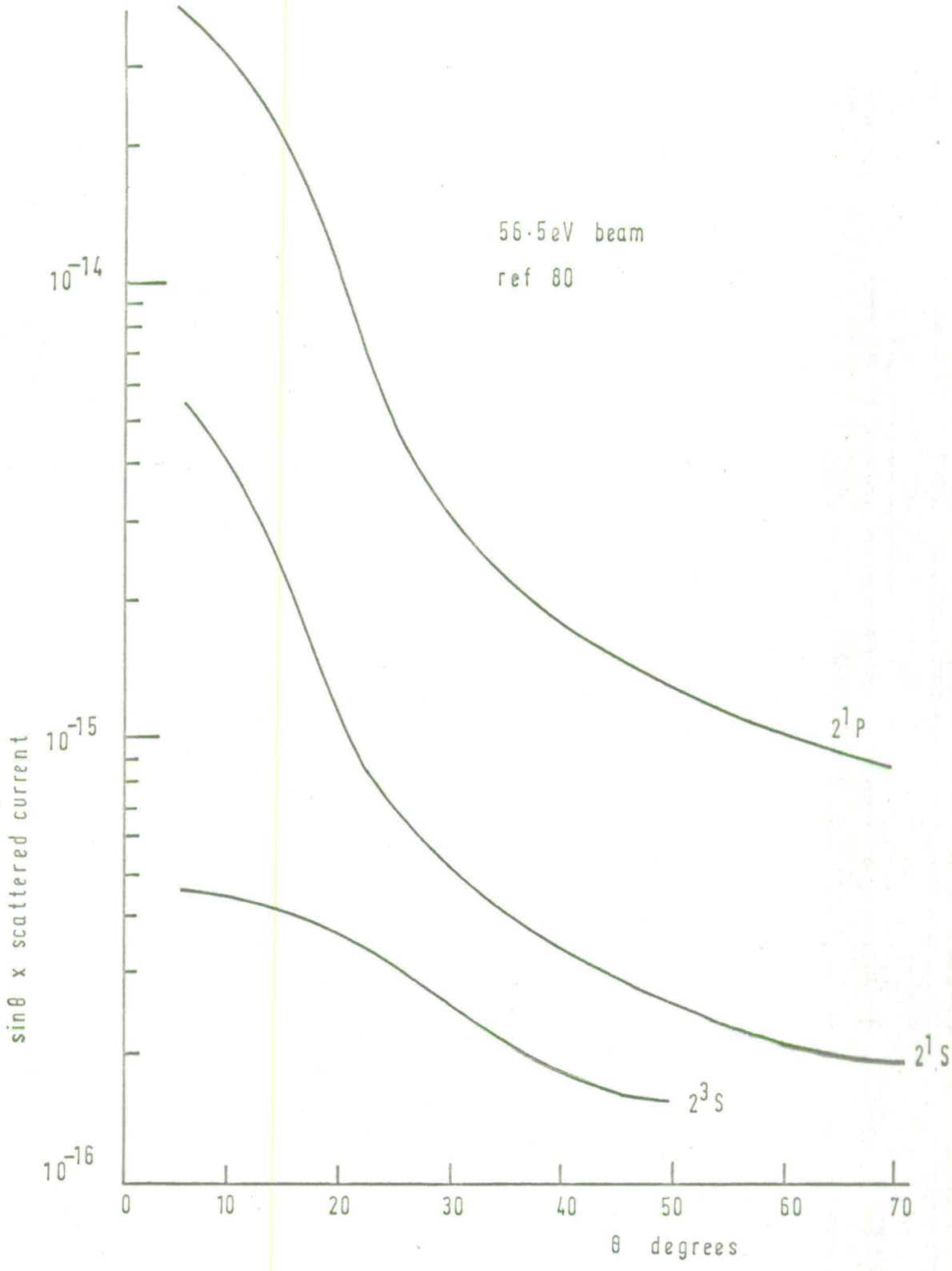

It begins to seem as if the results obtained by the retarding potential difference method may be spurious; however the 2^3S state has been observed at 56.5eV and 50° by Simpson, Menendez, and Mielczarek (80). They found that it was 7 times less intense than the 2^1P state, in agreement with Doering's conclusion above. The 2^1S state was also observed, appearing 5 times less intense than the 2^1P state. This last result contradicts the observations of Lassettre et al (Fig.33c), who found the two transitions occurring with equal intensity as low as 15° scattering angle. Therefore, although the qualitative agreement is good, there is not complete agreement among any of the workers about the intensities of the various transitions.

Because of uncertainties introduced by the method of data analysis used in the present work it does not seem justifiable to put much weight on the relative intensities of the peaks seen: the shape of the derivative curve is too sensitive to the smoothing procedure, a fact which must also have been true in the Kuppermann and Raff experiment. However it should be remembered that the occurrence and position of a peak is clearly marked by a discontinuity in the current against voltage curve. It is only the intensity which is doubtful.

Since ethylene has been studied by all the above workers we will consider briefly their results for this gas before continuing the discussion.

The electron impact spectrum of ethylene:

At high energies and low angle the main feature of the spectrum is a continuum peaking at 7.66eV - Fig.(35a), ref.(43) -, which was resolved in a later experiment - Fig.(35b), ref.(67).

At low energies, 40 - 75eV, Kuppermann and Raff observed inelastic transitions at 4.8, 6.5, 7.7, 8.8 and 10.7eV, Fig. (35d). The first two peaks were assigned to optically forbidden transitions, one corresponding well with the value of 4.6eV proposed by Evans (85) for the singlet → triplet $T \leftarrow N$

FIG 35 ELECTRON IMPACT SPECTRA OF ETHYLENE

(a) AT HIGH ENERGIES

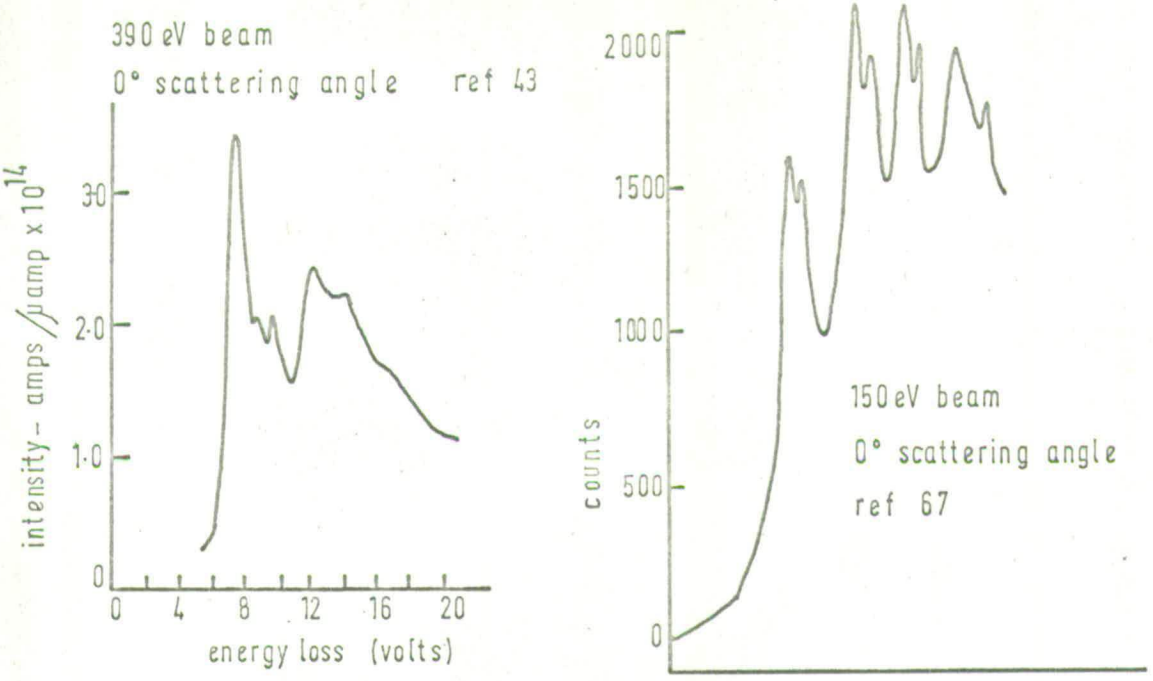

(b) AT LOW ENERGIES

I – give the positions of the Rydberg bands

50eV beam; scattering angle < 20mrad

ref 77

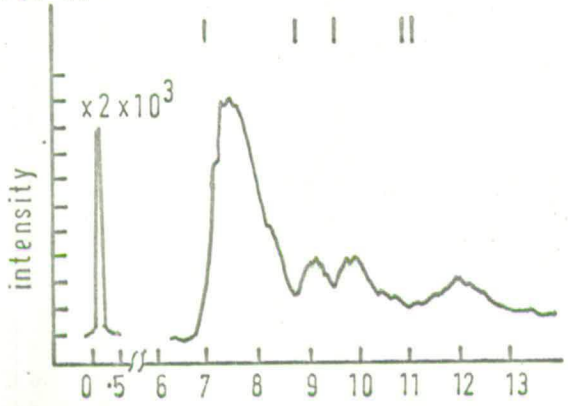

50 eV beam

large scattering angle

ref 73

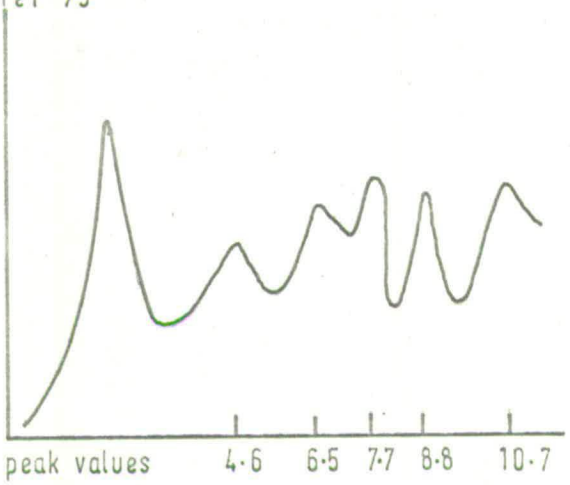

energy loss (eV)

FIG 36 ELECTRON IMPACT SPECTRUM OF ETHYLENE

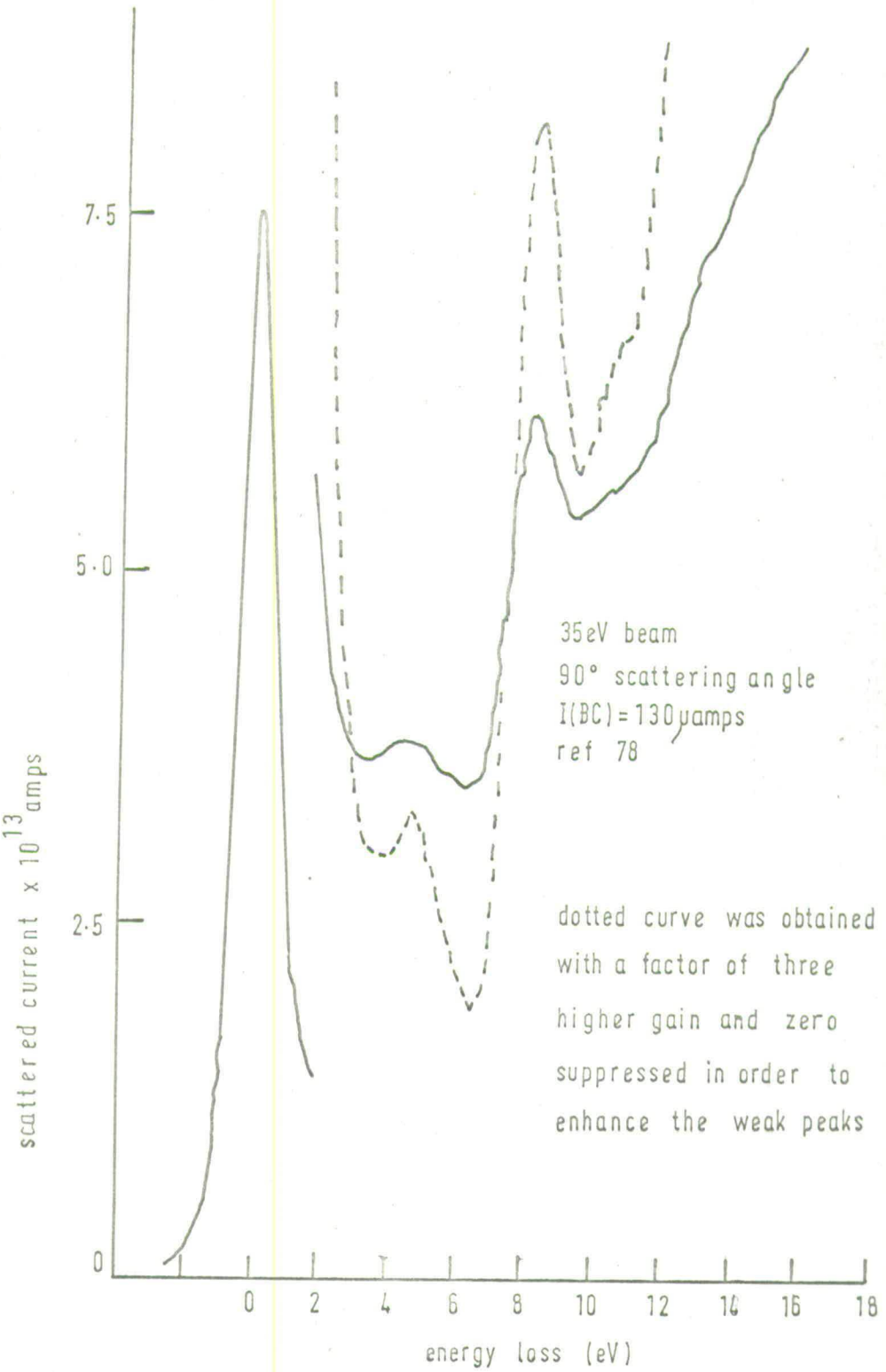

transition, and the other they suggest is an angular momentum forbidden transition. The 7.7 and 8.8eV peaks agree with observed transitions in the ultraviolet absorption spectrum, and the 10.7eV peak was attributed to the ionisation limit.

Simpson and Mielczarek obtained a spectrum with peaks between 7 and 13eV only. They observed no transitions below 7.1eV, or at the ionisation limit - see Fig.(35c), and ref.(77).

Doering's results are shown in Fig.(36). Because ethylene interfered seriously with the emission from the cathode, necessitating a much higher operating temperature than normal, and because of difficulties in achieving a satisfactory signal to noise ratio, the energy resolution in this experiment was 1.2 eV at best. The major features of his spectra agree well with those of Simpson and Mielczarek, while there is qualitative agreement with Lassettre's high energy work. He does however see an "unmistakeable" peak at 4.7 eV, not seen by either of the above authors, but present in the spectra of Kuppermann and Raff.

Both Doering and Kuppermann and Raff found an identical variation with electron energy of the intensity of the 4.7 eV transition relative to the 8 eV transition: As the energy was increased from 35 to 50 eV, the 4.7 eV peak became less prominent, and by 75 eV it had disappeared altogether from Raff's spectrum. They therefore agree over its assignment as a $T \leftarrow N$ transition. Doering does not see a peak at 6.5 eV and concludes that it is at least a factor of 3 less intense than the 4.7 eV transition, in contradiction to Kuppermann and Raff. All the workers found a peak at 10.7 eV, only Kuppermann and Raff observing a prominent one, assigned by them to the ionisation limit. The others, however, favour its assignment as an allowed transition to a bound state near the ionisation limit.

Summarising the position we see that, apart from the 6.5 eV peak in ethylene and the ionisation limit in helium, all the peaks observed by Kuppermann and Raff in these two gases have been observed by other workers, there being disagreement among all of them over the relative intensities. It does appear that as the scattering angle is increased from 0 to 90° there is not such a radical change in the spectra as was first thought from Raff's work. However, the optically allowed transitions do become much weaker relative to optically forbidden ones so that forbidden transitions, masked at small angles, can be observed at 90°. Doering has obtained some data on N_2 in which he finds that the optically allowed transitions agree well with the high energy work of Lassettre, but at energies less than 100 eV, and 90° scattering angle, singlet-triplet transitions are very clearly resolved (83). There is therefore much useful information to be gained from low energy, high angle scattering spectra and it remains to decide whether the present method can yield reliable results.

The greatest discrepancy between the present results and those of the other workers is the prominence of the optically forbidden transitions. This does suggest that, in some way, the method used here may be more sensitive to the occurrence of weak transitions. A possible explanation arises when the results obtained by the trapped electron technique (see Chapter 1) are studied. Bowman and Miller have measured the electron impact spectra of helium and ethylene by this method (84). In their apparatus 93% of all electrons scattered from a particular level are detected without regard to scattering angle, and their results for helium and ethylene are shown in Fig.(38). The incident electron energy scale was corrected for changes due to the potential well, and for contact potentials, in order to bring the excitation peaks into agreement with optical transitions, the 2^3S state of helium at 19.82 eV being used as a standard. Now there is a great difference in incident electron

FIG 38 ELECTRON IMPACT SPECTRUM OF HELIUM AND ETHYLENE OBTAINED BY THE TRAPPED ELECTRON TECHNIQUE

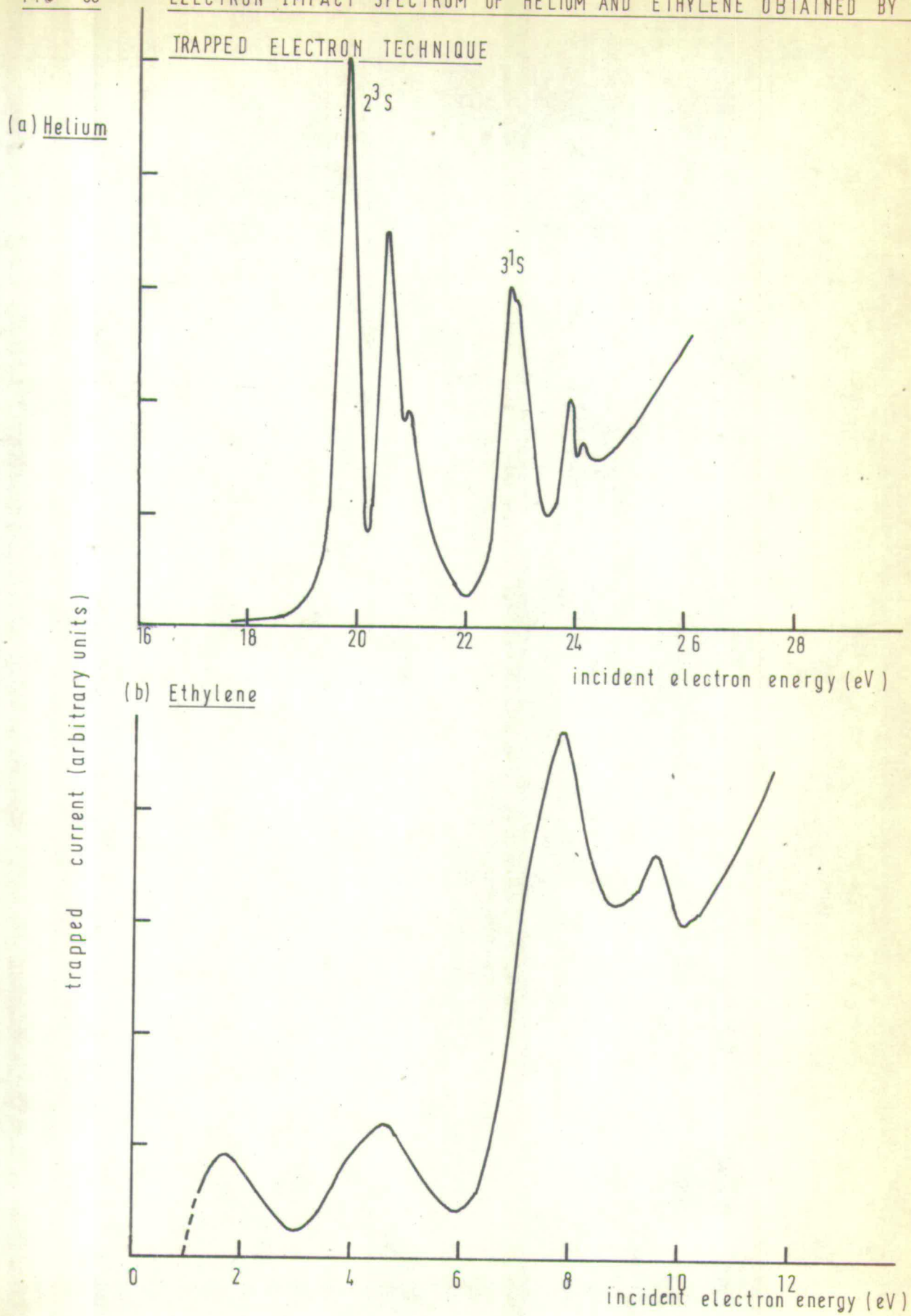

energy between this experiment and the present one, so that exact agreement is not expected. But the results bear a close resemblance to those obtained by the retarding potential difference technique. This suggests that what at first sight appears to be a disadvantage of the present method - the collection of electrons scattered through a wide range of angles - may in fact be responsible for the increased sensitivity of the instrument over the electrostatic analysers. A far greater percentage of the scattered electrons are being collected and therefore the weaker peaks are more easily observed.

There is good agreement between the data of Kuppermann and Raff and that of the present work, except that in this work the ionisation limit in argon is not clearly marked. However, before results, especially relative intensities, obtained from this experiment can be treated with real confidence, the difficulties inherent in dealing with an integral curve when it is the derivative that is required must be overcome.

3.2. Suggested Improvements to the Apparatus:

3.2.1. Electrical Differentiation of Retarding Potential Measurements:

Leder and Simpson (86) have suggested a method by which differential spectra may be obtained from retarding potential measurements. They were working at very high electron energies (keV), but it may be possible to adapt the method to the lower energies used here. Full details of circuitry and performance can be found in ref. (86) and only the principles of the method will now be discussed.

In the retarding potential difference technique the magnitude of the current, I, at any given value, E, of the retarding field is proportional to that fraction of the total current due to electrons of energy greater than E. The curve of I against E is thus an integral curve of the energy distribution of the electrons reaching the collector, i.e. $\int_{E}^{\infty} I(E)\,dE$ against E.

FIG 39 ELECTRICAL DIFFERENTIATION OF RETARDING POTENTIAL MEASUREMENTS

(a) Integral curve of current against retarding voltage showing the ac output ΔI resulting from the ac modulating voltage ΔV at retarding potential E

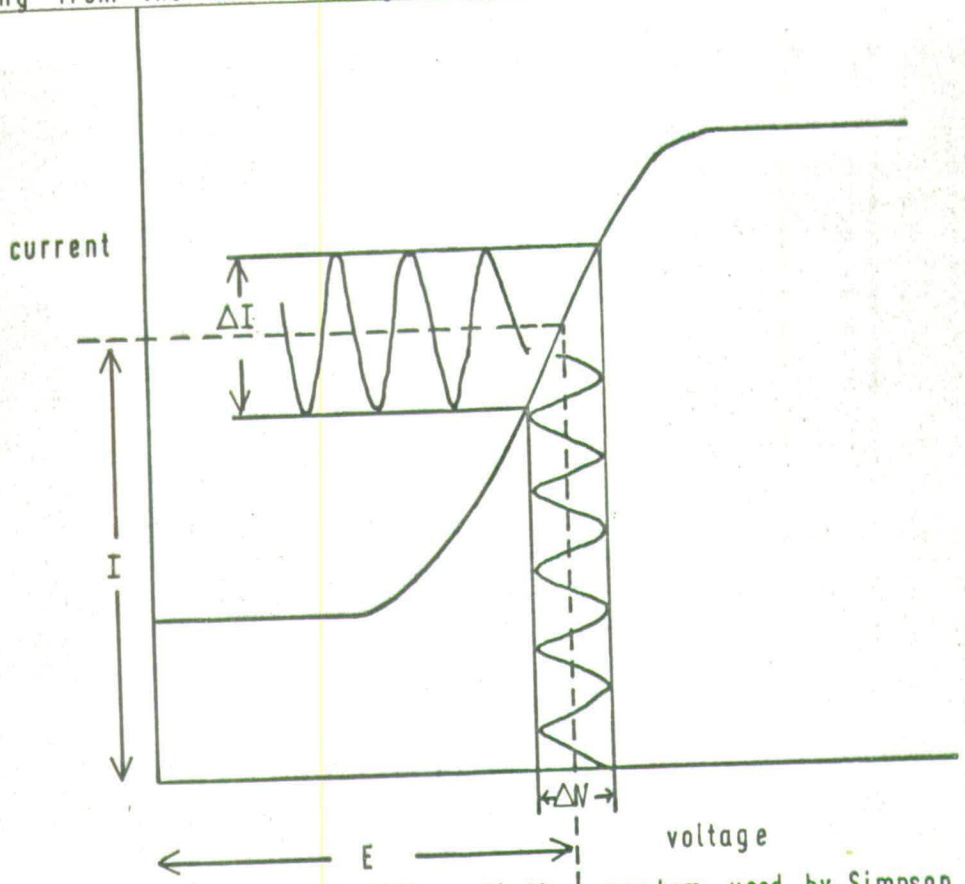

(b) Block diagram of electrical differentiating system used by Simpson and Leder

The dotted line denotes the vacuum part of the system

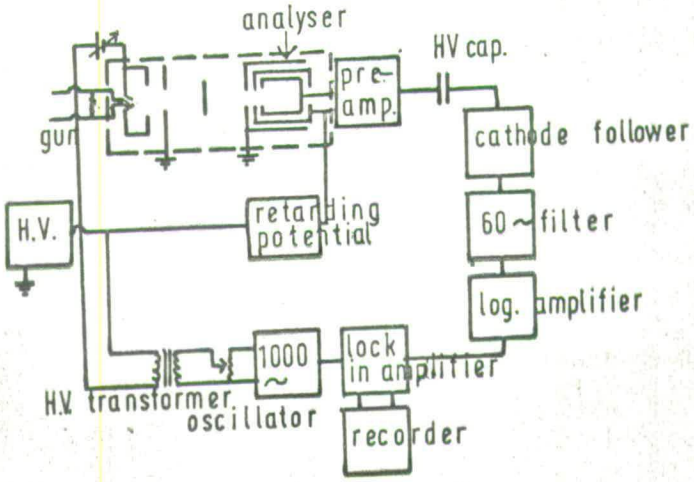

If a small ac voltage ΔV is superimposed on the retarding potential E, then the current I has added to it an ac component ΔI whose magnitude is proportional to the slope of the integral curve at the point E, and whose frequency is the same as that of ΔV. The process is illustrated in Fig.(39a). Changing E while keeping ΔV constant leads the magnitude of ΔI to sweep out a difference curve corresponding to the integral curve. As ΔV is decreased in amplitude the difference curve approaches a true differential curve. A block diagram of the electrical differentiating system designed by Leder and Simpson is shown in Fig.(39b). Their retarding potential was obtained from dry batteries and a continuous rotation potentiometer driven by a 2 r.p.m. motor.

Using this method it would become possible to obtain spectra much more rapidly, and the exceedingly laborious and uncertain analysis previously employed could be avoided. A further advantage is that by transforming a dc signal into an ac one, problems of voltage stability are alleviated. The disadvantage of the method is that the energy of the electrons is fluctuating within the amplitude of the modulating signal, 0.1 volts in Simpson's work; but the magnitude of ΔV could perhaps be reduced, and since the resolution of the instrument is limited by the energy spread of the beam, about 0.3 eV, the fluctuation may not be a problem at all. Simpson found no appreciable broadening of the energy profile he obtained for an electron beam from a tungsten filament, having a known half width of 0.6 eV.

With the possibility of overcoming the major drawback of the technique we will now consider what further improvements could be made.

3.2.2. Stabilisation of Beam Current and Pressure:

As was mentioned in Chapter 2, section 2, very many spectra had to be discarded because the system became unstable. The main sources of instability were found to be fluctuations in beam current, and fluctuations in pressure.

Stablisation of the beam current can be achieved by using the already amplified output from the electrometer in a servo system to modulate the voltage on E_1, and hence the emission.

Instabilities in pressure can be overcome by incorporating a servo controlled needle valve in the gas inlet system. A Granville Phillips Automatic Pressure Controller has been purchased for this purpose and is now installed between the Balzer's needle valve and the inlet flange. It will be operated by the signal from the ionisation gauge in the gun chamber, since the ionisation gauge in the collision chamber cannot be switched on during measurements without giving rise to a significant positive ion current at the grids.

3.2.3. Improved Angular Discrimination:

By splitting the scattered electron collector, electrons scattered through a smaller range of angles could be studied, while retaining the facility of measuring the total current reaching the collector in cases where intensity problems are acute. It has been ascertained that this modification could be carried out without difficulty by 20th Century Electronics.

3.3. Conclusions:

At first sight it appears that the electrostatic analyser is a preferable technique to the present one, since higher resolution is possible, and the derivative is obtained directly. However with the above modifications the retarding potential difference method becomes more attractive. Even at present the resolution of the apparatus is higher than any achieved by Doering. It is all a question of intensity. The situation is somewhat analogous to the position of Schulz with the electron trap and the double electrostatic analyser. The second technique is the more refined, but because of intensity it could be used to study only those transitions with high cross-sections.

Similarly, Lassettre's work was limited to low scattering angles, the loss of intensity preventing investigations at angles greater than 15°. Indeed, in the double analyser experiment only zero angle scattering could be studied, even with an electron multiplier in the detection system. At the much higher angles studied by Doering signal to noise problems were severe, and the resolution was limited to between 0.7 and 1.2 eV. However, for the purpose of studying cross sections in detail the advantages lie entirely with the electrostatic analyser techniques. They are inherently capable of the high resolution necessary, if the intensity problems can be overcome.

The above discussion leads to the conclusion that the present method can best be used in more qualitative studies of electron impact spectra. The positions of many singlet-triplet transitions have been predicted by quantum mechanical calculations.

In particular, Pariser and Parr (87) have developed a molecular orbital type of calculation for the electronic spectra of conjugated molecules. Their theory has since been refined by other workers and there exist predictions of the energies and intensities of transitions in the electronic spectra of many hydrocarbons and heteromolecules. Experimental evidence is available for the optically allowed transitions, but there is very little information with which to test the accuracy of predictions concerning the optically forbidden ones.

The present electron impact spectrometer, after incorporation of the improvements suggested above, should provide a suitable method for the location of optically forbidden transitions in a wide variety of molecules. Collecting electrons over a wide range of angles as it does, gives the apparatus a higher sensitivity than is possible with the more refined techniques. In addition, the variation of intensity with incident electron energy allows assignment of the type of transition involved. However in order to examine cross sections, and hence transition probabilities in more detail, a different type of apparatus is required, in which the differential scattering can be studied.

REFERENCES:

1. C. Ramsauer, Ann.der, Physik Lpz, 1921, 64, 513; 1921, 66, 546
2. C. Ramsauer, R. Kollath, Ann. der, Physik Lpz., 1929, 3, 536; 1930, 4, 91
3. C.E. Normand, Phys. Rev., 1930, 35, 1217
4. D.E. Golden, H.W. Bandel, Phys. Rev., 1965, 138, A14
5. J.S. Townsend, 'Motion of Electrons in Gases', 1925, London, Oxford University Press
6. H.S.W. Massey, E.H.S. Burhop, 'Electronic and Ionic Impact Phenomena', 1952, London, Oxford University Press
7. J.B. Hasted, 'Physics of Atomic Collisions', 1964, London, Oxford University Press
8. D.R. Bates (Ed.), 'Atomic and Molecular Processes', 1962, New York, Academic Press
9. T.L. Cottrell, I.C. Walker, Quart. Rev. Chem. Soc., 1966, 30, 153.
10. C.B.O. Mohr, F.H. Nicoll, Proc. Roy. Soc., 1932, 138A, 229
11. W.L. Fite, R.T. Brackmann, Phys. Rev., 1958, 112, 1141; W.L. Fite, R.F. Stebbings, R.T. Brackmann, Phys. Rev., 1959, 116, 356
12. R.M. St. John, F.L. Miller, C.C. Lin, Phys. Rev., 1964, 134, A888
13. W.L. Fite, R.F. Stebbings, D.G. Hummer, R.T. Brackmann, Phys. Rev., 1960, 119, 1939
14. J.D. Craggs, H.S.W. Massey, 'Handbuch der Physik', 1959, Vol.37, Berlin, Springer-Verlag
15. L.S. Frost, A.V. Phelps, Phys. Rev., 1962, 127, 1621
16. R. Haas, Z. Physik, 1957, 148, 177
17. G.J. Schulz, Phys. Rev., 1959, 116, 1141
18. H.S. Taylor, G.V. Nazaroff, A. Golebiewski, J. Chem. Physics, 1966, 45, 2872
19. K. Takayanagi, J. Phys. Soc. Japan, 1965, 20, 562; 20, 2297
20. K. Takayanagi, J. Phys. Soc. Japan, 1966, 21, 507
21. N.F. Mott, H.S.W. Massey, 'Theory of Atomic Collisions', 1965, London, Oxford University Press

22. H. Maier-Liebnitz, Zeit. fur Physik, 1935, 95, 489.

23. G.J. Schulz, Phys. Rev., 1958, 112, 150

24. G.J. Schulz, Phys. Rev., 1964, 135, A988

25. G.J. Schulz, J.T. Dowell, Phys. Rev., 1962, 128, 174

26. G.J. Schulz, J. Chem. Physics, 1960, 33, 1661

27. G.J. Schulz, J. Chem. Physics, 1961, 34, 1778

28. A.L. Hughes, V. Rojansky, Phys. Rev., 1929, 34, 284.

29. E.M. Clarke, Can.J. Phys., 1954, 32, 764

30. P. Marmet, L. Kerwin, Can. J. Phys., 1960, 38, 787

31. G.J. Schulz, Phys. Rev., 1959, 116, 1141

32. G.J. Schulz, Phys. Rev., 1962, 125, 229

33. J.A. Simpson, Rev. Sci. Instruments, 1964, 35, 1698

34. C.E. Kuyatt, J.A. Simpson, S.R. Mielczarak, Phys. Rev., 1965, 138A, 385

35. H.G.M. Heidemann, C.E. Kuyatt, G.E. Chamberlain, J. Chem. Physics, 1966, 44, 355.

36. L.C. van Atta, Phys. Rev., 1931, 38, 876

37. A.L. Hughes, J.H. McMillen, Phys. Rev., 1932, 41, 39

38. H. Jones, R. Whiddington, Phil. Mag., 1928, 6, 889

39. E. Rudberg, Proc. Roy. Soc., 1930, 129A, 628

40. J.E. Roberts, R. Whiddington, Proc. Roy. Soc., 1936, 156A, 270

41. E. Rudberg, Proc. Roy. Soc., 1930, 130A, 182

42. N. Thorley, R. Whiddington, Proc. Leeds Phil. Sci. Soc., 1937, 3, 265

43. E.N. Lassettre, S.A. Francis, J. Chem. Physics, 1964, 40, 1208

44. E.N. Lassettre, E.A. Jones, ibid, 1964, 40, 1222

45. E.N. Lassettre, A.S. Berman, S.M. Silverman, M.E. Krasnow, ibid, 1964, 40, 1232

46. E.N. Lassettre, M.E. Krasnow, S.M. Silverman, ibid, 1964, 40, 1242

47. E.N. Lassettre, M.E. Krasnow, ibid, 1964, 40, 1248

48. E.N. Lassettre, S.M. Silverman, ibid, 1964, 40, 1256

49. E.N. Lassettre, S.M. Silverman, M.E. Krasnow, ibid, 1964, 40, 1261

50. E.N. Lassettre, S.M. Silverman, ibid, 1964, 40, 1265

51. A.M. Skerbele, E.N. Lassettre, ibid, 1964, 40, 1271

52. A.M. Skerbele, E.N. Lassettre, V.D. Meyer, M.S. Longmire, ibid, 1964, 41,2952

53. E.N. Lassettre, S.M. Silverman, ibid, 1964, 41, 3727

54. A. Skerbele, E.N. Lassettre, ibid, 1964, 42, 395

55. E.N. Lassettre, V.D. Meyer, M.S. Longmire, ibid, 1964, 42, 807

56. E.N. Lassettre, S.M. Silverman, ibid, 1964, 42, 3420

57. E.N. Lassettre, F.M. Glaser, V.D. Meyer, A. Skerbele, ibid, 1964, 42, 3429

58. E.N. Lassettre, V.D. Meyer, ibid, 1964, 42, 3436

59. E.N. Lassettre, S.M. Silverman, ibid, 1964, 43, 194

60. E.N. Lassettre, J.C. Shiloff, ibid, 1965, 43, 560

61. E.N. Lassettre, V.D. Meyer, A. Skerbele, ibid, 1965, 43, 805

62. E.N. Lassettre, V.D. Meyer, A. Skerbele, ibid, 1965, 43, 817

63. E.N. Lassettre, V.D. Meyer, A. Skerbele, ibid, 1965,43, 3769

64. V.D. Meyer, E.N. Lassettre, ibid, 1966, 44, 2535

65. A. Skerbele, E.N. Lassettre, ibid, 1966, 44, 4066

66. A.Skerbele, E.N. Lassettre, V.D. Meyer, ibid, 1966, 44, 4069

67. K.E. Ross, E.N. Lassettre, V.D. Meyer, ibid, 1966, 44, 4635

68. E.N. Lassettre, A. Skerbele, ibid, 1966, 45, 1077

70. F.L. Arnot, G.O. Baines, Proc. Roy. Soc., 1935,151A, 256

71. A. Womer, Phys. Rev., 1934, 38, 876

72. A. Kuppermann, L.M. Raff, Disc. Faraday Soc., 1963, 35, 30

73. A. Kuppermann, L.M. Raff, J. Chem. Physics, 1962, 34, 2497

74. L.M. Raff, Ph.D. Thesis, Illinois, 1962

75. T.L.Cottrell, B.M. Lowe, A.W. Read, unpublished work

76. A.W. Read, unpublished work

77. J.A. Simpson, S.R. Mielczarek, J. Chem. Physics, 1963, 39, 1606

78. J.P. Doering, J. Chem. Physics, 1966, 45, 1065

79. G. Rutledge, Phys. Rev., 1932, 40, 262

80. J.A. Simpson, M.G. Menendez, S.R. Mielczarek, Phys. Rev., 1966, 150, 76

81. A. Kuppermann, L.M. Raff, J. Chem. Physics, 1963, 39, 1608

82. J.P. Doering, J. Chem. Physics, 1967, 46, 1194

83. J.P. Doering, private communication

84. C.R. Bowman, W.D. Miller, J. Chem. Physics, 1964, 42, 681

85. D.F. Evans, J. Chem. Soc., 1960, 1735

86. L.B. Leder, J.A. Simpson, Rev. Sci. Instruments, 1958, 29, 571

87. R. Pariser, R.G. Parr, J. Chem. Physics, 1955, 23, 711

ACKNOWLEDGMENTS

I am grateful to Dr. A.W. Read, Dr. T.L. Cottrell, and Dr. B.M. Lowe for their help and encouragement during this research. I also wish to thank Mr. T.D. Sheddan, Mr. A.H. Young, Mr. A. King and the other members of the technical staff for their assistance throughout the work.

I am indebted to the University of Edinburgh for the provision of library and laboratory facilities, and the Science Research Council for the award of a studentship.

Offprinted from the *Transactions of The Faraday Society*,
No. 512, Vol. 61, Part 8, August, 1965

VIBRATIONAL RELAXATION OF CARBON MONOXIDE AT ROOM TEMPERATURE

Vibrational Relaxation of Carbon Monoxide at Room Temperature

By Margaret G. Ferguson and A. W. Read

Chemistry Dept., Edinburgh University.

Received 15*th January*, 1965

The vibrational relaxation time of carbon monoxide has been determined with the spectrophone, comparing the amount of vibrational energy lost by collision to the amount lost by fluorescence. Using a carefully purified sample a value of 0·8 sec was established as a shorter limit to the relaxation time at 290°K. This result, longer than previously determined room-temperature values, agrees with the value predicted by the high-temperature shock-tube data. The shorter values are shown to be due to impurity effects.

Vibrationally excited carbon monoxide can lose its energy by two mechanisms:

(1) collision, $CO(v = 1)+M \rightarrow CO(v = 0)+M+$kinetic energy,

(2) radiation, $CO(v = 1) \rightarrow CO(v = 0)+h\nu$.

The relaxation time for the first process with M = CO has been well established at higher temperatures by shock-tube experiments [1–3] and the extrapolation of these results indicates that at room temperature the rate of collisional loss should be much slower than that of radiative loss, whose time constant can be calculated from spectral data.[4] This conclusion has been verified by Millikan [5] who studied vibrational fluorescence in a flow experiment. Thus, pure carbon monoxide should lose vibrational energy by radiation rather than by collision and should give zero response in the spectrophone, which detects changes in translational energy.[6] This is in contradiction to the observations of Woodmansee and Decius,[7] but their result can be attributed to the presence of impurities shortening the relaxation time to the reported value of 2×10^{-3} sec.

We have re-investigated the behaviour of carbon monoxide in the spectrophone and by comparison of the proportion of energy loss by collision to that by radiation have established a new value for the relaxation time at room temperature.

EXPERIMENTAL

The spectrophone is shown diagramatically in fig. 1. It was constructed from brass, vacuum sealed with a Viton O ring. The diaphragm was of 30 gauge metallized Melinex film and was clamped between two metal rings which were screwed to the cell. Diaphragm tension and backplate position were adjustable for maximum sensitivity. The pressure in the cell equilibrated by long-time-constant leaks across diaphragm, tensioning ring and backplate. The absorption cell was a cylinder 2·5 cm diam. by 2 cm long, with windows of calcium aluminate glass (Barr and Stroud, type BS.39B) sealed to the ends with Viton O rings. Gas flow into the spectrophone was controlled by an all-metal needle valve which was closed when measurements were taken to avoid acoustic resonance effects in the gas line. The spectrophone was connected to a conventional high-vacuum system and the vacuum measured with an ionization gauge. When required the system could be heated to 120°C for bake-out purposes.

The exerimental parrangement is shown diagramatically in fig. 2. A front silvered mirror focussed the radiation from a Nernst filament through a modulating disc into the cell.

Radiation was absorbed by the gas and some transferred to translational modes giving rise to pressure fluctuations. These caused variations in the position of the diaphragm which frequency modulated the 10·7 Mc/sec oscillator at the chopping frequency. The frequency modulation was detected in a conventional ratio-type discriminator and after pre-amplification fed to a selective amplifier of 2·5 mV full-scale sensitivity. In later experiments this was increased to 50 μV full-scale sensitivity. The d.c. output from the discriminator gave an indication of mean diaphragm position. The sensitivity of the entire system could be checked by noting the signal from a standard pressure of nitrous oxide.

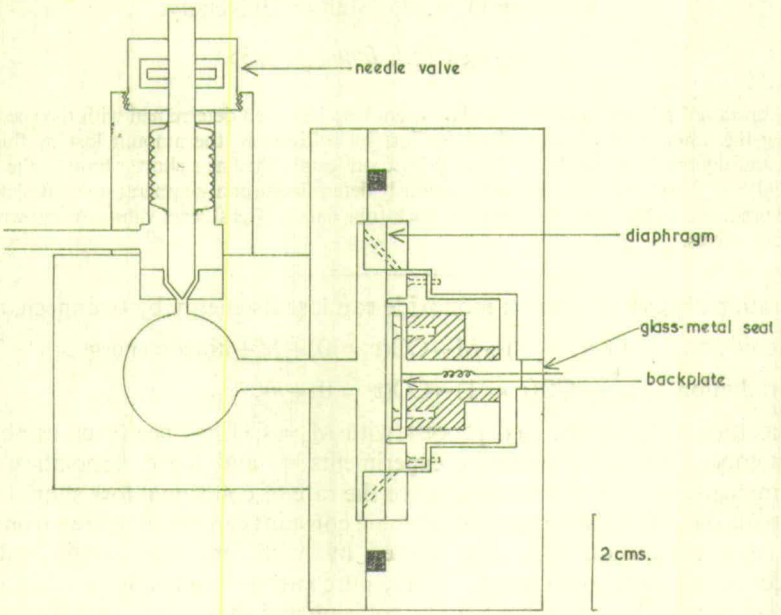

FIG. 1.—Diagram of Spectrophone.

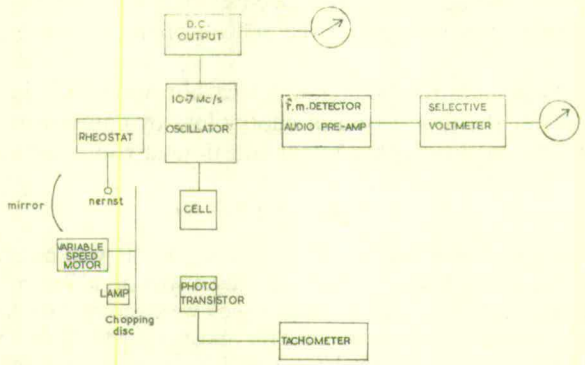

FIG. 2.—Experimental arrangement.

MATERIALS

Carbon monoxide was obtained from a cylinder (I.C.I. Ltd.), mass-spectrometer and infrared analysis indicated small amounts of CO_2 and H_2O with no detectable H_2. It was further purified by passage through several cold traps at $-196°C$, one of which contained pellets of alumina,[5] and dried by passage through phosphoric oxide. A new sample of CO was prepared for each experiment. When required, H_2 was obtained from a cylinder and used without further purification.

RESULTS

The cell was filled with pure CO to a pressure of 40 cm and with the selective amplifier at 2·5 mV sensitivity and 140 c/sec chopping frequency no signal was detected until 5 h after filling the cell. The signal then rose to a maximum value over a period of 40 h. It seemed probable that this rise was due to impurity molecules from the cell walls shortening the overall relaxation time, thus the spectrophone was baked for 40 h at 120°C after which the pressure fell from 3×10^{-5} to 3×10^{-6} torr and the pressure rise from 2×10^{-3} to 4×10^{-4} torr/h. On repeating the previous experiment it was found that a maximum value was not reached after 140 h. The sensitivity was checked and found to be unchanged. Hereafter, the spectrophone was baked before each experiment.

Even in pure CO a little vibrational energy will be lost by collision, the exact amount depending on the relative rates of processes (1) and (2). With the more sensitive electronics it was possible to detect a very small initial signal as soon as the cell was filled with purified gas. H_2, which is known to be an efficient collision partner for the de-excitation of CO ($\tau_{CO-H_2} = 10^{-4}$ sec at 290°K [5]) was then allowed to diffuse into the cell so that the rate of process (1) became very much faster than that of process (2) and the signal rose to a final steady value.

The small initial signal is proportional to the energy lost by collision in pure carbon monoxide which is given by $f_{10}n_1h\nu$ sec^{-1} cm^{-3}, where f_{10} is the transition probability per molecule per second for the $1\rightarrow0$ process, n_1 is the number of vibrationally excited molecules per unit volume and ν is the vibrational frequency.[8] The final steady signal after the addition of H_2 is proportional to the total energy loss both by collision and by radiation in pure CO, assuming that the radiation density remains constant and that the 10-20 % of added H_2 does not affect the absorption process. The total energy loss is given by $(f_{10}+1/\tau_{rad})n_1h\nu$ sec^{-1} cm^{-3}, where $1/\tau_{rad}$ is the number of spontaneous transitions per sec per molecule (31 sec^{-1}).

For CO, $f_{10} = 1/\tau_{CO-CO}$ [6], where τ_{CO-CO} is the relaxation time. Thus:

$$\text{initial signal/final signal} = 1/\tau_{CO-CO}/1/\tau_{CO-CO}+1/\tau_{rad}$$

At a pressure of 39 cm the initial signal was found to be 15 μV and the final signal to be 780 μV. This gives the relaxation time of CO at 290°K and 1 atm as 0·8 sec.

Molecular relaxation times depend inversely upon pressure whereas the radiative lifetime is independent of pressure. Thus, a good test of the experimental method is to measure the initial and final signals at two pressures and see if they are self-consistent. This must be done with the same sample of gas to eliminate the possibility of slight differences in the degree of purity. With a pressure of 40 cm the initial signal was found to be 30 μV, the pressure in the cell was then reduced, as rapidly as possible, to 20 cm when the initial signal was found to be 20 μV. After the introduction of hydrogen the final signal at 20 cm was 460 μV whereas for 40 cm it was 760 μV. From the figures at 40 cm and the final signal at 20 cm the initial signal expected at the lower pressure was 10 μV compared to the experimental value of 20 μV. The probable reason for the slight discrepancy is the impurity which degassed from the cell walls during the time taken to lower the pressure in the cell. The impurity will shorten the relaxation time and hence increase the initial signal over the expected value.

In order to investigate the effects of impurities from the walls measurements were then made on a sample of pure CO which was left in the cell for a period of 90h. The results are plotted in fig. 3. The theoretical curve was calculated using the equation for the relaxation time of a mixture [6]:

$$1/\tau_{mixture} = 1-x_B/\tau_{CO-CO}+x_B/\tau_{CO-B},$$

where B is the impurity, probably H_2O, and x_B is its mole fraction. It was assumed that B was desorbing from the walls at a steady rate (taken as the degassing rate of the empty cell) and that $\tau_{CO-B} = 1 \times 10^{-6}$ sec.

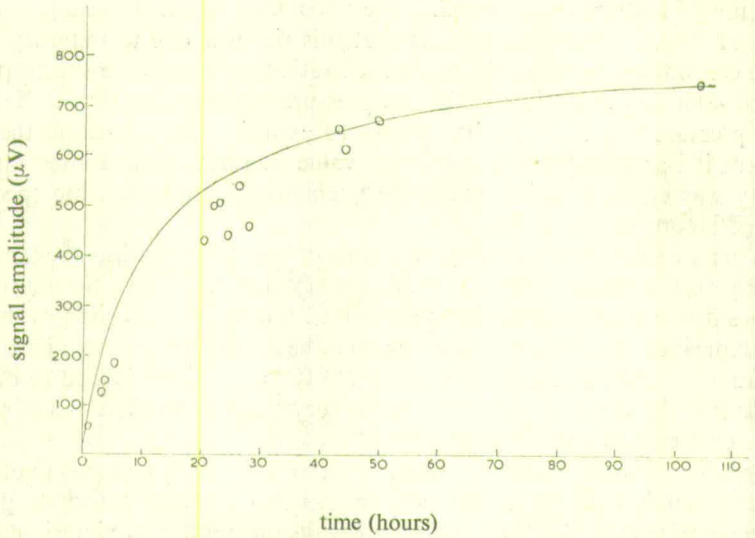

FIG. 3.—Plot of signal amplitude against time; Continuous line is the theoretical curve.

DISCUSSION

It is impossible to obtain an accurate figure for the initial signal because of the difficulties in the purification and the time necessary to fill the cell after the gas has been purified. The value of 15 μV for the initial signal at a pressure of 39 cm therefore represents an upper limit to the signal due to CO—CO collisions and thus the value for the relaxation time is a lower limit. All experiments were carried out at frequencies above 70 c/sec thus energy loss to the walls is not likely to be significant,[6] this has been directly confirmed by McCaa and Williams who observed the fluorescence from pure CO using a modulation frequency of 13 c/sec.[9] There is probably some re-absorption of a quantum before it is emitted from the cell, this will lead to an overall increase in the probability of collisional loss and again makes the value of 0·8 sec a shorter limit to the true relaxation time.

The result in this paper is in good agreement with that of Millikan [5] who observed infra-red fluorescence in a flow experiment for a period of 0·2 sec and deduced a relaxation time of this order or longer. The value predicted by the exptrapolation of the high-temperature shock tube data is around 5 sec and that predicted by the theory is around 3 sec[10], both of which are in good agreement with the present result.

The agreement of experimental and theoretical curves in fig. 3 is reasonable considering the assumptions made and it serves to emphasize the extreme efficiency of polyatomic molecules as collision partners for CO. It should be possible to study these effects further with this apparatus and also to study other gases which have predicted long relaxation times. It should be noted that the very small spectrophone signal from pure CO means that the Luft type of gas analyser,[11] which uses the same principle, will only detect impure samples of this gas.

The authors acknowledge helpful discussions with Prof. T. L. Cottrell and Prof. J. C. Decius.

[1] Windsor, Davidson and Taylor, *7th Symp. Combustion* (Butterworths, London, 1958), p. 80.
[2] Matthews, *J. Chem. Physics*, 1961, **34**, 639.
[3] Hooker and Millikan, *J. Chem. Physics*, 1963, **38**, 214.
[4] Penner, *Quantitative Molecular Spectroscopy and Gas Emissivities* (Pergamon Press, London, 1959), p. 21.
[5] Millikan, *J. Chem. Physics*, 1963, **38**, 2855.
[6] Cottrell and McCoubrey, *Molecular Energy Transfer in Gases* (Butterworths, London, 1961).
[7] Woodmansee and Decius, *J. Chem. Physics*, 1962, **36**, 1831.
[8] Kaiser, *Can. J. Physics*, 1959, **37**, 1499.
[9] McCaa and Williams, *J. Opt. Soc. Amer.*, 1964, **54**, 326.
[10] Dickens and Ripamonti, *Trans. Faraday Soc.*, 1961, **57**, 735.
[11] Luft, *Z. tech. Physik*, 1943, **24**, 97.

PRINTED IN GREAT BRITAIN AT
THE UNIVERSITY PRESS
ABERDEEN

Offprinted from the *Transactions of The Faraday Society*,
No. 529, Vol. 63, Part 1, January, 1967

VIBRATIONAL RELAXATION OF HYDROGEN CHLORIDE, DEUTERIUM CHLORIDE AND HYDROGEN BROMIDE AT ROOM TEMPERATURE

Vibrational Relaxation of Hydrogen Chloride, Deuterium Chloride and Hydrogen Bromide at Room Temperature

By Margaret G. Ferguson and A. W. Read *

Chemistry Dept., Edinburgh University

Received 26th August, 1966

The vibrational relaxation times of HCl, DCl and HBr have been determined by a spectrophone method. Shorter limits to the relaxation times are $1{\cdot}1 \times 10^{-2}$, 1×10^{-2} and $1{\cdot}5 \times 10^{-3}$ sec respectively. These results agree better with vibration-rotation theory than with vibration-translation theory. The results for HCl is compared with high-temperature shock-tube data.

Little is known about the vibrational relaxation of the hydrogen halides. Observations of the infra-red emission from shock-heated gas indicate that the relaxation times of hydrogen chloride and hydrogen bromide at 2000°K are several orders of magnitude shorter than predicted by theory.[1] The discrepancy is greater than any previously found for diatomic molecules, and it is therefore important to know the relaxation times of these molecules at lower temperatures. Because of their high vibrational frequencies, the room temperature equilibrium vibration populations are very low and prevent the use of the ultrasonic interferometer.[2] This limitation does not apply to the optic-acoustic method and we have investigated the vibrational relaxation of HCl, DCl and HBr using the spectrophone developed during work on carbon monoxide.[3] The basis of this method is that vibrationally excited molecules with long relaxation times ($>10^{-3}$ sec) will lose energy both collisionally and radiatively. The time constant of the radiiative process, which is known from the absorption intensity, provides a time scale by which the efficiency of the collisional process can be determined.

EXPERIMENTAL

A description of the spectrophone and experimental arrangement are given elsewhere.[3] In the present work the final amplification of the spectrophone signal was by a General Radio Company Tuned Amplifier and Null Detector, type 1232A. During the experiments the Melinex diaphragm was replaced frequently since the gases used, even when pure and dry, slowly attacked the metal coating.

MATERIALS

Hydrogen chloride was prepared (i) from NH_4Cl and H_2SO_4, and (ii) by reacting HCl with conc. H_2SO_4. In both cases the gas was dried with H_2SO_4 and P_2O_5, condensed at $-196°$, degassed and distilled into the spectrophone.

Hydrogen bromide was obtained from a cylinder (Matheson Co. minimum purity 99·8 %), dried over P_2O_5 and further purified as for HCl.

Deuterium chloride was prepared by reacting $SiCl_4$ with D_2O.[4] Infra-red analysis showed that the gas contained 10-20 % of HCl. This arose from an exchange mechanism with the

* present address: Central Electricity Generating Board, Regional Research and Development Department, Kirkstall Power Station, Leeds, 4.

water adsorbed on the walls of the gas-handling system, despite precautions to eliminate such contamination. After several preparations in the same system the percentage of HCl was greatly reduced. In the later runs DCl was obtained from a cylinder (Merck, Sharpe and Duohme), condensed at $-196°$, degassed and distilled at $-120°$.

In all cases, a new sample was prepared for each experiment.

RESULTS

A gas sample was allowed to diffuse rapidly into the baked, degassed spectrophone and the initial signal found. During a period of several hours the signal rose to a steady value. This rise is caused by impurity molecules from the walls which shorten

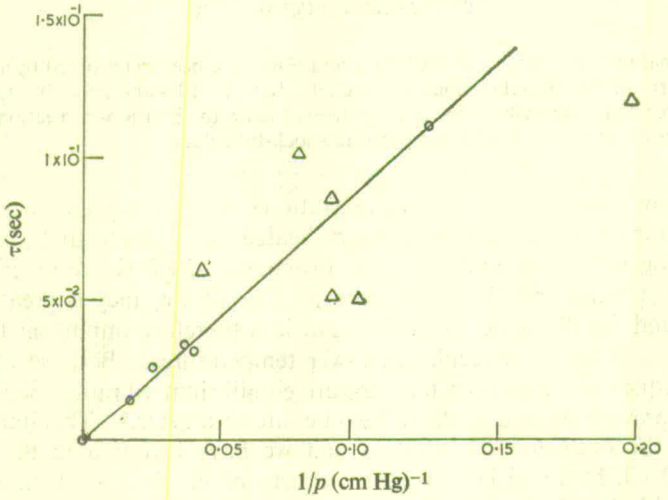

FIG. 1.—Relaxation times in HCl and DCl as a function of 1/pressure : ○, HCl results ; △, DCl results. Line is drawn for a relaxation time of $1{\cdot}1 \times 10^{-2}$ sec.

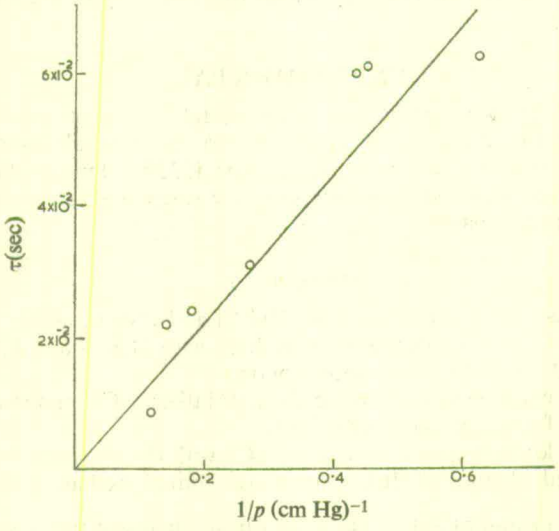

FIG. 2.—Relaxation times in HBr as a function of 1/pressure. Line is drawn for a relaxation time of $1{\cdot}5 \times 10^{-3}$ sec.

the relaxation time until all the vibrational energy is lost by collision. Measurements with mixtures of HCl and H_2 (10 %) which would be expected to have short relaxation times, showed no such rise with time indicating that the effect is not due to attack on the diaphragm.

From the initial and final signals the relaxation time τ was calculated using the expression [3]: initial signal/final signal $= 1/\tau/(1/\tau+1/\tau_{rad})$. The radiative lifetimes

TABLE 1.—RELAXATION TIMES AT 290°K (APPROX.) FOR HCl, DCl AND HBr

compound	radiative lifetime (sec)	relaxation time (sec)
HCl	0·03	$>1{\cdot}1\times10^{-2}$
DCl	0·12	$\sim1\times10^{-2}$
HBr	0·15	$>1{\cdot}5\times10^{-3}$

(τ_{rad}) were derived from absorption intensities using the method of Penner.[5] The absorption intensities for HCl and DCl were taken from measurements by Benedict, Herman, Moore and Silverman,[6] and for HBr from Babrov.[7]

The relaxation times as a function of 1/pressure are shown in fig. 1 and 2 and the values for 1 atm. are given in table 1. The large scatter of the DCl results is almost certainly due to impurity effects, since it is extremely difficult to obtain DCl without small, varying amounts of HCl.

DISCUSSION

Because of the difficulties of obtaining pure gas samples all the relaxation times are shorter limits to the true values, this effect being most important at lower pressures. At higher pressures some re-absorption of an emitted quantum may take place; this will again lead to a shorter relaxation time. The magnitude of the re-absorption effect has been investigated by Doyennette and Henry,[8] who found that the spectrophone value of 0·8 sec for the relaxation time of carbon monoxide [3] should be increased to 6 sec to take account of re-absorption. The relaxation times in table 1 are therefore quoted as lower limits.

The experimental relaxation times may be compared with those calculated by vibration-translation theory.[9] Values of α were obtained by method B of Herzfeld and Litovitz,[10] using the Kreiger potential function as amended by Monchick and Mason.[11] The theoretical results are given in table 2 where they are compared with the experimental values.

TABLE 2.—THEORETICAL RELAXATION TIMES AT 290°K FOR HCl, DCl AND HBr

compound	α (cm^{-1})	$\tau_{theor.}$ (sec)	$\tau_{theor.}/\tau_{expt.}$
HCl	$5{\cdot}84\times10^{8}$	6·5	$<5{\cdot}9\times10^{2}$
DCl	$5{\cdot}84\times10^{8}$	$1{\cdot}6\times10^{-2}$	$<1{\cdot}6$
HBr	$5{\cdot}9\times10^{8}$	$5{\cdot}1\times10^{4}$	$<3{\cdot}4\times10^{7}$

Whilst the theoretical value for DCl is nearly correct those for HCl and HBr are too long, even allowing a factor of 5 for re-absorption effects. The same theory gives good results for such gases as CO, O_2 and N_2, all of which have long relaxation times at room temperature. Possibly, with the hydrogen halides, vibrational energy

is relaxing by some other mechanism so that the vibration-translation theory does not apply. Such a mechanism could be that suggested by Cottrell and Matheson,[12] involving vibration-rotation energy transfer. This process is expected to be most efficient for molecules with low moments of inertia and correspondingly high rotational velocities. The hydrogen halides are such molecules, the hydrogen atom effectively rotating about the much heavier halogen atom. The vibration-rotation mechanism has been treated theoretically by Moore [13] and the results of his treatment, expressed as ratios, are given in table 3 where they are compared with the ratios derived from vibration-translation theory and the experimental results.

TABLE 3.—RATIOS OF RELAXATION TIMES AT 290°K

ratio	vib-trans. theory	vib-rot. theory	expt.
τ_{HCl}/τ_{DCl}	$4{\cdot}1\times10^{2}$	$1{\cdot}1\times10^{-1}$	~1
τ_{HCl}/τ_{HBr}	$1{\cdot}3\times10^{-4}$	2·5	7·3

The agreement between theory and experiment is much improved, particularly for the τ_{HCl}/τ_{HBr} ratio. The theory assumes that rotational energy is continuous which may not be justified for the hydrogen halides where the rotational levels are

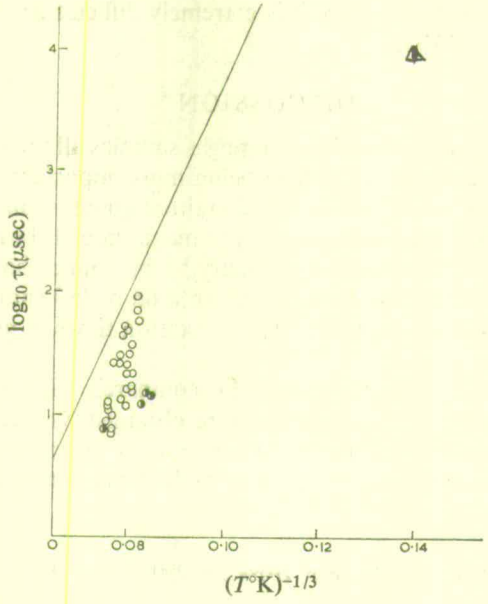

FIG. 3.—Relaxation times in HC as a function of (temperature)$^{-1/3}$: ○, 3-0 results [14]; ◑, 1-0 results [1]; △, present work.

separated by 10-20 cm^{-1}, and a more refined treatment might give better agreement with experiment.

Results for the 3-0 transition on HCl have been obtained by Borrell and Gutteridge [14] using a shock tube. The $v = 3$ level of HCl would be expected to relax rapidly to $v = 1$ by resonance collisions of the type:

$$HCl(v = 3)+HCl(v = 0)\rightarrow HCl(v = 2)+HCl(v = 1)$$
$$HCl(v = 2)+HCl(v = 0)\rightarrow 2HCl(v = 1).$$

Thus the 3-0 relaxation time should be effectively that of the 1-0 process which will be much slower than the resonance processes. The results of Borrell and Gutteridge are plotted in fig. 3 for comparison with the present result. The approximate 1-0 results for HCl [1] are also plotted and the line is drawn according to the translation-vibration theory. It appears that the shock tube results do not extrapolate towards the low temperature result.

We thank the S.R.C. for a maintenance grant to M. G. F.

[1] P. Borrell, *Chem. Soc. Spec. Publ.* no. 20 (Academic Press, 1966), p. 263.
[2] T. L. Cottrell, *Int. Inst. Chem., 12th Conference*, 1962 (Interscience Publications, New York, 1964).
[3] M. G. Ferguson and A. W. Read, *Trans. Faraday Soc.*, 1965, **61**, 1559.
[4] A. E. de Vries and F. S. Klein, *J. Chem. Physics*, 1964, **41**, 3428.
[5] S. S. Penner, *Quantitative Molecular Spectroscopy and Gas Emissivities* (Addison-Wesley, 1959).
[6] W. S. Benedict, R. Herman, G. E. Moore and S. Silverman, *J. Chem. Physics*, 1957, **26**, 1671.
[7] H. J. Babrov, *J. Chem. Physics*, 1964, **40**, 831.
[8] L. Doyennette and L. Henry, *J. Physique*, to be published.
[9] T. L. Cottrell, R. C. Dobbie, J. McLain and A. W. Read, *Trans. Faraday Soc.*, 1964, **60**, 241.
[10] K. F. Herzfeld and T. A. Litovitz, *Absorption and Dispersion of Ultrasonic Waves* (Academic Press, 1959).
[11] L. Monchick and E. A. Mason, *J. Chem. Physics*, 1961, **35**, 1676.
[12] T. L. Cottrell and A. J. Matheson, *Trans. Faraday Soc.*, 1962, **58**, 2336.
[13] C. B. Moore, *J. Chem. Physics*, 1965, **43**, 2979.
[14] P. Borrell and R. Gutteridge, private communication.

PRINTED IN GREAT BRITAIN AT
THE UNIVERSITY PRESS
ABERDEEN